

SYNAPSE FORMATION IN THE ZEBRAFISH SPINAL CORD

by

COURTNEY NICHELLE EASLEY-NEAL

A DISSERTATION

Presented to the Department of Biology
and the Graduate School of the University of Oregon
in partial fulfillment of the requirements
for the degree of
Doctor of Philosophy

September 2011

DISSERTATION APPROVAL PAGE

Student: Courtney Easley-Neal

Title: Synapse Formation in the Zebrafish Spinal Cord

This dissertation has been accepted and approved in partial fulfillment of the requirements for the Doctor of Philosophy degree in the Department of Biology by:

Monte Westerfield	Chairperson
Philip Washbourne	Advisor
Judith Eisen	Member
Tory Herman	Member
Mike Wehr	Outside Member

and

Kimberly Espy	Vice President for Research and Graduate Studies/Dean of the Graduate School
---------------	--

Original approval signatures are on file with the University of Oregon Graduate School.

Degree awarded September 2011

© 2011 Courtney Nichelle Easley-Neal

DISSERTATION ABSTRACT

Courtney Nichelle Easley-Neal

Doctor of Philosophy

Department of Biology

September 2011

Title: Synapse Formation in the Zebrafish Spinal Cord

Approved: _____
Philip Washbourne

This dissertation describes research to elucidate the early steps in the process of synapse formation in the zebrafish spinal cord. One question is how presynaptic proteins are trafficked and recruited to nascent synapses. Previous work has suggested two possible models of presynaptic transport, either 1) most presynaptic proteins are transported together or 2) two types of transport packets, synaptic vesicle (SV) protein transport vesicles (STVs) and Piccolo-containing active zone precursor transport vesicles (PTVs), transport the necessary components separately. We tested these models using *in vivo* imaging in zebrafish spinal cord and found that the recruitment of at least three distinct transport packets during presynaptic assembly of a glutamatergic synapse occurs in an ordered sequence. First, STVs are stabilized at future synaptic sites, then PTVs, followed by a third transport packet type carrying Synapsin, a cytosolic protein that can tether SVs to actin. These results identify an order to the assembly of the presynaptic terminal *in vivo*, suggesting that a single synaptogenic interaction may precipitate the cascade of recruitment steps. We next examined the Cadm/SynCAM family of cell adhesion molecules, a family of proteins that has been shown to be able to induce synapse formation *in vitro* and was

thought to play a role in recruitment of presynaptic proteins. As the role of these proteins *in vivo* was not well understood, we chose to examine the role of the *cadms* in zebrafish spinal cord. We found that zebrafish possess six *cadm* genes, and all are expressed throughout the nervous system both during development and in the adult. We then looked at the role of one of the Cadms, Cadm2a, *in vivo* in the zebrafish spinal cord. We found that knockdown of *cadm2a* significantly decreases the ability of zebrafish embryos to respond to touch. We also found that there is a significant reduction in the number of synapses, as shown by immunohistochemistry, formed between Rohon-Beard and CoPA neurons, the first two cell types in the touch response circuit. These data suggest that Cadm2a plays an important role in synapse formation *in vivo*.

This dissertation contains both my previously published and unpublished co-authored material.

CURRICULUM VITAE

NAME OF AUTHOR: Courtney Nichelle Easley-Neal

GRADUATE AND UNDERGRADUATE SCHOOLS ATTENDED:

University of Oregon, Eugene
University of Washington, Seattle

DEGREES AWARDED:

Doctor of Philosophy, Biology, 2011, University of Oregon
Bachelor of Science, Biology, 2005, University of Washington
Bachelor of Arts, Psychology, 2005, University of Washington

AREAS OF SPECIAL INTEREST:

Neuroscience
Developmental biology

PROFESSIONAL EXPERIENCE:

Graduate Teaching Fellow, UO Biology Department, 2005-06

Undergraduate research assistant, UW Department of Laboratory Medicine,
Dr. A.R. LaSpada 2002-05

Undergraduate Summer Research Fellow, PNNL, Dr. M.J. Feldhaus, 2003

Undergraduate Summer Research Fellow, PNNL, Dr. K.D. Rodland, 2002

GRANTS, AWARDS, AND HONORS:

NIH Developmental Training Grant Appointee, 2006-07, 2007-08, 2008-09,
2009-10

UOWGS Travel Award, Axon Guidance, Synaptogenesis and Neural Plasticity
Meeting, 2008

PUBLICATIONS:

Easley-Neal C, Buchanan J, & Washbourne P. Ordered assembly of the presynaptic terminal of glutamatergic synapses *in vivo*. J Neurosci, manuscript in review.

Pietri T*, Easley-Neal C*, Wilson C, Washbourne P (2008) Six *cadm/SynCAM* genes are expressed in the nervous system of developing zebrafish. Dev Dyn 237:233-246.

Weydt P, Pineda VV, Torrence AE, Libby RT, Satterfield TF, Lazarowski ER, Gilbert ML, Morton GJ, Bammler TK, Strand AD, Cui L, Beyer RP, Easley CN, Smith AC, Krainc D, Luquet S, Sweet IR, Schwartz MW, La Spada AR (2006) Thermoregulatory and metabolic defects in Huntington's disease transgenic mice implicate PGC-1alpha in Huntington's disease neurodegeneration. Cell Metab 4:349-62.

*co-first authors

ACKNOWLEDGMENTS

It has been a privilege to carry out my dissertation research in the uniquely caring and supportive environment of the UO Institute of Neuroscience. I consider myself exceedingly fortunate to have worked in an environment where I consider my colleagues to be friends. My thanks go first to Dr. Philip Washbourne, to whom I am indebted for helping me to complete the transformation from student to scientist during the course of my studies. His unfailing eagerness to discuss results and new experiments was a constant source of motivation. I wish to thank Dr. Judith Eisen for her constant willingness to share her time and tremendous expertise. I thank Dr. Monte Westerfield for his thoughtful comments and critiques which always proved to be helpful in improving my work. I would also like to thank Dr. Tory Herman for her insightful questions and Dr. Mike Wehr for providing a unique perspective on my work. I would like to thank the ION and Biology department staff for all of their help during my time at UO, especially Peg Morrow, Ellen McCumsey, Donna Overall, and Lynne Romans. My thanks also go out to the UO zebrafish facility for fish husbandry.

I would like to express my heartfelt thanks to my family for their unwavering support and encouragement over the course of my graduate career. Finally, I'd like to thank my husband, JT Neal, for going on this journey with me.

This investigation was supported in part by a National Institutes of Health Developmental Training Grant, Number NIH 5-T32-HD07348, and by a grant from the National Institute of Neurological Disorders and Stroke, R01 NS065795-01A2, to Dr. Philip Washbourne at the University of Oregon.

This work is dedicated to my family. Thank you for always believing in me.

TABLE OF CONTENTS

Chapter	Page
I. INTRODUCTION	1
II. ORDERED ASSEMBLY OF THE PRESYNAPTIC TERMINAL OF GLUTAMATERGIC SYNAPSES <i>IN VIVO</i>	4
Introduction.....	4
Results.....	7
Rohon Beard Cells Form Synapses onto CoPA Cell Bodies.....	8
Ultrastructural Identification of Immature Synapses on CoPA Cell Bodies. ...	12
Presynaptic Proteins Arrive in a Specific Order	14
Pausing of STVs Is Predictive of Synapse Formation	18
Synapsin I Is Recruited to Sites of Synapse Formation at Least One Hour After STVs.....	22
PTVs Are Recruited Before Synapsin	24
Synapsin I Is Transported in Axons Independently of STVs and PTVs.....	26
Discussion.....	30
Experimental Procedures	34
Analysis of Zebrafish <i>synapsin</i> Genes.....	34
DNA Constructs.....	35
Zebrafish Husbandry.....	36
Imaging.....	37

Chapter	Page
Immunofluorescence Labeling.....	38
Analysis.....	39
<i>In Situ</i> Hybridization.....	40
Electron Microscopy.....	41
III. SIX <i>CADM/SYNCAM</i> GENES ARE EXPRESSED IN THE NERVOUS SYSTEM OF DEVELOPING ZEBRAFISH.....	42
Introduction.....	42
Results and Discussion	46
Isolation and Characterization of the <i>cadm</i> Genes from Zebrafish	46
Expression Patterns of <i>cadm</i> Genes.....	54
<i>cadm</i> Expression in Developing and Adult Brain.....	56
<i>cadm</i> Expression in the Developing and Adult Visual System	62
<i>cadm</i> Expression in the Developing Spinal Cord	65
Concluding Remarks.....	67
Supplementary Results.....	68
<i>cadm</i> Expression in the Brain: Developing Brain.....	68
Adult Brain.....	70
Experimental Procedures	73
Cloning the <i>cadm</i> Genes	73
Protein Alignment and Phylogenetic Analysis	74
Mapping and Conserved Synteny	75

Chapter	Page
<i>In Situ</i> Hybridization.....	75
IV. <i>CADM2A</i> IS NECESSARY FOR THE FORMATION OF GLUTAMATERGIC SYNAPSES IN THE DEVELOPING ZEBRAFISH SPINAL CORD	77
Introduction.....	77
Materials and Methods.....	79
Zebrafish Husbandry.....	79
Fluorescent <i>In Situ</i> Hybridization	79
Morpholinos.....	79
Morpholino Injections.....	80
RT-PCR.....	80
Behavioral Analysis	80
Immunohistochemistry	82
Imaging	82
Results.....	82
Cadm2a Is Expressed in RB cells	82
Knockdown of Cadm2a Leads to a Decrease in Touch Response.....	84
Knockdown of Cadm2a Leads to a Decrease in Synapse Number.....	87
Discussion.....	89
V. CONCLUSION.....	91

Chapter	Page
REFERENCES CITED.....	93

LIST OF FIGURES

Figure	Page
Chapter II	
1. RBs synapse on CoPA interneurons	9
2. Axosomatic synapses onto CoPA-like cells.	13
3. Presynaptic components arrive sequentially during development.....	15
4. Zebrafish <i>synapsin</i> genes are expressed in RBs	18
5. Paused STVs predict sites of synapse formation	20
6. Delayed Synapsin recruitment to paused VAMP2-mKate2 puncta.....	23
7. Ncadherin recruitment precedes Synapsin.....	25
8. Synapsin1, STVs, and PTVs are transported independently of each other	27
Chapter III	
1. Structure and sequence of zebrafish Cadm proteins	49
2. Phylogeny of Cadm proteins.....	50
3. Genomic analysis of zebrafish <i>cadm</i> genes	51
4. Expression of <i>cadms</i> at 24 hours post-fertilization (hpf).....	55
5. Expression of <i>cadms</i> in the brain	57
6. Expression of <i>cadms</i> in the visual system.....	63
7. Expression of <i>cadms</i> in the developing spinal cord.....	66
Chapter IV	
1. <i>cadm2a</i> is expressed in RB cells.....	83
2. Cadm2a knockdown decreases touch response	86
3. Cadm2a knockdown decreases RB-CoPA synapse number	88

LIST OF TABLES

Table	Page
Chapter III	
1. Nomenclature of the <i>Cadm</i> Gene Family	43
2. Summary of <i>cadm</i> Expression in Brain at 48 Hours Postfertilization	60
3. Summary of <i>cadm</i> Expression in Adult Brain	61

CHAPTER I

INTRODUCTION

Studying neuronal connections to understand human disease

The brain is a fantastically complex organ. In order for it to function properly, correct connections need to be made between the 100 billion neurons (10^{11}) that are estimated to populate the human brain. The connections between these neurons, called synapses, allow for communication between neurons in a unidirectional fashion. Each neuron is estimated to make approximately 7000 synaptic connections with other neurons; this means that the adult human brain contains a staggering one quadrillion (10^{15}) synapses (Drachman, 2005).

Given the sheer number of connections that must be made, it is easy to imagine that in some cases the development of synapses could go awry. In fact several neurological disorders have been shown to involve synapse misformation or malfunction. These include Autism spectrum disorder, Fragile X syndrome, Alzheimers disease, and schizophrenia (Luscher and Isaac, 2009; Penzes et al., 2011). This makes understanding the process of synapse formation a vital goal on the road to better understanding and treatment of these conditions.

Building a synapse

Currently, there are thought to be at approximately 1000 unique proteins at a synapse (Grant, 2006). In order for a properly functioning synapse to develop, all of these proteins must arrive at a synapse at the correct time and in the correct order. To this

point, most studies on synapse formation have been done *in vitro* in cell culture or on fixed tissue in electron microscopy studies. These methods invariably fail to capture the full complexity of the process as it occurs in an intact, living organism. For that reason I used the zebrafish spinal cord as a model to study some early events in synapse formation including presynaptic protein trafficking and the role of adhesion molecules in synapse formation. The zebrafish was an excellent model for these studies due to its relative simplicity; there are only 15 identified types of neurons in the spinal cord during the developmental stages examined in this work (Bernhardt et al., 1990; Hale et al., 2001; Drapeau et al., 2002). In addition, zebrafish embryos are highly amenable to *in vivo* studies due to their optical clarity during early development (Nikolaou and Meyer, 2011).

There are several major steps in the process of synapse formation. First, contact is made between the pre and postsynaptic cell; this contact is stabilized by neuronal adhesion molecules. Next, proteins are recruited to the pre and postsynaptic terminals to form the active zone and the post synaptic density, respectively. Finally, additional proteins are recruited as the synapse matures (McAllister, 2007). Though these processes have received considerable attention from investigators, significant questions remain regarding the initial recruitment of proteins to the synapse, and the signaling process that triggers the recruitment of those proteins.

To better understand how a developing synapse is initially formed *in vivo*, I examined the order and timing of recruitment of presynaptic transport packets to a defined synapse in the zebrafish spinal cord. I discuss this work in Chapter II; this chapter contains work co-authored with J. Buchanan and P. Washbourne.

The role of adhesion molecules in synapse formation

I also studied the role of the Cadm family of adhesion molecules in synapse formation. Cell adhesion molecules are important not just for physically connecting two cells at the point of a synapse, but also play an important role in signaling (Dalva et al., 2007; Biederer and Stagi, 2008). Signaling by Cadm1 has been shown to be important for recruitment of glutamate receptors (Hoy et al., 2009). In addition, Cadm1 has been shown *in vitro* to bind to scaffolding molecules such as CASK (Biederer et al., 2002), and signaling via such interactions could further act to recruit synaptic components.

To examine the function of Cadms in synapse formation *in vivo*, I first characterized the spatiotemporal expression patterns of the zebrafish *cadm* genes during development and in the adult. I then examined the role of Cadm family member Cadm2a in the formation of a defined synapse in the zebrafish spinal cord. I discuss this work in Chapters III and IV; these chapters contain work co-authored with T. Pietri, C. Wilson, and P. Washbourne.

Finally, Chapter V provides a discussion of some of the implications suggested by my dissertation research.

CHAPTER II
ORDERED ASSEMBLY OF THE PRESYNAPTIC TERMINAL OF
GLUTAMATERGIC SYNAPSES *IN VIVO*

The work described in this chapter was co-authored by myself, J. Buchanan, and P. Washbourne. P. Washbourne and I designed the study and wrote the manuscript. I performed the majority of the experiments and analysis. P. Washbourne performed some of the analysis. J. Buchanan prepared and examined samples by electron microscopy.

INTRODUCTION

Synapses are highly complex sites of neuronal contact at which unidirectional communication occurs. Both pre- and postsynaptic sides of the contact contain up to 1000 distinct proteins (Valor and Grant, 2007), that must be assembled correctly for the synapse to function. The vast array of proteins in the presynaptic terminal direct release of synaptic vesicles (SVs) at active zones, whereas the postsynaptic proteome is organized around neurotransmitter receptors, signaling proteins and scaffolding molecules. Recently, several families of cell adhesion molecules have been shown to be sufficient to induce the formation of presynaptic terminals, these include Neuroligins, SynCAMs, Ephrin receptors, and Netrin-G-ligands (Washbourne et al., 2004; Dalva et al., 2007; Tallafuss et al., 2010). However, the order in which they recruit presynaptic components is unclear. Two modes of transport for presynaptic proteins to the terminal have been identified: SV protein transport vesicles (STVs) and presynaptic active zone or

piccolo transport vesicles (PTVs ; Zhai et al., 2001; Sabo et al., 2006), suggesting that there may be at least two steps to the process of presynaptic assembly.

STVs transport an array of SV proteins including VAMP2 (also called Synaptobrevin), Synaptotagmin, and SV2, all of which are found on mature SVs (Ahmari et al., 2000). STVs vary widely in size from clusters the size of a few SVs to larger tubulovesicular aggregates of SV material (Kraszewski et al., 1995; Ahmari et al., 2000). In contrast, PTVs are more uniform 80nm dense-core vesicles that carry active zone cytomatrix proteins, as well as proteins involved in calcium sensing and vesicle fusion, such as piccolo, bassoon, N-cadherin, and SNAP-25 (Zhai et al., 2001; Shapira et al., 2003). Both STVs and PTVs are transported bidirectionally along axons, pausing for varying lengths of time (Kraszewski et al., 1995; Ahmari et al., 2000; Zhai et al., 2001; Shapira et al., 2003; Sabo et al., 2006). While STVs are trafficked at velocities ranging from 0.1-1 $\mu\text{m}/\text{second}$ (Kraszewski et al., 1995; Ahmari et al., 2000; Sabo et al., 2006), PTVs travel at speeds of around 0.1-0.54 $\mu\text{m} /\text{second}$ (Shapira et al., 2003; Jontes et al., 2004). However, because the transport kinetics of STVs and PTVs have not been examined in parallel, it is unknown whether or not the methods of transport of these presynaptic transport packets are distinct.

Little is known about the timing or order of arrival of STVs and PTVs at nascent synapses. Competing models suggest either that most presynaptic components are transported together (Ahmari et al., 2000; Tao-Cheng, 2007) in a single type of transport packet, or that STVs and PTVs transport the necessary components (Zhai et al., 2001; Shapira et al., 2003), although the order in which these two transport packet types would arrive is not clear. If presynaptic proteins are transported in more than one type of

transport packet, several possibilities for the order of recruitment of these transport packets exist: 1) they could stop at nascent synapses randomly i.e. either STVs or PTVs could stabilize first at the site of a new synapse depending on which transport packet approaches this site first; 2) STVs and PTVs could arrive concurrently; 3) STVs and PTVs could arrive in a specific order. Each of these possibilities suggests a different signaling cascade that would be required to underlie the process of synaptogenesis. Therefore, experiments to determine the order of recruitment of these transport packets could inform future studies of signaling involved in synapse formation.

What is carried in each of these transport packet types is also of interest. One protein in particular, Synapsin I, is of consequence due to its relative abundance in the central nervous system (CNS; 0.4% of total brain protein; Kelly, 1991) and due to the recent discovery that it is present at >99% of all cortical synapses (Micheva et al., 2010). Synapsins hold a reserve pool of SVs within the presynaptic terminal by binding both SVs and the actin cytoskeleton (Fornasiero et al., 2010). Though Synapsin function is unnecessary for synapse formation or neurotransmitter release, genetic ablation of Synapsins in mice leads to deficits in synaptic transmission, including changes in neurotransmitter release kinetics (Gitler et al., 2004; Coleman and Bykhovskaia, 2009). Some studies suggest that Synapsins are transported to the presynaptic terminal in association with STVs (Ahmari et al., 2000), whereas other studies propose that PTVs associate with STVs during transport and that these large complexes also contain Synapsins (Tao-Cheng, 2007).

In this study, we examined *in vivo* the order in which STVs, PTVs, and Synapsins traffic to the site of a newly forming synapse. Immunofluorescence images from fixed

samples revealed that Synapsins arrived significantly later than STV proteins. Live imaging studies confirmed that STVs, PTVs, and Synapsin1 traffic independently in axons: STVs arrived at nascent synapses first, followed by PTVs after a ~1 hour delay, and then Synapsin after an additional ~30 minutes had elapsed. This is the first study to show that presynaptic assembly proceeds in an ordered fashion, and that Synapsin1 is transported as part of a discrete transport packet, distinct from STVs and PTVs.

RESULTS

Previous studies examining the trafficking of presynaptic components to CNS synapses have almost exclusively been performed *in vitro*, due to the lack of an appropriate *in vivo* model for synapse assembly. Recent live imaging studies in zebrafish (*Danio rerio*; Jontes et al., 2000; Jontes et al., 2004; Nikolaou and Meyer, 2011) have suggested that this organism possesses the characteristics necessary to facilitate examination of when and how synaptic proteins are brought to the site of a nascent synapse *in vivo*. Zebrafish develop rapidly and are optically clear through early development (McLean and Fetcho, 2008; Nikolaou and Meyer, 2011). Rohon-Beard (RB) sensory neurons in the zebrafish spinal cord lend themselves to live-imaging studies as their central axons are linear, allowing fast imaging within a narrow range of focus (Figure 1A, B; Jontes et al., 2004). These cells transduce the sense of touch (Artinger et al., 1999; Douglass et al., 2008) to mediate a very early behavior: touch-evoked coiling by one day postfertilization (dpf; Saint-Amant and Drapeau, 1998; Drapeau et al., 2002; Saint-Amant, 2006). However, it was not clear which cells RBs form synapses with in the spinal cord. We recently demonstrated that tactile stimuli to the trunk and tail elicit

AMPA-type glutamate receptor-specific synaptic currents in commissural primary ascending (CoPA) interneurons (Pietri et al., 2009), suggesting that RBs synapse directly onto CoPAs (Figure 1B; Downes and Granato, 2006). We first set out to determine whether this RB-CoPA pair would provide a model of CNS synaptogenesis, with which we could examine the recruitment of proteins to a homogeneous population of newly forming glutamatergic synapses *in vivo*. Next, we focused on immunolabeling experiments using synaptic markers and time lapse imaging of fluorescent synaptic fusion proteins to examine the order of arrival and the mode of transport of various presynaptic components.

Rohon Beard cells form synapses onto CoPA cell bodies

We began by examining whether RB axons contact CoPA cells in the spinal cord of zebrafish embryos at 25 hpf, a developmental stage at which embryos can respond to touch (Drapeau et al., 2002). By this stage, RB axons expressing GFP from a *neurogenin1*:GFP transgene (*ngn1*:GFP, [TG(-3.1ngn1:GFP)sb2]) had already extended along the length of the dorsal longitudinal fascicle (dlf; arrow in Figure 1C). These axons lay directly adjacent to CoPA interneuron cell bodies, as visualized by immunolabeling with con-1 antibody (arrowhead in Figure. 1C; Bernhardt et al., 1990). This confirms that, at this stage, the central axons of RBs and CoPA cell bodies are in close proximity, making it feasible for synaptogenesis to occur.

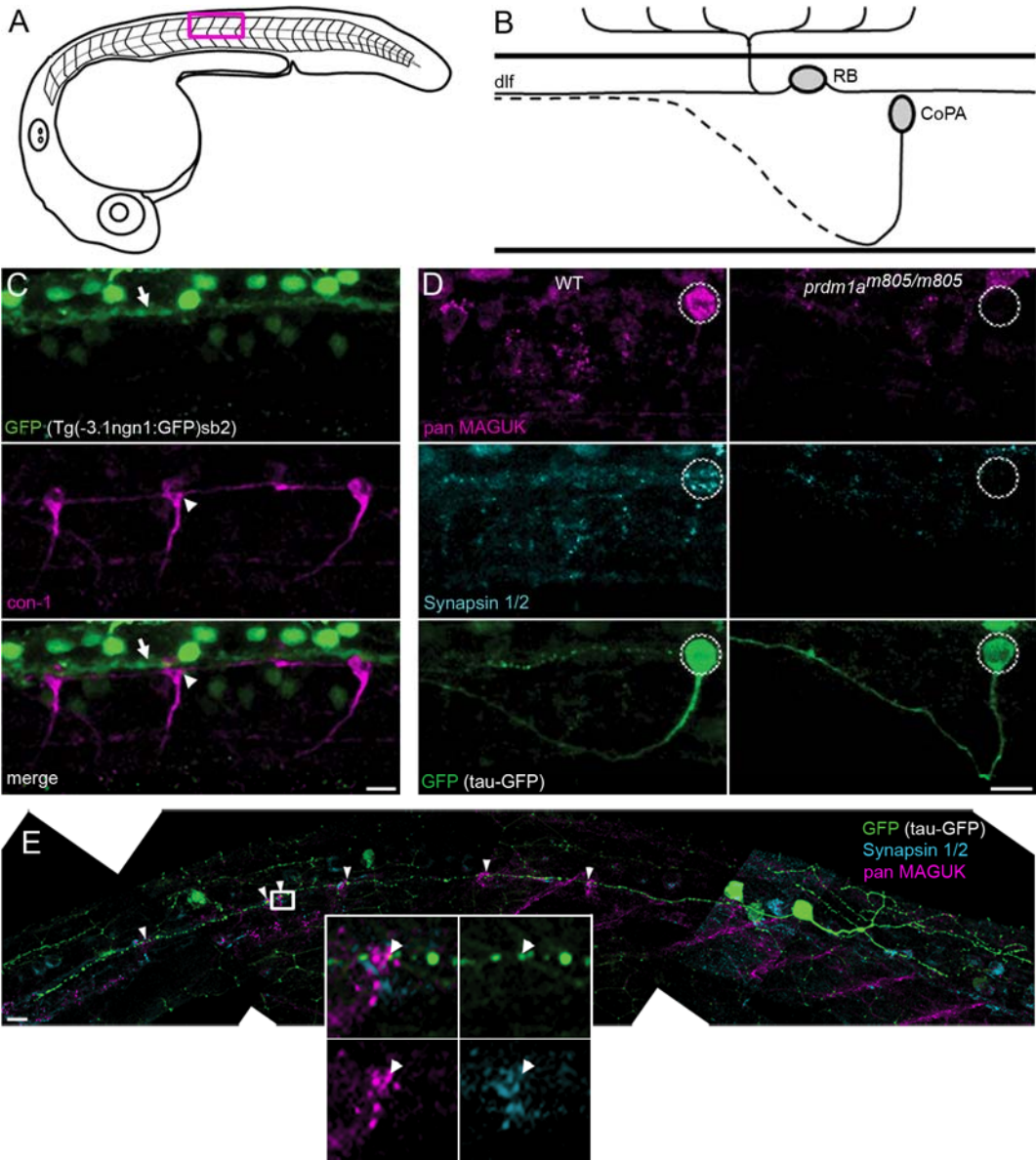


Figure 1. RBs synapse onto CoPA interneurons. (A) Diagram of a lateral view of a 25 hpf zebrafish embryo. Red box outlines the region of the trunk between segments 11 and 15 where these studies were performed. (B) Diagram depicting the cell body location and axon trajectories of an RB cell and a CoPA cell, in a lateral view of the developing spinal cord. The dotted axon represents a contralateral projection. (C) CoPA cell bodies, labeled with con-1 antibody (magenta), were in close proximity to RB axons expressing GFP, in *ngn1*:GFP transgenic embryos. Scale bar, 10 μ m. (D) pan MAGUK (magenta) and Synapsin 1/2 (cyan) immunolabeling on WT and *prdm*^{m805/m805} embryos with GFP-labeled CoPA cells. Left panel: WT embryo showed overlap of many pre and postsynaptic puncta on CoPA cell body. Right panel: No pre- or postsynaptic puncta were seen on CoPA cell bodies in embryos lacking RB cells. Dotted outline indicates location of CoPA cell body in each panel. Scale bar, 10 μ m. (E) Composite image of a RB cell expressing GFP (green), including the entire central axon extending rostrally, with labeling for Synapsin 1/2 (cyan) and pan MAGUK (magenta). Distinct clusters of colocalized pan MAGUK and Synapsin 1/2 immunofluorescence were at CoPA cell bodies, see arrowheads. Inset shows distinct MAGUK and Synapsin 1/2 puncta, arrowhead indicates a MAGUK puncta adjacent to a Synapsin 1/2 puncta that is within a varicosity in the GFP-expressing RB axon. Scale bar 10 μ m.

To confirm the presence of synapses on CoPA cells at this stage of development, we next performed immunolabeling using antibodies to the presynaptic proteins Synapsin1 and 2 and postsynaptic density membrane associated guanylate kinase proteins (MAGUKs) PSD-95, PSD-93 and SAP102 (pan MAGUK antibody; Meyer et al., 2005). To identify and visualize CoPA cells, we expressed Tau-GFP fusion protein in a mosaic distribution by injecting a neuronal expression vector into fertilized eggs at the one cell stage. The preferential targeting of Tau-GFP to axons facilitated the identification of CoPA cells by virtue of their ascending, commissural axon (Bernhardt et al., 1990). We observed punctate labeling of both Synapsin 1/2 and pan MAGUK antibodies at the cell bodies of CoPA cells at 24-26 hpf (Figure 1D, left panel). Further analysis with multiple GFP transgenic zebrafish lines (data not shown; A. Tallafuss and P. Washbourne) confirmed that CoPA interneurons are the only neurons in the dorsal spinal cord at 25 hpf that exhibit punctate MAGUK immunoreactivity. When we examined images in which

Synapsin and MAGUK immunolabeling was overlaid (Figure 1D, and see inset in Figure 1E), we saw colocalization in distinct puncta at CoPA cell bodies, suggesting the presence of numerous synapses.

As axons from several neuronal populations project in the dlf, including the contralateral axons of CoPA cells, it was conceivable that the synapses located on CoPA cell bodies might represent a mixed population of synapses from RBs, CoPAs, and other neurons. The narrowminded (*nrd*, *prdm1a*^{*m805/m805*}) mutation disrupts the *prdm1a* gene resulting in a deficit in neural crest cell development, including loss of the RB cells (data not shown; Artinger et al., 1999; Hernandez-Lagunas et al., 2005), while sparing all other neurons examined in the spinal cord (data not shown). *prdm1a*^{*m805/m805*} embryos showed no punctate immunoreactivity for MAGUKs or Synapsin on CoPA cell bodies (Figure. 1D, WT n = 4, *prdm1a*^{*m805/m805*} n = 3). As no synapses, defined by adjacent Synapsin and MAGUK puncta, were observed at CoPA cell bodies in the absence of RB cells, we conclude that all synapses onto CoPAs are from RBs at this stage of development.

There are between 50 and 78 RB cells along each side of the entire spinal cord (Grunwald et al., 1988; Eisen and Pike, 1991), but on average only 23 CoPA interneurons (Eisen and Pike, 1991). For our further studies of synapse assembly, it was important to take into account the overall connectivity between RBs and CoPAs. For example, if a given RB synapses with only a subset of CoPA cells, it would be challenging to monitor the region of axon that would eventually form synapses with a ‘correct’ CoPA. To address this, we examined embryos that had only a single fluorescently-labeled RB. Immunolabeling with Synapsin and pan MAGUK antibodies revealed that, at 25 hpf, 87.1% of CoPAs (n = 31 CoPAs from 13 embryos; arrowheads in Figure 1E) had formed

synapses with single labeled RB axons as indicated by Synapsin immunoreactivity in the RB axon adjacent to the MAGUK puncta. Furthermore, on average, a single synapse (1.33 ± 0.14 ; $n = 18$ CoPAs from 8 embryos) was observed between an RB axon and each CoPA cell. By 28 hpf, we observed as many as 39 postsynaptic puncta at a single CoPA (average = 18.77 ± 2.27 ; see Figure 1E, and 3C, D), suggesting that eventually every RB may synapse onto every CoPA within a hemi-spinal cord. Importantly for our studies, these results suggest that every RB contacts the overwhelming majority of CoPAs on one side of the spinal cord and that a single synapse forms at each contact site.

Ultrastructural identification of immature synapses on CoPA cell bodies

We next examined the ultrastructure of RB-CoPA synapses, to determine whether the classical hallmarks of synapses could be resolved at this early developmental time point. We performed transmission electron microscopy on transverse sections of embryos at 25 and 28 hpf. We found that CoPA cells could be identified in cross section due to (1) their cell body shape, (2) their dorso-lateral location within the spinal cord, and (3) their proximity to the dlf (Figure 2A). At 25 and 28 hpf, we were able to identify axons forming the dlf lying lateral to CoPA cell bodies. Many of these axons contacted the lateral face of a CoPA cell body (Figure 2B-D). At 25 hpf, some axons were contacted by small filopodial extensions from the CoPA cell body, and these contact sites showed accumulations of SVs (Figure 2D, in 3/3 CoPA-like cells examined). Filopodial extensions from the cell bodies of CoPA cells were not observed at 28 hpf (Figure 2B, C, 4/4 cells).

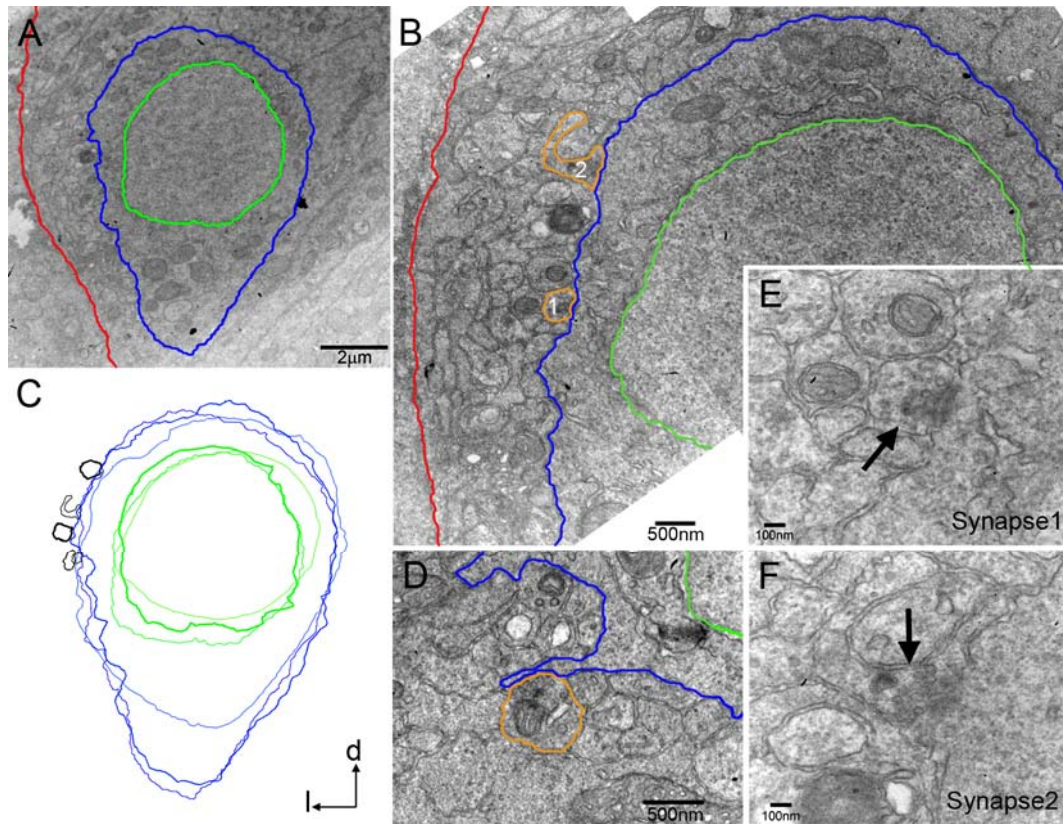


Figure 2. Axosomatic synapses onto CoPA-like cells. (A) Electronmicrograph (EM) of a transverse section of the zebrafish embryo at 28 hpf. CoPA-like cells were identified based on their cell body shape and dorso-lateral location in the spinal cord. The plasma membrane and nuclear envelope were traced in blue and green for clarity, respectively. The basal lamina of the spinal cord is in red. (B) Synapses (orange tracing) from axons in the dlf were identified on the CoPA-like cell body in A (see E and F, for higher magnification). (C) Synapses were found on the lateral face of CoPA-like cells in a stereotypical location, as demonstrated by an overlay of three cell profiles with their synapses (black). (D) At 25 hpf, synapses were located on small filopodial extensions from the cell body. Higher magnification images of Synapse1 (E) and Synapse2 (F) in B, with accumulations of synaptic vesicles (arrows), smooth apposed synaptic membranes and weakly-labeled postsynaptic densities.

At 28 hpf, a few axon profiles directly in contact with the cell body (in 4/4 cells examined) demonstrated accumulations of SVs (Profiles 1 and 2 in Figure 2B). Analysis of contacts with accumulations of SVs at higher magnification revealed an even apposition and a thickening of the pre- and postsynaptic membranes (Figure 2E, F).

Furthermore, we noted weakly labeled postsynaptic densities, suggesting that these contacts are immature synapses (Ahmari and Smith, 2002). Interestingly, upon overlay of multiple cell body profiles together with their impinging presynaptic axon terminals, we discovered that synapses were clustered within a defined region upon the dorsal, lateral face of the CoPA cell bodies (Figure 2C). This suggests that synapse formation may be confined to a stereotypical location between dlf axons and CoPA cell bodies. From these experiments, we conclude that at 25–28 hpf synapse formation is ongoing between axons of the dlf, which we previously identified as being from RBs, and CoPA cells in the zebrafish spinal cord.

Presynaptic proteins arrive in a specific order

We next examined the time course over which SVs and Synapsins accumulated at RB-CoPA synapses. Embryos from transgenic *ngn1:GFP* zebrafish, which express GFP in RBs, were immunolabeled with antibodies to Synaptotagmin2b (Synaptotagmin), to label SVs and STVs, and antibodies to Synapsins and MAGUKs. Embryos were fixed and labeled at 19, 22, 25, and 28 hpf. These ages flank the onset of the touch response at 21 hpf (Saint-Amant and Drapeau, 1998; Drapeau et al., 2002; Saint-Amant, 2006; Pietri et al., 2009), when we would hypothesize that RB-CoPA synapses form and become functional.

At 19 hpf punctate immunoreactivity for Synaptotagmin was seen along the dlf. When we co-labeled with antibodies that label CoPA cells within the spinal cord (con-1), we found that punctate aggregates of Synaptotagmin in RB axons were adjacent to CoPA cell bodies where they contact the dlf (Figure 3A, B). When we quantified these puncta,

we found an average of $2 (\pm 0.27, n = 8 \text{ CoPAs})$ puncta per CoPA with Synaptotagmin immunoreactivity, and this number increased at each developmental time point examined (Figure 3B, D). These results suggest that STVs are transported in axons at early stages of development and that the number of synaptic SV puncta increases over the developmental time period examined.

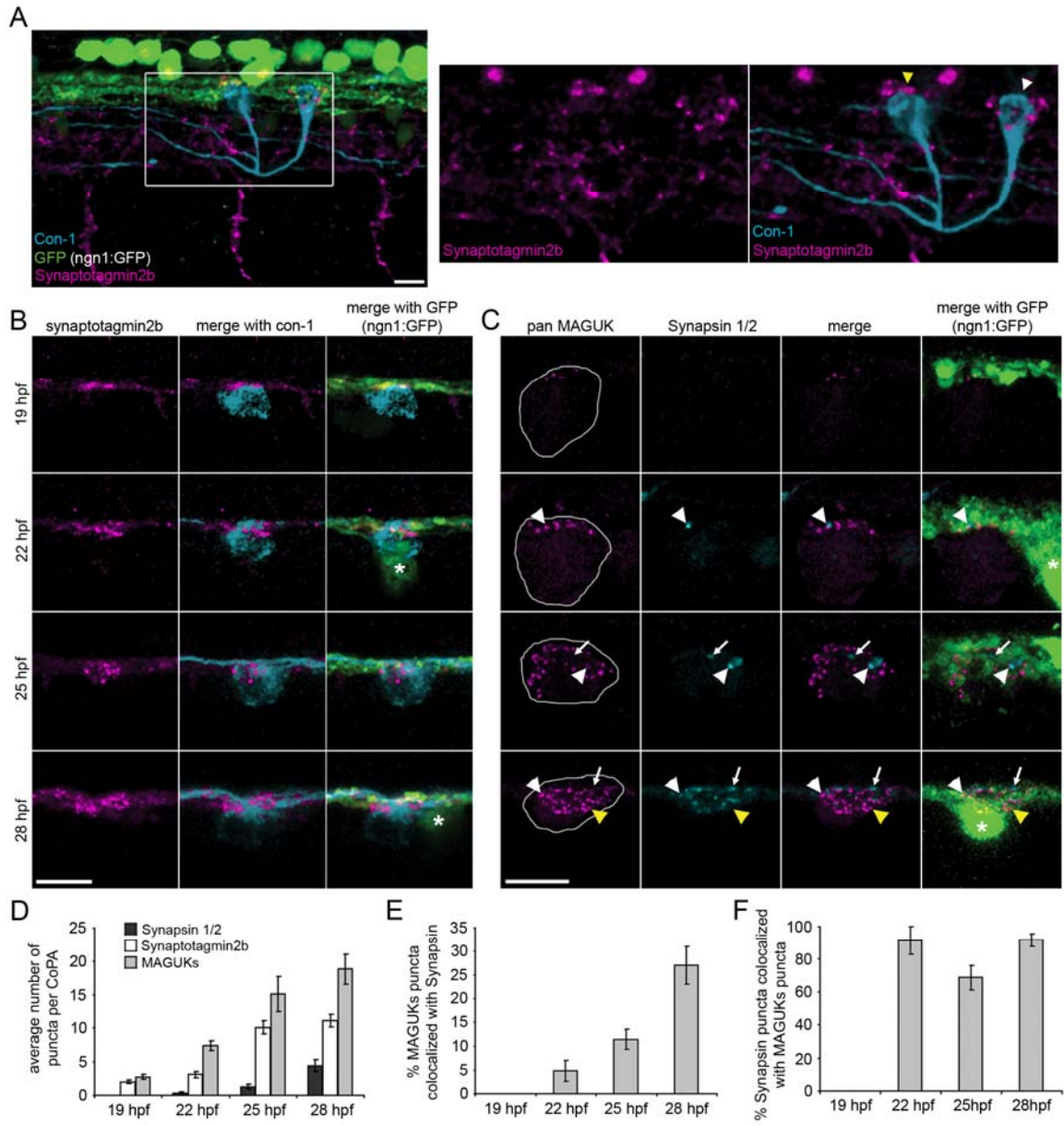


Figure 3. Presynaptic components arrive sequentially during development. (A) Left panel: lateral view of 3 segments of a 25 hpf embryo expressing *ngn1:GFP* (green) labeled with antibodies to Synaptotagmin2b (magenta) and CoPA neurons (*con-1*, cyan). Notice Synaptotagmin2b puncta were colocalized with CoPA cell bodies at the dlf. Right panels: zoom of box in left panel. Yellow arrow indicates CoPA cell body in distal dlf, white arrow indicates CoPA cell body in proximal dlf. Scale bar 10 μ m. (B) Dorsal view of IF labeling for Synaptotagmin2b (magenta) colocalized with CoPA cell bodies (cyan) in *ngn1:GFP* embryos from 19-28 hpf. Asterisk labels RB cell bodies. Scale bar 10 μ m. (C) Dorsal view of IF labeling for MAGUKs (magenta) and Synapsin 1/2 (cyan) from 19-28 hpf. Asterisk labels RB cell bodies. Outlines of CoPA cell bodies were generated by increasing the gain of the MAGUK IF. Scale bar 10 μ m. (D) Histogram shows the number of Synapsin 1/2, Synaptotagmin2b, and MAGUK puncta per CoPA cell from 19-28 hpf. (E-F) Histograms show the percentage of MAGUK puncta colocalized with Synapsin puncta, and the percentage of Synapsin puncta colocalized with MAGUK puncta, respectively, from 19-28 hpf. Error bars show standard error of the mean (s.e.m.).

In contrast to the early appearance of STV immunoreactivity, immunolabeling for Synapsin was first seen at 22 hpf (Figure 3C, D), 3 hours later than the SV protein Synaptotagmin. A portion of the Synapsin labeling was diffuse throughout the dlf, but large, intense puncta were occasionally seen in axons, and especially at sites adjacent to CoPA cell bodies (Figure 3C). Between 8.5 – 31.3% of Synapsin puncta were at locations in the dlf other than CoPAs during the developmental window examined. The numbers of Synapsin puncta steadily increased with development (Figure 3C, D). To determine whether Synapsin puncta were indeed synaptic, we examined MAGUK immunoreactivity. This postsynaptic marker was detected earlier than Synapsin, at 19 hpf, and an increasing number of MAGUK puncta were seen in CoPA interneurons at each later time point (Figure 3C, D). Importantly, adjacent Synapsin and MAGUK puncta were seen at CoPA cell bodies at around 22 hpf (arrowhead, Figure 3C-F). Interestingly, only a small proportion ($4.79\% \pm 2.21\%$, $n = 16$ CoPAs) of the many MAGUK puncta were adjacent to Synapsin early in development, but this proportion steadily grew to over

25% over the next 6 hours of growth (Figure 3E). However, the proportion of Synapsin puncta that were adjacent to MAGUK proteins was much higher and remained relatively constant over time, averaging 69% - 91% (19 hpf, n = 16 CoPAs; 22 hpf, n = 15 CoPAs; 25 hpf, n = 21 CoPAs; 28 hpf, n = 18 CoPAs) over the stages examined (Figure 3F).

Based on the different developmental time points at which markers for STVs and Synapsin appear, our immunolabeling studies suggest that there is a sequential arrival of synaptic proteins at the RB-CoPA synapse, which would imply that these proteins are trafficked separately to synapses.

At this level of analysis, it is important to consider that the 3 hour delay in the arrival of Synapsin at RB-CoPA synapses as compared to Synaptotagmin may not be solely due to differential trafficking. This delay could also depend on the developmental expression pattern of *synapsin* genes in the zebrafish embryo. We identified and isolated the coding regions of three zebrafish *synapsin* genes, *synapsins1*, *2a* and *2b*. No ortholog of mammalian *synapsin3* was identified in the zebrafish genome, although *synapsin2* was present as duplicate co-orthologs (data not shown). *In situ* hybridization at 17, 19, 22 and 25 hpf, revealed that transcripts for these genes did not appear until 19 hpf (Figure 4A, B, and data not shown). Based on our immunolabeling studies (Figure 3C), we conclude that there is a ~2 hour delay in the generation of Synapsin protein as Synapsins were not detected by immunohistochemistry until 21 hpf. While the developmental expression pattern explains the late arrival of Synapsins at RB-CoPA synapses, it nonetheless underscores the possibility of independent, sequential arrival of STVs and Synapsins at the presynaptic terminal.

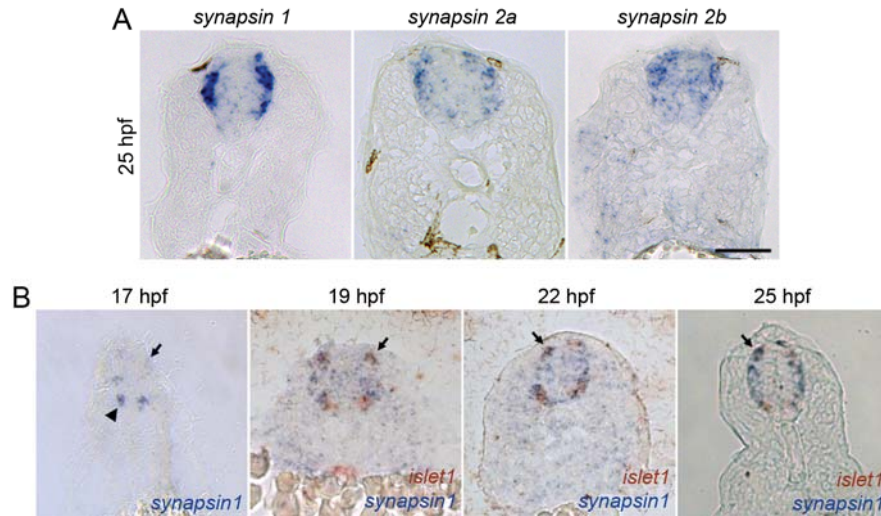


Figure 4. Zebrafish *synapsin* genes are expressed in RBs. (A) *In situ* hybridization (ISH) for zebrafish *synapsins 1*, *2a*, and *2b* at 25 hpf in transverse sections. *synapsin1* showed the strongest expression of the three in RBs. Scale bar 50 μ m. (B) *synapsin1* ISH on 17, 19, 22, and 25 hpf transverse sections (2 color ISH with *islet-1* to label RBs and motor neurons in 19, 22, and 25 hpf images). *synapsin1* transcript was first seen at 17 hpf in motor neuron domain (arrowhead), but not in RBs (arrow). *synapsin1* and *islet1* were seen in RBs from 19 hpf on (arrows). Scale bar 50 μ m.

Pausing of STVs is predictive of synapse formation

To investigate the order and timing of arrival of synaptic proteins at individual synapses, we turned to live imaging at 24 hpf, a stage when all presynaptic markers that we examined are expressed. We drove the expression of the SV protein VAMP2 fused to the red fluorescent protein mKate2 (UAS:VAMP2-mKate2) by injecting DNA into fertilized zebrafish eggs from the et101.2 Gal4 line (Scott et al., 2007) which expresses Gal4 in RB cells. By titrating the concentration of the plasmid, embryos were obtained that expressed VAMP2-mKate2 in only one or two RB neurons (Figure 5A).

Immunolabeling of VAMP2-mKate2 expressing embryos showed that VAMP2-mKate2 puncta colocalize with the SV proteins SV2 ($95.2\% \pm 3.7\%$, $n = 3$) and Synaptotagmin ($86.7\% \pm 3.9\%$, $n = 3$), suggesting that VAMP2-mKate2 is a component of STVs (data

not shown). Live imaging of the central axons of expressing RB cells demonstrated that VAMP2-mKate2 puncta are transported in both anterograde and retrograde directions with frequent pauses. Our control experiments and comparisons with previous studies of trafficking of VAMP2 in neurons in live zebrafish embryos and in mammalian cultures (Ahmari et al., 2000; Jontes et al., 2004; Sabo et al., 2006) suggest that VAMP2-mKate2 is a reliable marker for the visualization of STV transport in RB axons.

To examine the accumulation of STVs at RB-CoPA synapses, we acquired image stacks of segments of RB axons expressing VAMP2-mKate2 every 30 sec over a two hour period from 24-26 hpf (selected frames from an imaging session presented in Figure 5B). Embryos were fixed within five minutes of the end of the imaging period, and then immunolabeled for postsynaptic MAGUK proteins (Figure 5C). The VAMP2-mKate2 puncta that had been tracked during the imaging session were identified in the immunofluorescence (IF) images. The length of time that each VAMP2-mKate2 puncta was paused was then measured from the end of the live imaging period to generate a retrospective stability map (Figure 5C). This analysis revealed a wide variety of stabilities, ranging from puncta that were not paused at the end of imaging (0 hours, dark blue in Figure 5C), puncta that paused during imaging and remained stable until the end of imaging (e.g. 0.5 hours, arrow, light blue in Figure 5C), to puncta that were paused for the entire imaging period (>2 hours, arrowhead, magenta in Figure 5C).

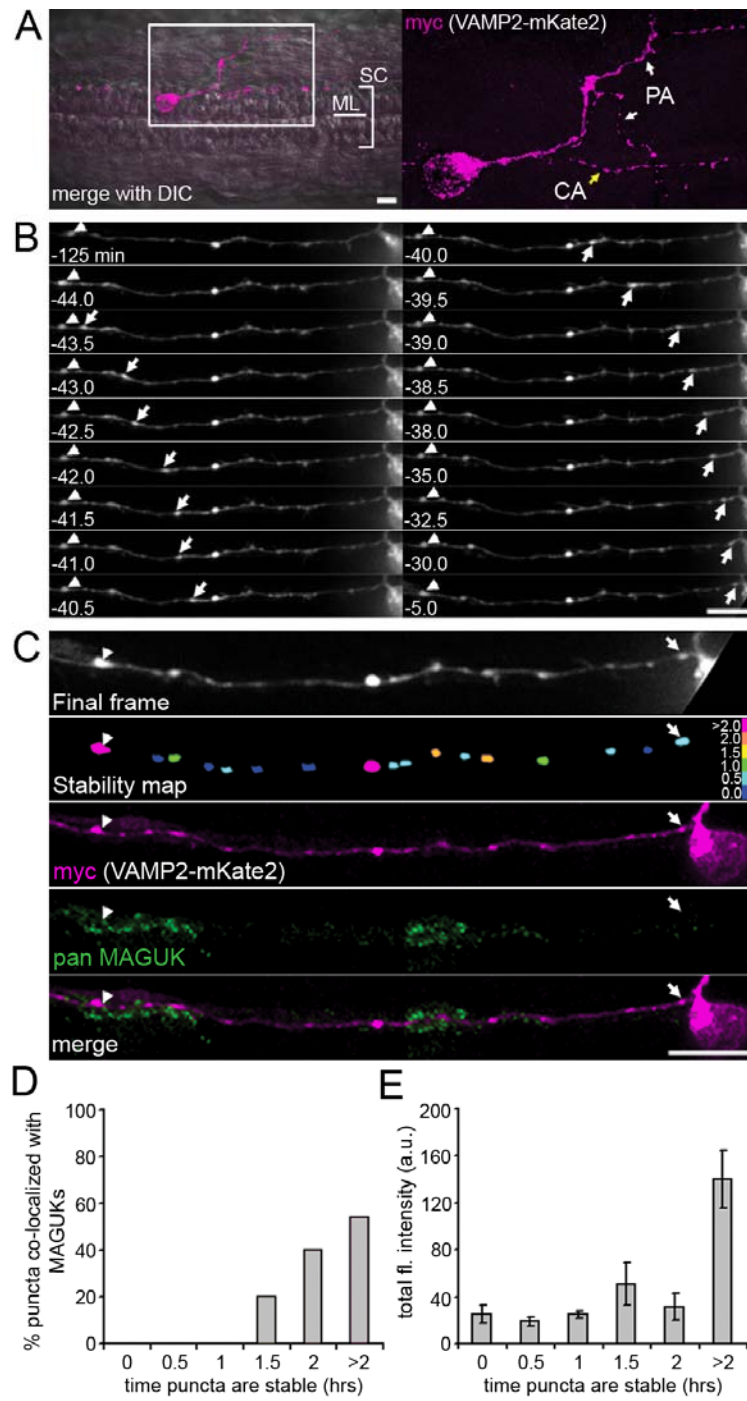


Figure 5. Paused STVs predict sites of synapse formation. (A) An RB neuron expressing VAMP2-mKate2 at 25 hpf in a dorsal view, with rostral to the left. Left panel, IF for VAMP2-mKate2 overlaid on a bright field image. The midline (ML) and extent of the spinal cord (SC) are indicated. Right panel, magnification of myc IF labeling, showing the peripheral arbor (PA) and central axon (CA) of the RB. Scale bar, 10 μ m. (B) Selected frames from a 2 hour time-lapse movie (from 24-26 hpf) of VAMP2-mKate2 expressed by an RB cell. While some puncta remained stable for the entire imaging period (arrowheads) others stabilized during imaging (arrow). Scale bar, 10 μ m. (C) Post-imaging IF labeling demonstrates the presence of MAGUKs (green) at a VAMP2-mKate2 punctum that was paused for at least 2 hours (arrowhead), but not at a punctum paused for 29 minutes (arrow). The stability map uses a color code to report the time each punctum was paused before the end of imaging. Bins were as follows: non-paused puncta (0.0), paused for 0 - 0.5 hours (0.5), 0.5 – 1 hour (1), etc. to puncta paused for the entire imaging period (>2.0). Scale bar, 10 μ m. (D) Stability histogram shows quantification of the percentage of VAMP2-mKate2 puncta colocalized with MAGUKs. n = 7 RB axon segments analyzed. (E) Intensity histogram shows the total fluorescence intensity for VAMP2 puncta. A significant increase in total fluorescence intensity was seen at puncta paused for >2 hours. Bins for each as described for the stability map. Error bars show s.e.m.

When colocalization between MAGUK protein IF and VAMP2-mKate2 puncta was analyzed, we found that only VAMP2-mKate2 puncta that had been paused for at least 1.5 hours prior to fixation were colocalized with MAGUK puncta (average stability with MAGUK localization = 94.8 min \pm 14.7 min, n = 7 RB axon segments; Figure 5D). VAMP2-mKate2 puncta that had been paused for shorter lengths of time or that were not paused at the end of the imaging period never colocalized with MAGUK puncta (arrow in Figure 5C, D; n = 7 RB axon segments). These data suggest that STVs stabilize at nascent synaptic sites and that stabilization precedes accumulation of postsynaptic MAGUK scaffolding proteins by about 1.5 hours.

Interestingly, the total fluorescence intensity (sum of intensities at each pixel within the punctum) was highest for VAMP2-mKate2 puncta that had been stable for the longest amount of time (Figure 5E). In fact, the total fluorescence intensity of VAMP2-

mKate2 puncta that had been stable for longer than 2 hours was 2.7 - 7.3 fold higher than puncta that had stabilized during imaging, suggesting that additional VAMP2-mKate2 positive STVs are added to synaptic sites more than 2 hours after initial stabilization.

Synapsin1 is recruited to sites of synapse formation at least one hour after STVs

Having established that stable STVs are eventually colocalized with postsynaptic markers with a time course of around 1.5 hours, we next examined whether Synapsin was recruited to individual presynaptic terminals with a delay with respect to STVs. We imaged VAMP2-mKate2 expressing RB axons as described above, and then performed retrospective IF labeling for Synapsin and MAGUK proteins. Synapsin was never colocalized with VAMP2-mKate2 transport packets that had been moving at the end of the imaging session or that had paused at the end of the imaging session (arrow Figure 6A-C). Thus, we can conclude that Synapsin does not transport with VAMP2-mKate2 positive STVs.

However, Synapsin was colocalized with VAMP2-mKate2 clusters that had been stable for at least one hour (arrowhead Figure 6B, C; n = 13 RB axon segments). In addition, 100% of stable VAMP2-mKate2 puncta that colocalized with Synapsin were also localized opposite MAGUK puncta (arrowhead Figure 6B, C). These data suggest that Synapsin is recruited to synapses with a significant delay with respect to VAMP2-mKate2 containing STVs. Furthermore, we conclude that Synapsin and postsynaptic MAGUK proteins are recruited to new synapses concurrently or with a similar time course.

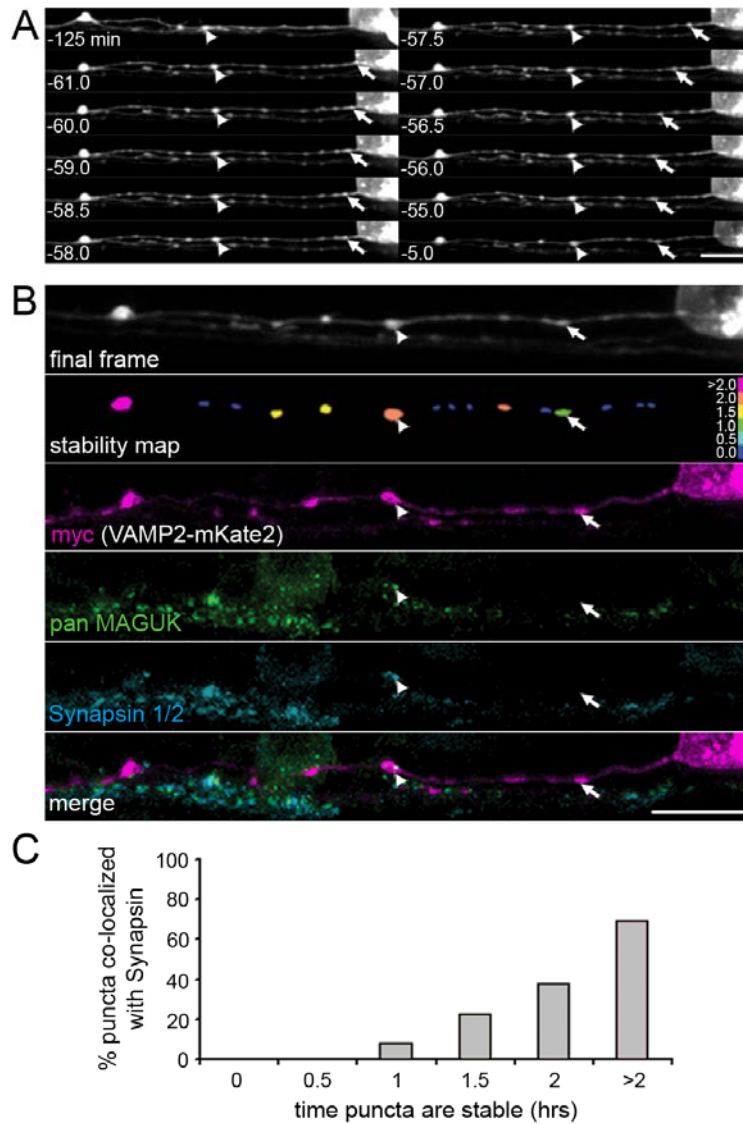


Figure 6. Delayed Synapsin recruitment to paused VAMP2-mKate2 puncta. (A) Selected frames from a 2 hour time-lapse movie (from 24-26 hpf) of VAMP2-mKate2 expressed by an RB cell. While some puncta remained paused for the entire imaging period (arrowheads) others paused during imaging (arrow). Scale bar, 10 μ m. (B) Post-imaging IF labeling demonstrates the presence of Synapsin 1/2 (cyan) and MAGUKs (green) at VAMP2-mKate2 (magenta) a punctum that was paused for 110 min (arrowhead), but not at a punctum paused for 51 min (arrow). The stability map uses the color code bins described in Figure 5. Scale bar, 10 μ m. (C) A stability histogram quantifying the percentage of Synapsin 1/2 that colocalized with VAMP2-mKate2 puncta reveals that, on average, recruitment of VAMP2-mKate2 preceded that of Synapsin by 83.7 min (\pm 12.5 min). Bins are as described for Figure 5. n = 13 RB axon segments analyzed.

PTVs are recruited before Synapsin

We next examined the time course of recruitment of PTVs to the RB-CoPA synapse. To monitor the trafficking of PTVs, we expressed Ncadherin-GFP in RB cells (Ncad-GFP, *cadherin2*; Jontes et al., 2004). Ncadherin is an integral component of PTVs (Zhai et al., 2001). Since Bassoon and Piccolo antibodies were not immunoreactive in zebrafish embryos, we performed IF for the PTV marker Bassoon on rat hippocampal neurons expressing zebrafish Ncad-GFP. This analysis showed strong colocalization between Bassoon puncta and Ncad-GFP puncta ($95.36\% \pm 3.49\%$; $n = 5$ neurons; Figure 7A), confirming that Ncad-GFP is a good marker of PTVs. The majority of Ncad-GFP did not colocalize with the SV protein Synaptotagmin ($16.6\% \pm 3.4$, $n = 3$ embryos; Figure 7B) in RB axons, suggesting that it is present in a different transport organelle than SV proteins. Live imaging showed that Ncad-GFP was trafficked in punctate structures both anterogradely and retrogradely in RB axons (Figure 7C; Jontes et al., 2004).

Live imaging of Ncad-GFP and post-imaging IF labeling for Synapsin and MAGUKs were performed as previously described. Puncta that were actively trafficking at the end of the imaging period almost never colocalized with Synapsin and MAGUKs (Figure 7E), suggesting that Synapsin is not transported with PTVs. We found that Ncad-GFP puncta colocalize with Synapsin, on average, 37.6 min (± 8.0 min) after stabilizing ($n = 13$ RB axon segments; arrows Figure 7C-E). 100% of Ncad-GFP puncta that colocalized with Synapsin were also found to be apposed to MAGUK puncta. These data suggest that PTVs arrive at synapses around 30 minutes before Synapsin, and with a distinct time course to VAMP2 transport packets (gray bars, Figure 7E).

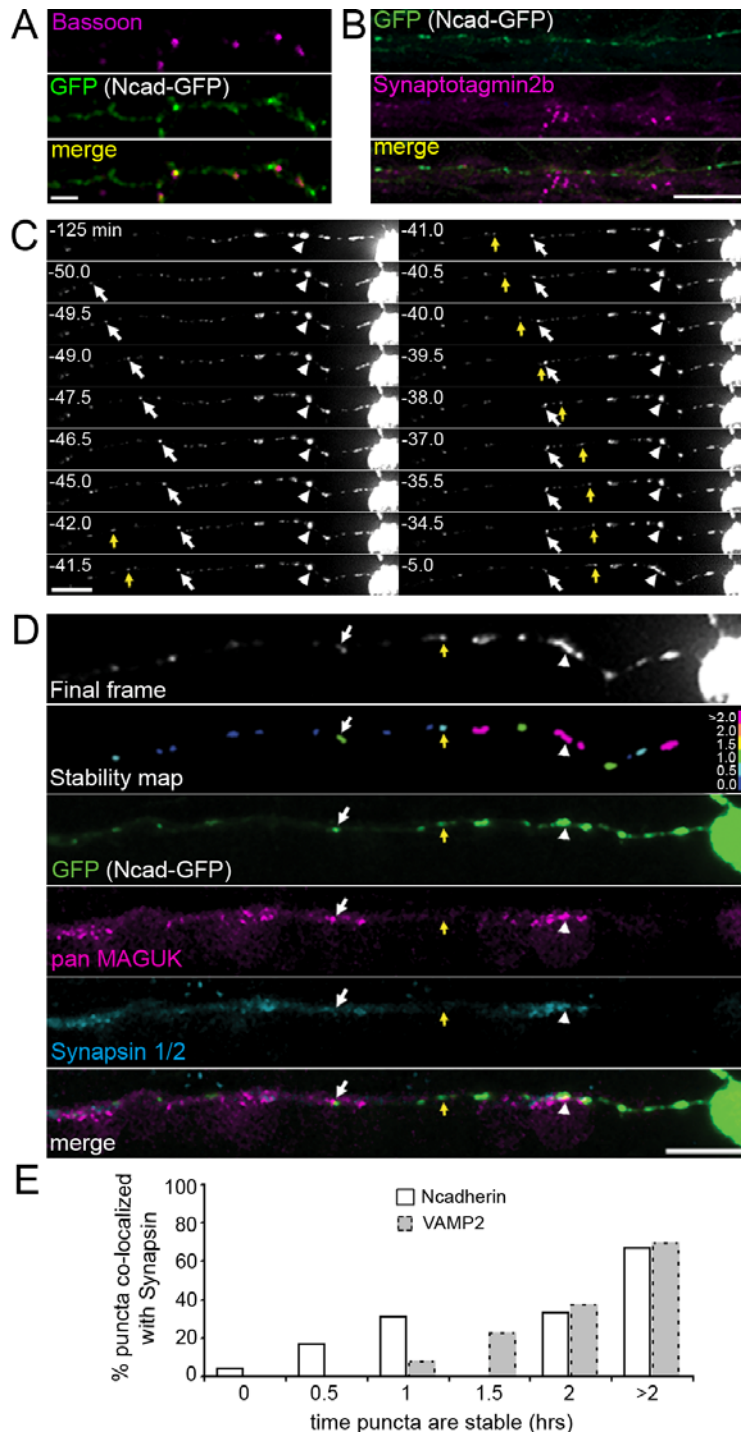


Figure 7. Ncadherin recruitment precedes Synapsin. (A) IF for bassoon on Ncad-GFP transfected rat hippocampal neurons shows that the majority of Bassoon puncta colocalize with Ncad-GFP puncta. (B) IF for Synaptotagmin2b colocalized with only a small percentage of Ncad-GFP puncta in RB axons. (C) Selected frames from a 2 hour time-lapse movie (from 24-26 hpf) of Ncad-GFP expression in an RB cell. Some puncta were paused for the entire imaging period (arrowhead), while others paused during imaging (arrow). Scale bar, 10 μ m. (D) Post-imaging IF labeling demonstrates the presence of Synapsin 1/2 (cyan) and MAGUKs (magenta) at an Ncadherin-GFP (green) punctum that was paused for the entire imaging period (arrowhead) and for 34.5 min preceding the end of imaging (arrow), but not at a punctum that was paused for only 29.5 min preceding the final frame (yellow arrow). A stability map (with bins as described in Figure 5) reports the time each puncta was paused preceding the end of imaging. Scale bar, 10 μ m. (E) A stability histogram quantifying the percentage of Synapsin 1/2 puncta that colocalized with Ncadherin-GFP (white bars) reveals that recruitment of Ncadherin precedes Synapsin by 37.6 min (\pm 8.0 min). Gray bars show data for VAMP2-mKate2 from histogram in Figure 6C to emphasize the difference in the time delay with which Synapsin colocalization is first seen. Bins were as described for Figure 5. n = 6 RB axon segments analyzed.

Synapsin1 is transported in axons independently of STVs and PTVs

Although previous studies have suggested that Synapsin is trafficked to synapses with STVs (Ahmari et al., 2000) or PTVs (Tao-Cheng, 2007), our data suggest that Synapsin arrives at synapses independently of STVs and PTVs, and with a delay. To answer the question of how Synapsin is transported in RB axons, we imaged fluorescently tagged Synapsin in RBs co-expressed with either our STV or PTV marker constructs, VAMP2-mKate2 and Ncadherin-GFP, respectively. Our *in situ* hybridization experiments (Figure 4A) revealed that all three *synapsin* genes (1, 2a, and 2b) were expressed in RB cells, with *synapsin1* showing the strongest expression. Thus, we chose to examine the trafficking of Synapsin1 in RB axons.

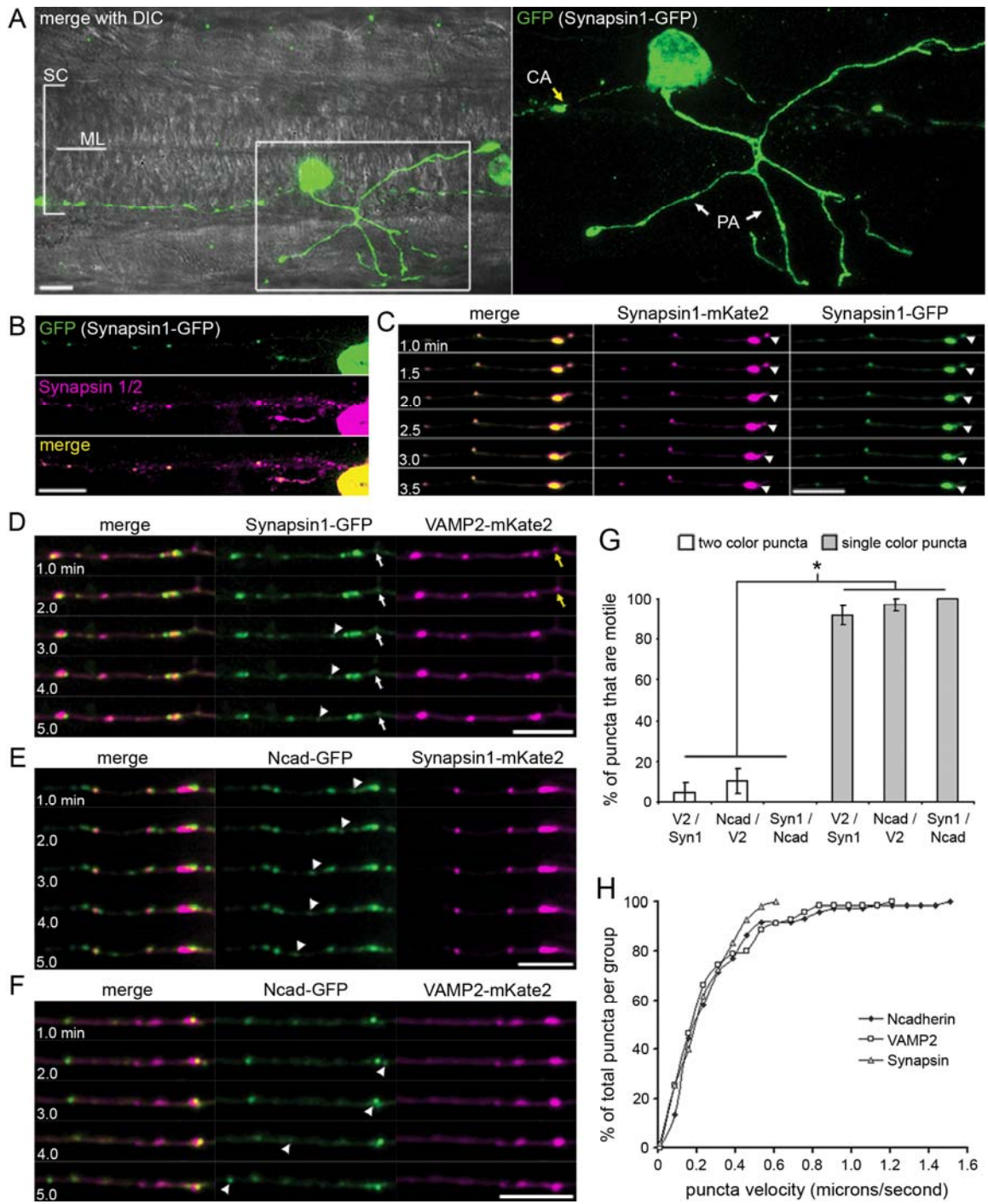


Figure 8. Synapsin1, STVs, and PTVs are transported independently of each other.

(A) Synapsin1-GFP in an RB neuron in the zebrafish spinal cord at 25 hpf. Left panel: Dorsal view of IF labeling of GFP overlaid with a brightfield image. The midline (ML) and extent of the spinal cord (SC) are indicated. Right panel: enlargement of IF outlined in box showing Synapsin1-GFP. PA: peripheral arbor, CA: central axon. Scale bar, 10 μ m. (B) Synapsin1-GFP was localized with a similar distribution as endogenous Synapsin 1/2 in RB axons in the zebrafish spinal cord. (C) Selected sequence of 6 frames, 30 seconds apart, from a 30 minute movie. Arrowheads highlight puncta labeled with both Synapsin1-GFP and Synapsin1-mKate2 moving together. (D-F) Selected sequence of 5 frames, 1 min apart, from 30 min time-lapse movies showing differential transport of Synapsin1-GFP and VAMP2-mKate2 (D) Synapsin1-mKate2 and Ncadherin-GFP (E) and Ncadherin-GFP and VAMP2-mKate2 (F) in RB axons. Movies acquired between 24-26 hpf. Arrows and arrowheads highlight puncta positive for only one of the two fluorescent fusion proteins that are transported independently of the other. Yellow arrow (D) denotes a punctum that is initially paused with another color puncta. Scale bars, 10 μ m. (G) Histogram showing the number of two color puncta vs. single color puncta that are motile over a 30 minute imaging period. Two color puncta are those labeled for both transport packet markers imaged in a given pair, single color puncta are those expressing only one of the two markers. Error bars show s.e.m. * $p < 0.005$. (H) Cumulative plot showing percentage of each type of puncta (Ncadherin, VAMP2, Synapsin) moving at each velocity. The maximum velocity measured for a Synapsin1 puncta was 2.49 and 1.98 fold slower than the maximum velocity for an Ncadherin or a VAMP2 puncta, respectively.

Zebrafish Synapsin1 was expressed as a fusion with either mKate2 or GFP in RB cells (Figure 8A). We found that Synapsin1-GFP and Synapsin1-mKate2 both trafficked anterogradely and retrogradely in RB axons as puncta (data not shown). Immunolabeling of Synapsin1-GFP expressing embryos with Synapsin 1/2 antibody showed 100% colocalization (100%, $n = 3$ embryos; Figure 8B), suggesting that fluorescently-tagged Synapsin1 behaves like the endogenous protein. In addition, to ensure that the mKate2 and GFP tags do not alter the transport of Synapsin1, RB axons coexpressing Synapsin1-mKate2 and Synapsin1-GFP were imaged. The two tagged versions of Synapsin were seen to move together all the time (Figure 8C).

Next, we expressed all chromatically-distinct combinations of VAMP2-mKate2, Ncadherin-GFP, Synapsin1-GFP and Synapsin1-mKate2. When RBs expressing Synapsin1-GFP and VAMP2-mKate2 were imaged, we found that the two were transported independently (Figure 8D, G). Puncta expressing only one of the fluorescently-tagged markers could be seen moving along the axon (arrowheads Figure 8D-F). Immobile puncta were often observed where both VAMP2 and Synapsin1 were colocalized, however, in many instances ($n = 14$), one of the two fusion proteins moved away while the other stayed stable (white and yellow arrows Figure 8D). Many puncta expressed both VAMP2-mKate2 and Synapsin1-GFP, but the majority of these puncta ($95.0 \pm 4.9\%$) were paused (Figure 8D, G). This same pattern was seen with the other pairs of presynaptic markers. Ncad-GFP and Synapsin1-mKate2 never trafficked together, and Ncad-GFP and VAMP2-mKate2 rarely did ($10.4\% \pm 6.1\%$, $n = 58$ puncta; arrows Figure 8D-F).

We then examined the percentages of puncta that were mobile during a 30 minute imaging session. We separated puncta that were positive for only one marker or that contained two presynaptic marker proteins. For each of the singly-labeled presynaptic markers, on average 96.2% of the puncta observed during an imaging session were mobile, while very few two-color puncta moved (Figure 8G).

Finally, we examined the dynamics of puncta movement. The instantaneous velocities of Ncad-GFP, VAMP2-mKate2, and Synapsin1-GFP displayed a wide range as seen in the cumulative percentage plot (from 0.01– 1.44 $\mu\text{m}/\text{sec}$; Figure 8H). However, the maximal velocities of Synapsin1-GFP puncta were significantly below those of Ncad-GFP or VAMP2-mKate2 puncta. Synapsin1-GFP puncta did not move faster than 0.57

$\mu\text{m}/\text{sec}$, whereas more than 8% of VAMP2 and Ncad puncta moved with higher velocities (VAMP2 = 8.4%, Ncad = 8.1%; Figure 8H), reaching 1.14 and 1.44 $\mu\text{m}/\text{sec}$, respectively. This result suggests that Synapsin may be transported by motor proteins distinct from those used by STVs and PTVs. Together with the analysis of co-movement (Figure 8G), our data demonstrate that PTVs, STVs and Synapsin are all transported independently to synapses.

DISCUSSION

In the current study, we have made two important advances in understanding the recruitment of presynaptic transport packets to nascent synapses. We have shown that there is a distinct order of recruitment of presynaptic transport packets to a nascent synapse and that Synapsin1 is transported to nascent synapses separately from STVs and PTVs. Using the RB-CoPA synapse in zebrafish spinal cord as a model glutamatergic synapse (Figure 1, 2), we first showed that immunofluorescence labeling revealed a time delay between the recruitment of STV proteins and Synapsin to presynaptic terminals (Figure 3). This delay was confirmed by time-lapse imaging and post-imaging IF (Figure 6). We next showed that the PTV marker Ncadherin was recruited to presynaptic terminals with a delay as compared to STVs, but before Synapsin (Figure 7), demonstrating a sequential recruitment of three distinct presynaptic components.

Our time-lapse imaging experiments with Synapsin1-GFP demonstrated that this SV-associated protein is trafficked independently of STVs and PTVs (Figure 8). This is surprising for two reasons: (1) Synapsin is tightly associated with SVs at mature synapses (Huttner et al., 1983), suggesting that Synapsin would also be transported by STVs

during synapse formation; (2) if Synapsin were not transported with STVs, it would be expected that this cytosolic protein might diffuse and then aggregate at synapses much like PSD-95 (Bresler et al., 2001; Barrow et al., 2009). Our studies instead suggest that Synapsins are associated either with a distinct vesicular transport organelle or with a complex of cytosolic proteins which is transported along microtubules.

The importance of understanding how Synapsin gets to nascent presynaptic terminals is underscored by a recent observation from array tomography experiments that Synapsin1 is present at >99% of cortical synapses (Micheva et al., 2010). Thus, Synapsin is clearly a fundamental component of almost all synapses, though synapses can form in its absence (Chin et al., 1995). Synapsin plays a role in synaptogenesis, as Synapsin1 deficient neurons in culture show a reduced number of synapses for the first 10 days *in vitro* (Chin et al., 1995). It is possible that Synapsin plays a signaling role that is temporally controlled, requiring its later arrival at the presynaptic terminal to enable a synaptic maturation step. Our data demonstrate a second recruitment of STVs to presynaptic terminals at least 30 min after the initial STV localization (Figure 5C, E), a step that might be regulated by Synapsin.

Previous studies of the transport of presynaptic components to new synapses have remained contradictory. Two reports suggest that all of the proteins necessary to form a presynaptic terminal, including STV proteins, PTV proteins, and Synapsin are co-transported (Ahmari et al., 2000; Tao-Cheng, 2007). On the other hand, immunisolated PTVs contain active zone proteins such as piccolo, bassoon, cadherin, SNAP-25 and calcium channel subunit $\alpha 1$, but not VAMP2 or other SV proteins such as Synaptotagmin and Synaptophysin (Zhai et al., 2001; Shapira et al., 2003). It is entirely possible that at

certain times during transport, all three transport packets, STVs, PTVs and Synapsin transport packets, pause at common sites along the axon (Sabo et al., 2006; Bury and Sabo, 2011). This would explain the colocalization of a wide variety of presynaptic proteins in post imaging IF and immuno-EM studies (Ahmari et al., 2000; Tao-Cheng, 2007). Indeed, in our live imaging studies it was common to see STVs, PTVs and Synapsin1 colocalized when paused (Figure 8D-G).

In our experiments, Synapsin did not reach maximal velocities similar to those measured for STVs and PTVs, suggesting it may be transported by distinct motor proteins. However, the transport properties of STVs and PTVs were indistinguishable (Figure 8). This is in line with similar studies also performed in RB cells using Ncadherin and VAMP fusion proteins (Jontes et al., 2004). However in that study, Ncad-GFP and VAMP-GFP puncta were deposited in RB axons in the wake of an extending growth cone with the same kinetics, suggesting a similar time line for the recruitment of the proteins to synapses (Jontes et al., 2004). Since the postsynaptic component was not identified in these experiments, it is possible that these depositions were just paused, an occurrence that was frequently observed in our current study. This presynaptic precursor material may be deposited behind the advancing growth cone at predefined sites along the axon such as those described by Sabo et. al. (Sabo et al., 2006). From these sites, STVs and PTVs could then be recruited to developing synapses.

Two recent studies have begun to examine the question of how these three presynaptic components traffic *in vitro*. Work by Bury and Sabo suggests that a significant fraction of STVs and PTVs co-transport along axons of neurons in culture (Bury and Sabo, 2011). While we see that our STV and PTV markers can co-transport,

we find that the great majority of the time, STVs and PTVs traffic separately *in vivo* in zebrafish (Figure 8G). Our studies are supported by the fact that they also find that STVs and PTVs co-pause at the same sites, however Bury and Sabo did not examine the order of recruitment to synaptic sites. Another study, by Scott et al (2011), suggests that Synapsin can traffic along axons either slowly as part of molecular motor driven cytosolic protein aggregates, or quickly by associating with transport packets carrying the SV associated protein Synaptophysin. However, the slow cytosolic transport of Synapsin in cultured hippocampal neurons was diffuse and not clearly punctate and was much slower than that which we observed (Scott et al., 2011). While it is unclear what proportion of Synapsin clusters are co-transported with Synaptophysin (Scott et al., 2011), it will be interesting to determine whether this is simply a very rare event that we did not observe in our studies, or whether this represents an actual difference in methods of transport between cultured neurons and sensory neurons *in vivo*.

In this study we found that STVs are recruited to sites of developing synapses significantly before other presynaptic components. This leads to the intriguing question of why STVs would be needed at a presynaptic site before structural active zone components arrive. Although many reasons can be imagined, there are two possibilities that seem likely: 1) signaling by an SV component could be required to recruit PTVs and 2) low levels of fusion and release of SV contents at presynaptic sites could be important for recruitment of postsynaptic proteins. STVs cycle with the plasma membrane at low rates during transport pauses (Sabo et al., 2006), and therefore could also release glutamate, or other signaling molecules such as BDNF, as soon as they arrive at a nascent presynaptic site. This release may then help influence development of the synapse by

paracrine or trans-synaptic mechanisms (Maletic-Savatic et al., 1999; Demarque et al., 2002; Lohmann et al., 2002; Kwon and Sabatini, 2011).

The ordered arrival of synaptic components observed in this study suggests that a single triggering event could be sufficient to recruit all presynaptic components through a recruitment cascade. This would allow for a parsimonious signaling model in which a single event at the nascent synapse initiates the cascade. Binding, for example, of a synaptic adhesion molecule to its postsynaptic partner could recruit STVs, which could in turn recruit PTVs, which could then stabilize Synapsin. Indeed, SVs can be linked directly to active zone components through numerous interactions including through the protein RIM. Deletion of RIM decreases the SV readily releasable pool and the density of Ca channels (Han et al., 2011). Additionally, the PTV protein Piccolo can regulate the stabilization of Synapsin at presynaptic terminals through a calcium-calmodulin kinase II-dependent mechanism (Leal-Ortiz et al., 2008). It will be interesting to test our transport cascade model by preventing the biogenesis or transport of one of these transport packet types and then examining the effect on recruitment of one of the downstream transport packets.

EXPEREMENTAL PROCEDURES

Analysis of zebrafish *synapsin* genes

To obtain transcripts for the coding sequences for zebrafish *synapsins*, predicted sequences were identified using the Ensemble Genome browser (www.ensembl.org/index.html). 3 predicted *synapsin* gene transcripts were identified. An alignment was made with ClustalW2 (www.ebi.ac.uk/Tools/msa/clustalw2/) using a

Gonnet protein weight matrix and default alignment parameters (data not shown). Percent identity between mouse and zebrafish *synapsins* was calculated for the actin binding region using Jalview (www.jalview.org/help.html; data not shown; Waterhouse et al., 2009). To confirm that sequence identities were correctly assigned, we examined zebrafish, human, mouse and pufferfish chromosomes for syntenic regions surrounding the *synapsin* gene locations (Catchen et al., 2009; teleost.cs.uoregon.edu/acos/syteny_db/). Based on these analyses, we conclude that zebrafish possess one ortholog of mammalian Synapsin1, two orthologs of the mammalian Synapsin2 gene and no ortholog of Synapsin3. We call the two *synapsin2* orthologs *synapsin2a* and *synapsin2b*, based on existing annotation in the zebrafish genome assembly (Zv9).

Image clones of both *synapsin2a* and *2b* (Open Biosystems; *synapsin2a*: NM_001002597.1; *synapsin2b*: NM_001037576.1) were obtained to make in situ probes. A predicted coding sequence for *synapsin1* (NM_001126437) was used to design primers to amplify that sequence from 24hpf cDNA, made using the Superscript III first strand synthesis system for RT-PCR (Invitrogen, Carlsbad, CA). This PCR fragment was subcloned into the Zero Blunt TOPO cloning vector (Invitrogen).

DNA constructs

UAS:Synapsin1-GFP was constructed by inserting the *synapsin1* coding sequence into UAS:GFP by PCR using primers incorporating 5' EcoRI and 3' PstI restriction sites. UAS:GFP was generated by inserting a 10X UAS sequence, 1Eb minimal promoter, carp beta-actin transcriptional start, coding sequence for eGFP and a polyA site into a cloning

vector. UAS:Synapsin1-mKate2 was made by inserting the *synapsin1* coding sequence into UAS:mKate2 (a derivative of the UAS:GFP vector made by substituting the eGFP coding sequence for the red fluorescent protein mKate2 (Shcherbo et al., 2009) by PCR, incorporating 5' EcoRI, 3' PstI and the myc epitope tag sequence. mKate2 was chosen for these experiments due to its high fluorescence quantum yield and photostability (Shcherbo et al., 2009). Control experiments to determine that mKate2 did not adversely affect localization or trafficking of fusion proteins were performed by comparing the localization of mKate2 to GFP (data not shown).

Zebrafish VAMP2 coding sequence was identified using ensemble and cloned as described for *synapsin1* (NM_200005.1). UAS:VAMP2-myc-mKate2 (VAMP2-mKate2) was constructed by inserting the VAMP2 coding sequence into UAS:mKate2 as described above. The UAS:Ncadherin-GFP construct was a gift from Dr. James Jontes (Ohio State University, Columbus, OH). Islet1 coding sequence was obtained from pBS SK FL-islet1 plasmid (a gift from Dr. Judith Eisen, University of Oregon, Eugene, OR). The neuronal beta-tubulin (NBT):Tau-GFP expression construct was a gift from Dr. Steve Goldman (University of Rochester Medical Center, New York). All cloning steps were confirmed by sequencing.

Zebrafish husbandry

All zebrafish embryos, larvae, and adults were raised and maintained at 28.5°C according to standard protocols (Westerfield, 2000). Lines used include AB/Tübingen, *neurogenin1:GFP (Tg(-3.1ngn1:GFP)sb2)*, *narrowminded (nrd^{m805})*; provided by Dr. Kristin Artinger, University of Colorado, Denver), *s1102t:GAL4/UAS:Kaede [Et(-*

1.5hsp70l:Gal4-VP16; *s1102t*; *Tg(UAS-E1b:Kaede)*; *s1999t*; provided by Dr. Herwig Baier, University of California, San Francisco]. *s1102t:GAL4* embryos were obtained by outcrossing *s1102t:GAL4/UAS:Kaede* to AB/Tübingen and PCR genotyping DNA obtained from fin clips using primers specific for the GAL4 cassette and the UAS:Kaede cassette. DNA was pressure injected into 1-2 cell zebrafish embryos using a MPPI-2 pressure injector (ASI, Eugene, OR). DNA constructs were injected into the yolk singly or in combination at concentrations of 20-30ng/μl each and embryos were screened for GFP or mKate2 expression the following day. Embryos were staged according to (Kimmel et al., 1995).

Imaging

Embryos used for live imaging were dechorionated, then anesthetized in 0.003% tricaine in embryo medium (EM). Embryos were then mounted in 1.5% low melt agarose/EM. Dishes were flooded with EM plus 0.003% tricaine and the embryos were imaged at room temperature on a spinning disk microscope (McBain Instruments, Simi Valley, Ca) using a Leica 63x oil objective (1.40NA). For time lapse experiments with single fluorescent constructs, images were captured at 30 second intervals over 0.5 μm steps through the z depth traversed by the axon (from ~5-10 μm) over a 2 hour imaging period. For two-color imaging, embryos were live imaged for 30 to 60 minutes with z-stacks acquired with 0.5 μm steps through the depth traversed by the axon at 30 – 60 second intervals. Stacks were generated by obtaining images for each wavelength sequentially at each z-plane. This was a slower acquisition method than capturing all z-planes for one channel followed by all z-planes for a second channel, but allowed us to be

confident that any differences in movement of the two colors of puncta was due to differences in transport. All live imaging data was acquired using Volocity software and a Hamamatsu EMCCD camera. All IF was imaged on an inverted Nikon TU-2000 microscope with an EZ-C1 confocal system (Nikon) with either a 40x objective (0.95 NA) or a 100x oil-immersion objective (1.45 NA). Image stacks through the depth of the dlf (~10-15 microns) were acquired to capture synaptic puncta at all points of contact between RB axons and CoPAs unless otherwise noted. Images were acquired for each channel separately.

Immunofluorescence labeling

Immunofluorescence (IF) labeling was performed with the following primary antibodies and dilutions: mouse anti-panMAGUK (1:100 ; NeuroMab, Davis, CA), rabbit anti-Synapsin 1/2 (1:1000: Synaptic Systems, Goettingen, Germany) and rabbit anti-Piccolo (1:300; Synaptic Systems), chicken anti-c-myc (1:125; Aves, Tigard, Oregon), chicken anti-GFP (; 1:500; Abcam, Cambridge, MA), mouse anti-con-1 (1:150; gift from Dr. John Kuwada, University of Michigan, Ann Arbor), mouse anti-Synaptotagmin2b (znp-1; 1:750; Developmental Studies Hybridoma Bank, University of Iowa), and SV2 (1:1000 dilution; Developmental Studies Hybridoma Bank, University of Iowa), islet-1 (stock 39.4D, 1:200 dilution, Developmental Studies Hybridoma Bank, University of Iowa). Secondary antibodies used were: anti-Chicken Alexa 488, anti-chicken Alexa 546, anti-rabbit Alexa 546, anti-rabbit Alexa 633 (Molecular Probes) and anti-mouse Cy2, anti-mouse Cy3, (Jackson Immuno, West Grove, PA). For IF after live imaging, embryos were transferred from EM with 0.003% tricaine to fixative within 5 minutes of the

completion of live imaging. Please contact the authors for full whole-mount IF protocols. IF for endogenous Bassoon on cortical neurons was carried out as described in (Hoy et al., 2009) on 5 DIV neuron cultures. Anti-Bassoon (Enzo Life Sciences, Plymouth Meeting PA) was used at a 1:400 dilution.

Analysis

Analysis of imaging data was performed on maximum intensity projections for all fixed and live movies. Synaptic puncta were selected and counted using Image Pro Plus software (Figure 3, Figure 7; Media Cybernetics, Bethesda, MD) as described previously (Washbourne et al., 2002) but with one modification: background plus one standard deviation was subtracted from puncta fluorescence intensities prior to puncta selection. Background was calculated as the average intensity at points adjacent to the dlf. Puncta were counted as co-localized if they had at least one pixel overlap. Co-localization of puncta was verified in all cases by checking original z-stacks. Stability maps were generated by identifying paused puncta in kymographs made in Image J (Figure 5-7; rsb.info.nih.gov/ij/; Rasband, 1997-2011). Pausing was defined as movement of less than one puncta diameter between frames. Total fluorescence intensity (Figure 5C) was measured using Volocity software by summing the intensities at each pixel composing a punctum. Intensity data were normalized between images by subtracting a background value equal to the average background for a given image multiplied by the total number of pixels in a puncta. Velocities of puncta from live imaging experiments (Figure 8) were calculated from the beginning to the end of a movement for puncta that moved unidirectionally over at least 2 μm and for at least 3 frames using Image Pro Plus

software (Media Cybernetics). Prior to measuring puncta velocities, image stacks were aligned (to account for drift due to growth of the embryos during the imaging session) using the Stack Reg plugin for Image J (bigwww.epfl.ch/thevenaz/stackreg/; Thevenaz et al., 1998). Images were processed for presentation in Adobe Photoshop. Micrographs were prepared by using the despeckle filter and adjusting the levels to allow for good contrast upon printing. In the right hand panel of Figure 4A and 7A a mask was used over the RB cell body to prevent loss of detail when levels were adjusted to allow the RB processes to be clearly seen. All graphs were prepared in Microsoft Excel, and statistics were analyzed using an unpaired 2-tailed Students t-test.

***In situ* hybridization**

ISH was carried out and RNA probes were made according to the methods described by (Pietri et al., 2008). Briefly, embryos were hybridized with digoxigenin (DIG) and fluorescein labeled probes in 50% formamide hybridization buffer at 68°C over night. Antibodies to DIG and fluorescein conjugated to alkaline phosphatase (Roche, Mannheim, Germany) were used and detected with NBT/BCIP or INT/BCIP. Sense and antisense probe templates were in vitro transcribed from PCR fragments of *synapsin1a*, *1b* or *2b* linked to a T7 or T3 promoter sequence. *synapsin1a* probes cover nucleotides (nt) 1467 to 1872 of the coding sequence (CDS; NM_001126437.2), nt 1480 to 1883 of CDS for *synapsin2a* (NM_001002597.1), and the 157 nt preceding the start codon plus the first 250 nt of the CDS for *synapsin2b* (NM_001037576.1). DIG and fluorescein labeled probes were made according to manufacturer's protocol (Roche). Images were taken on a Zeiss Axioplan microscope using an Axiocam MRc5.

Electron microscopy

Zebrafish embryos at 25 and 28 hpf were anesthetized with 0.003% tricaine and then fixed and processed for EM essentially as described previously (Jontes et al., 2000). 70nm silver thin sections were placed on 200 mesh hexagonal copper grids and examined unstained in a JEOL 100 CX electron microscope at 80kV. Images were taken using a CCD digital camera system (XR-100 from AMT, Danvers, MA, USA). Please contact the authors for the full EM protocol.

CHAPTER III

SIX *CADM/SYNCAM* GENES ARE EXPRESSED IN THE NERVOUS SYSTEM OF DEVELOPING ZEBRAFISH

This work was previously published in Volume 237 of the journal *Developmental Dynamics* in January of 2008. I share first authorship with T. Petri. We performed the majority of the experiments and data analysis. P. Washbourne assisted with the data analysis. C. Wilson performed the radiation hybrid mapping experiments. The manuscript was written and edited by T. Pietri, P. Washbourne, and me.

INTRODUCTION

The Cadms (Cell Adhesion Molecules) are a family of type I transmembrane proteins that have been described in a number of pathological and physiological processes such as the progression of lung and other cancers (reviewed in Murakami, 2005), mast cell adhesion (Ito et al., 2003; Furuno et al., 2005; Ito and Oonuma, 2006; Ito et al., 2007b), spermatogenesis (Wakayama et al., 2001; Wakayama et al., 2003; Fujita et al., 2006; van der Weyden et al., 2006; Yamada et al., 2006), epithelium development and homeostasis (Ito et al., 2007b), and central nervous system development (Biederer et al., 2002; Sara et al., 2005; Spiegel et al., 2007).

Cadms have been independently identified in various model systems, thus these genes and the proteins they encode have acquired several different names, such as *Necl* (Nectinlike molecules), *Igsf4* (Ig-like spermatogenic factor), *TSLC* (tumor suppressor in lung cancer) and *SynCAM* (synaptic cell adhesion molecule; Table 1). Recently, the

Human Genome Organization (HUGO) Gene Nomenclature Committee renamed the genes *CADM* (Table 1). So far, four *Cadm* genes have been identified in tetrapod vertebrates and the proteins they encode show a strict conservation of their structural organization. *Cadm* proteins are composed of three extracellular Ig-like loop domains, a transmembrane domain and a highly conserved short cytoplasmic tail containing two known protein-protein interaction domains, namely a juxtamembrane protein 4.1 binding motif and a C-terminus type II PDZ-binding domain (Fig. 1A; Biederer, 2006). Interestingly, genes with this protein structure are only found in vertebrates and appear to be an innovation of this phylum (Biederer, 2006).

Table 1. Nomenclature of the *Cadm* Gene Family

Human gene name	<i>CADM1</i>	<i>CADM2</i>	<i>CADM3</i>	<i>CADM4</i>
Mouse gene name	<i>Cadm1</i>	<i>Cadm2</i>	<i>Cadm3</i>	<i>Cadm4</i>
Zebrafish gene name	<i>cadm1</i>	<i>cadm2</i>	<i>cadm3</i>	<i>cadm4</i>
Alternate gene and protein names	Nec12	Nec13	Nec11	Nec14
	SynCAM1	SynCAM2	SynCAM3	SynCAM4
	IGSF4A	IGSF4D	IGSF4B	IGSF4C
	Tslc1		Tsl11	
	sgIGSF RA175			

The human and mouse gene names were recently changed from IGSF4 to CADM by the HUGO gene nomenclature committee. We have adopted this nomenclature. Previous names given to these genes and proteins are shown at the bottom. GenBank ID numbers for the novel zebrafish *cadm* genes and isoforms are: *cadm1a*, EU182349, EU182350, EU182351; *cadm1b*, EU182352; *cadm2b*, EU182353; *cadm3*, EU182354.

The extracellular Ig-like domains of Cadm proteins can mediate both hetero- and homophilic interactions that are Ca²⁺ and Mg²⁺-independent. To date, in addition to various combinations of Cadm to Cadm interactions (Takai et al., 2003; Maurel et al., 2007), two types of heterophilic binding partners have been identified, the nectins and class I-restricted T-cell-associated molecules (CRTAM). Furthermore, the intracellular tails of the Cadms have been shown to interact with a number of scaffolding molecules in various *in vitro* systems. These include CASK (Biederer et al., 2002), syntenin (Biederer et al., 2002; Meyer et al., 2004), GRIP (Meyer et al., 2004), MPP3 (ortholog of the *Drosophila* tumor suppressor gene Dlg ; Fukuhara et al., 2003) and DAL-1 (Yageta et al., 2002). However, very little is known about how these interactions relate to the functions of the Cadms during development.

Extensive analyses have revealed that *Cadm1* is expressed during early development in rodents (Fujita et al., 2005; Ohta et al., 2005). It has been found in most epithelia and neuroepithelia, such as hair follicles, lung, liver, gut, tongue, olfactory epithelium, dorsal root ganglia, various regions of the central nervous system, being particularly enriched in the marginal zone of the cortex, the external granule layer of the cerebellum, the habenular nucleus and the thalamus (Fujita et al., 2005; Ohta et al., 2005). Additionally, *Cadm1* has been shown to be highly expressed in the testis, during germ cell development.

Of interest, inactivation of the *Cadm1* gene in mice produces infertile males (oligoastheno-teratozoospermia; Fujita et al., 2006). Infertility is probably caused by a delay in the maturation of sperm cells, leading to an increase in apoptosis. The deficit in sperm cell maturation is due to an alteration of the adhesion between spermatogenic cells

and the Sertoli cells (Wakayama et al., 2003; Fujita et al., 2006; van der Weyden et al., 2006; Yamada et al., 2006).

Given the widespread expression of *Cadm1*, it is interesting to note that no other deficits have been detected in *Cadm1* knock-out mice (Fujita et al., 2006), revealing probable compensation mechanisms in other tissues. Nonetheless, *in vitro* studies have determined several functions for *Cadm1* in the nervous system. *Cadm1* is expressed during the period of synaptogenesis and localizes to pre- and post-synaptic sites in the rodent brain. Its overexpression in cultured neurons increases spontaneous synaptic activity (Biederer et al., 2002; Sara et al., 2005). Moreover, the expression of recombinant *Cadm1* in nonneuronal cells co-cultured with neurons induces the formation of functional pre-synaptic terminals onto the non-neuronal cells. *Cadm1* may therefore act as a synaptogenic molecule during nervous system development (Biederer et al., 2002; Sara et al., 2005).

In addition to promoting neuron to neuron interactions, *Cadm1* also promotes a homophilic adhesion link between neurons and mast cells. This interaction grants *Cadm1* the ability to modulate the immune system by enhancing mast cell response to nerve activation (Ito et al., 2003; Furuno et al., 2005; Ito and Oonuma, 2006; Ito et al., 2007a). Another function of *Cadm1* in the immune system includes immunosurveillance. Loss of *Cadm1* may provide an escape mechanism from detection by natural killer (NK) cells and cytotoxic T cells, which express CRTAM (Murakami, 2005). Also, cell adhesion through *Cadms* appears necessary to promote tumor suppression. For instance, absence of *CADMI* expression and mutated forms of *CADMI* in carcinoma have been found to

enhance malignancy, through destabilization of cell-cell contacts (Fuchs and Colonna, 2006).

In contrast to *Cadm1*, *Cadm3* and *Cadm4* expression seems to be mostly restricted to neurons and glial cells (astrocytes, oligodendrocytes, and Schwann cells; Maurel et al., 2007; Spiegel et al., 2007). Recently, it has been proposed that a heterophilic interaction between *Cadm3* and *Cadm4* mediates Schwann cell adhesion to peripheral axons. Perturbation with dominant negative forms of either *Cadm3* or *Cadm4* or knockdown of their expression blocks the myelination process (Maurel et al., 2007; Spiegel et al., 2007). Expression patterns and function of *Cadm2* have not been reported to date.

As a prerequisite to better understanding the function and mechanism of all the *Cadm* genes during development, we have isolated orthologs of the tetrapod *Cadm* genes from the zebrafish (*Danio rerio*). We have characterized their pattern of expression during development and in the adult.

RESULTS AND DISCUSSION

Isolation and characterization of the *cadm* genes from zebrafish

In tetrapods, four distinct *Cadm* gene family members have been identified to date (Biederer, 2006). By searching the zebrafish genome database (http://www.ensembl.org/Danio_rerio) using mammalian family members as a template, we have identified six orthologs in zebrafish. In accordance with the HUGO Gene Nomenclature Committee and the nomenclature guidelines proposed by the Zebrafish Model Organism Database (www.zfin.org), we will call these genes *cadm* (Table 1).

By using a combination of reverse transcriptase (RT)-PCR and 5' rapid amplification of cDNA ends (RACE)-PCR, we have identified the coding sequences for the six *cadm* genes. This indicates that all six genes are expressed in zebrafish. The coding sequences show the same protein domain organization that characterizes the tetrapod *Cadm* family: a signal peptide followed by three immunoglobulin domains in the extracellular portions of the proteins, a transmembrane domain and a short cytoplasmic tail which encompass a juxtamembrane 4.1B binding domain and a C-terminal PDZ type II binding domain (Fig. 1A, C).

Alignment of the protein sequences of the six *cadm* genes (Fig. 1B, C) and comparison with tetrapod species (Fig. 2B, Supplementary Fig.1 available online at <http://onlinelibrary.wiley.com/doi/10.1002/dvdy.21397/supinfo>; data not shown) revealed that two genes are very similar to mouse *Cadm1*, whereas two other genes are very similar to mouse *Cadm2*. Given that the ancestor of teleost fish underwent a genome duplication prior to branching off from the tetrapod lineage during evolution (Postlethwait et al., 2004), we hypothesized that the genes similar to mouse *Cadm1* and 2 are co-orthologs. We have named these: *cadm1a* and *cadm1b*, and *cadm2a* and *cadm2b*. The respective co-ortholog protein sequences share higher homology between each other (80.6% and 74.1% identity for *cadm1* and 2 genes, respectively, Fig. 1B) than with any other *cadm* genes (42.2% average identity in pairwise comparison).

Analysis of conserved synteny between phyla can provide evidence of orthology and is necessary to determine whether genes are duplicates arising from a genome duplication (Postlethwait et al., 2004). Radiation hybrid mapping determined that *cadm1a*, *1b*, *2a*, *2b*, *3* and *4* map to linkage groups 21, 16, 2, 15, 10, and 15, respectively.

Since some of these locations differ from the assigned chromosomal locations in the latest zebrafish genome assembly (Zv7), we have compared the scaffolds containing the zebrafish *cadm* genes with the chromosomal region surrounding the murine *Cadm* genes. This analysis demonstrates that the neighboring genes of the zebrafish co-orthologs of *Cadm1* are also found flanking the murine gene. In fact, three orthologous genes are found in all three chromosomal regions: *jam3*, *igsf9b* and *grit* (Supplementary Fig. 2 data online; data not shown). This confirms that *cadm1a* and *1b* are derived from a duplication of the ancestral chromosomal region (Postlethwait et al., 2004).

Similar analyses revealed conserved synteny between zebrafish and murine *Cadm3* and *4* genes (not shown). However, comparison of syntenic regions for *cadm2a* and *2b* was not possible due to the paucity of neighboring genes. Further supporting the conclusion that *cadm1a*, *1b*, *2a* and *2b* arose from the teleost genome duplication, all *cadm* genes share the same gene structures as the respective mouse ortholog (Fig. 3). No duplicates have been found to date for *cadm3* and *4*. Since no duplicates have been found for these genes in other bony fish, we conclude that, subsequent to the genome duplication within the teleost lineage, these gene duplicates were probably lost.

Alignment of the six zebrafish *Cadm* protein sequences (Fig. 1B,C) reveals that the *Cadm2* protein sequences are more closely related to *Cadm3* (49.5% average identity) than to *Cadm1* and *4* (45.9% and 35.2% average identity, respectively). *Cadm4* is a more distant member of the family, with an average amino acid identity of 37.1%. The phylogenetic comparison between, human, mouse, toad and zebrafish sequences confirms this relationship of zebrafish *Cadm* proteins (Fig. 2A).

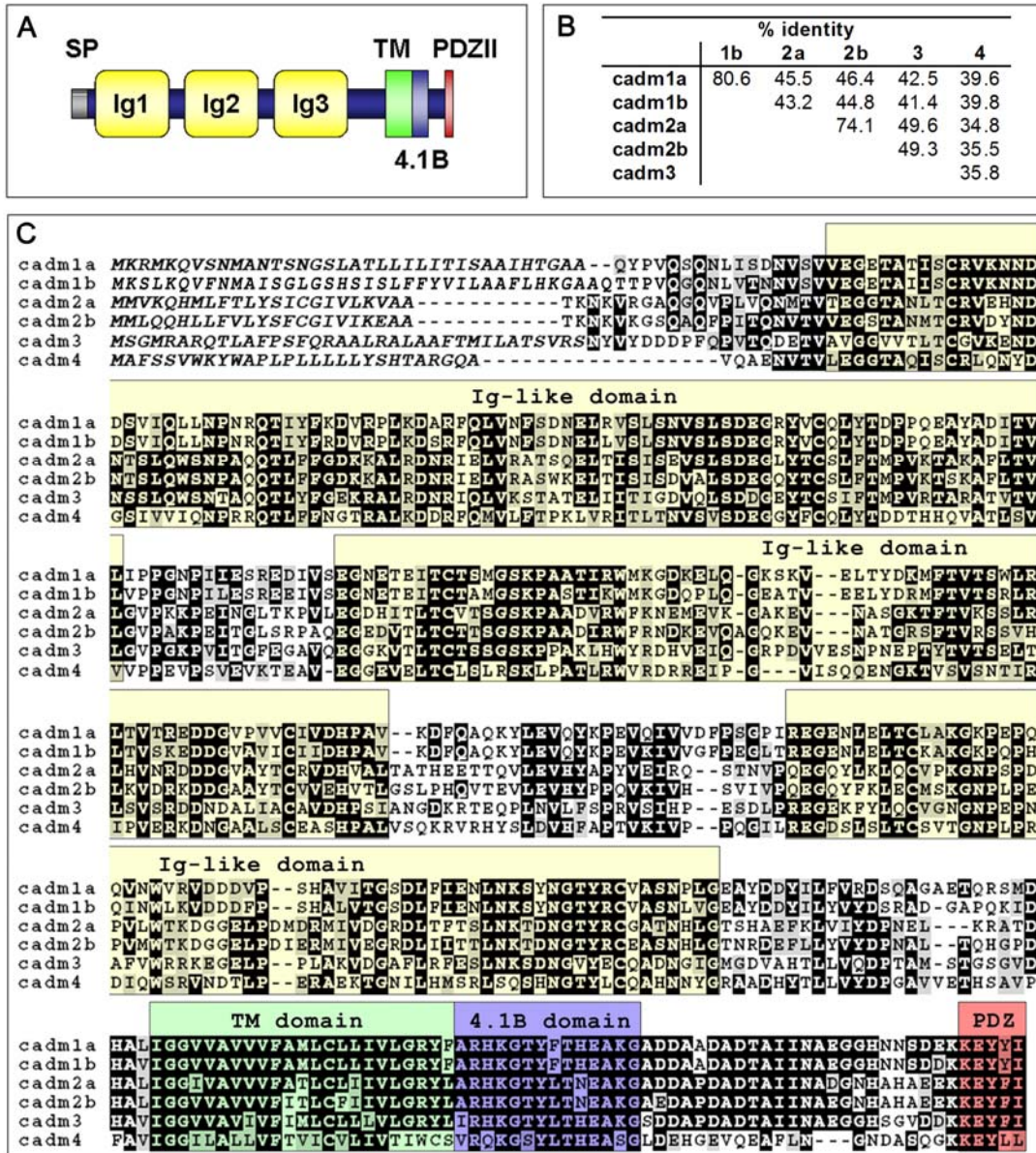


Figure 1. Structure and sequence of zebrafish Cadm proteins. **A:** Schematic representation of Cadm protein structure. All Cadms contain a signal peptide (SP), three Ig-like domains (Ig), a transmembrane (TM) domain and a cytoplasmic tail with a 4.1B binding domain (4.1B) and the PDZ type II binding domain (PDZII). **B:** Amino acid identity as a percentage in pairwise alignments for the six Cadm protein sequences. **C:** Protein alignment of the zebrafish Cadm protein sequences. Conserved positions with an identical amino acid (black) and conserved substitutions (grey) have been shadowed. Putative signal peptide for each cadm is in italic; each structural domain is indicated above the aligned sequences and color shaded as in A.

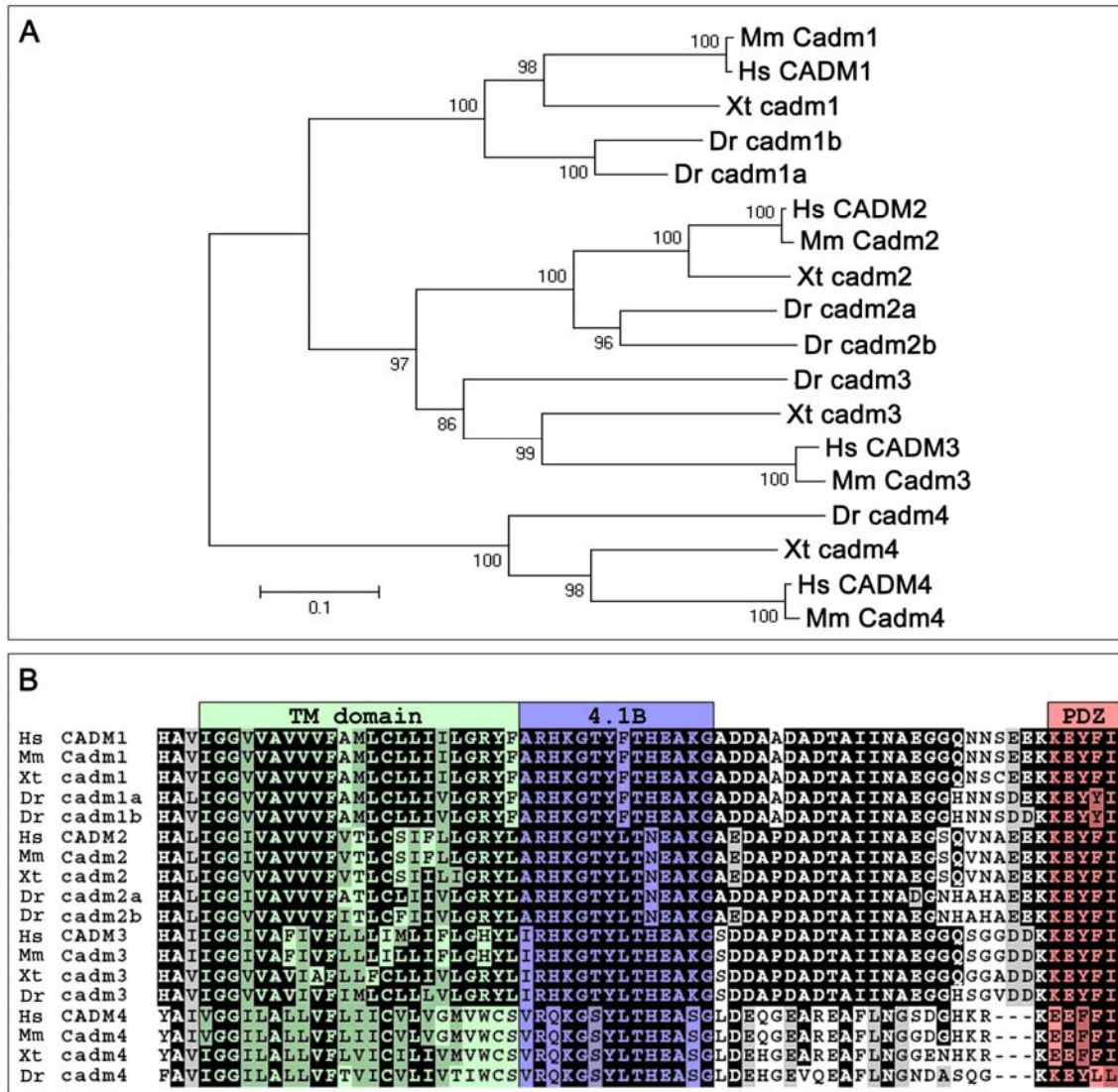


Figure 2. Phylogeny of the Cadm proteins. **A:** Relationships between the Cadm protein sequences of various vertebrates (Hs, Homo sapiens; Mm, Mus musculus; Xt, Xenopus tropicalis; Dr, Danio rerio) are shown in a phylogenetic tree. Amino acid sequences were aligned by Clustal-X. Sequences were trimmed to include unambiguously aligned regions, and phylogenetic analysis used the Poisson-corrected Neighbor-Joining method. The branch lengths (numbers) are the percentage of bootstrap values for 1000 replicas. Scale bar: 0.1 substitutions per site. **B:** Alignment of the transmembrane domain and cytoplasmic tail of the Cadm proteins highlight the high level of conservation of the structural domains among vertebrates. Conserved positions with an identical amino acid (black) and conserved substitutions (grey) have been shadowed; the color shading of domains is as in Fig. 1A.

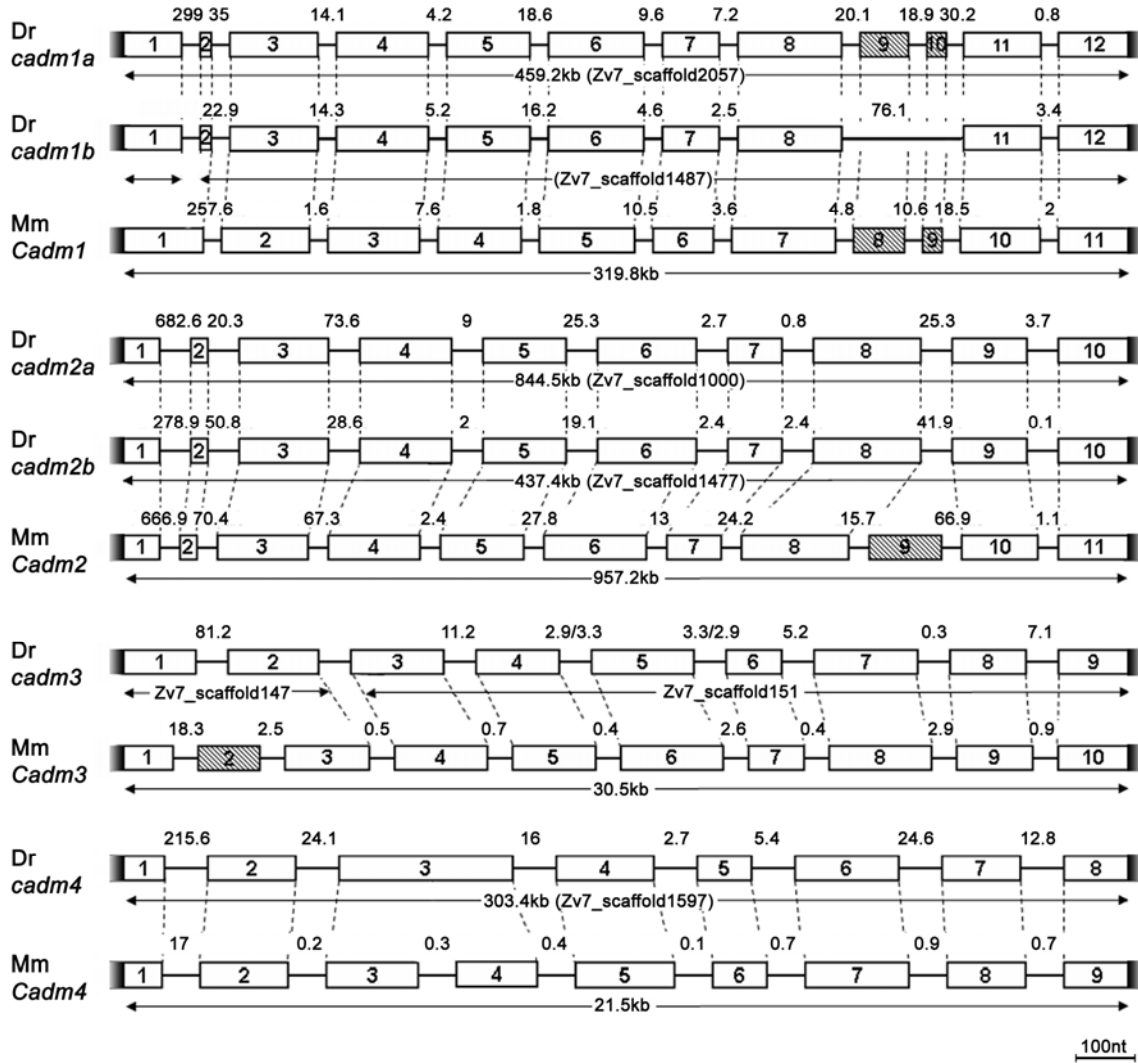


Figure 3. Genomic analysis of zebrafish *cadm* genes. Comparison of the zebrafish (Dr) and mouse (Mm) loci. Exons are represented by numbered boxes. Shaded boxes show exons subjected to alternative splicing. Exon-intron boundaries that correspond between zebrafish and mouse genes are represented by dashed lines. All corresponding exons between the two species are of identical length, unless indicated otherwise in the text. The scalebar (100nt) is for exons; the sizes of introns are indicated in kilobases. Notice that zebrafish *cadm1b* and *3* are both aligned on two different scaffolds in Zv7 assembled zebrafish genome. The first exon of *cadm1b* is found on Zv7_scaffold1472 while the other exons on Zv7_scaffold1487, suggesting a large first intron. Similarly, the first two exons of *cadm3* are found in Zv7_scaffold147, while the rest of the gene is on Zv7_scaffold151.

When compared to their murine orthologs, the zebrafish *Cadm* proteins show on average 55% identity (Supplementary Fig. 1 available online; data not shown). The strongest divergence is seen in the N terminus of the proteins, encoding the signal peptides. In contrast, the C-terminal portions of the *Cadms*, including the intracellular protein-protein interaction domains are highly conserved across phyla (Fig. 2B). This striking conservation reflects constraints upon evolutionary mechanisms, suggesting an important function for both the 4.1B and PDZ type II binding domains. The *Cadm1* PDZ binding domain is relevant to synaptogenesis as demonstrated by *in vitro* experiments (Biederer et al., 2002), while the 4.1B binding domain has been shown to mediate interactions with proteins important for actin cytoskeleton stabilization (Yageta et al., 2002).

We have also compared the genomic organization of mouse and zebrafish *Cadm* genes. We focused our attention on their coding sequences, excluding 5' and 3'-untranslated regions of the genes. Thus, the number of exons might be under-represented. Nevertheless, there are striking similarities between the mouse and zebrafish gene structures (Fig. 3). Almost all of the exons are of the same size and encode the same protein region, suggesting that despite the large evolutionary distance that separates these species the genes are remarkably well conserved. Here we highlight the few differences.

When comparing mouse and zebrafish genes, we see three cases of missing introns, resulting in extended exons. Loss of introns appears to have happened both in mouse and in zebrafish, such that zebrafish *cadm1a* and *1b* exons 1 and 2 correspond exactly to mouse *Cadm1* exon 1, and mouse *Cadm4* exons 3 and 4 appear to have been contracted into zebrafish exon 3. This loss of an intron from zebrafish *cadm4* gene is

substantiated by the medaka *cadm4* gene (Ensembl ENSORGL00000004868), which possesses the same structure as its zebrafish ortholog. Unusually, the lengths of the first two exons of the *cadm3* gene do not correspond to the lengths of the murine counterparts. We have confirmed the sequence of zebrafish *cadm3* by identifying expressed sequence tags which cover at least the first three exons of the gene (for example, EST CN507252).

Another interesting point is that the murine *Cadm* genes show an increased number of alternatively spliced exons when compared with the zebrafish genes (hatched boxes in Fig. 3). Both *Cadm2* and *Cadm3* show additional exons 9 and 2, respectively, which are alternatively spliced for exons 3 and 8. The zebrafish *cadm1* genes contain two exons (9 and 10) that can be alternatively spliced, and potentially produce four different isoforms, just as in mouse and human (Biederer, 2006). Using zebrafish adult brain cDNA, we were able to recover three of these isoforms for *cadm1a*, revealing an identical splice pattern between mouse and zebrafish. However, we have identified only one isoform for the *cadm1b* locus. Additionally, a third alternatively spliced exon in *Cadm1* has been identified in the mouse and human genomes (Biederer, 2006). It is probable that additional splice variants also exist in zebrafish, and that they are differentially regulated during development and in various tissues. This would explain the different number of isoforms we recovered for the *cadm1* loci by screening adult central nervous system cDNA.

In conclusion, despite their relatively large evolutionary distance, the *cadm* genes are remarkably conserved between zebrafish and mammals, suggesting that their functions are probably also conserved. In addition, the maintenance of the duplicated *cadm1* and *cadm2* loci in zebrafish indicates that multiple functions of the mammalian

orthologs may have been partitioned to the co-orthologs. On the other hand, it is possible that the co-orthologs may carry out the same function but in different tissues or at different times during development, as has been seen for other co-orthologs in teleost fish (Postlethwait et al., 2004).

Expression patterns of *cadm* genes

We assayed the temporal and spatial distribution of *cadm* gene expression during zebrafish development by whole mount RNA *in situ* hybridization (ISH), from about 10 hours postfertilization (hpf) through 72 hpf. We are confident that the probes to all six genes are specific and do not cross-react, given their distinct expression patterns and the fact that ISH using sense probes did not show any staining.

No expression was seen at 10 hpf, but by 15 hpf all of the *cadm* genes showed evidence of expression, in particular in the developing head (not shown). At 24 hpf, development has progressed to the point that most major organ systems have begun to form, and expression of all six *cadms* was seen throughout the central nervous system, including the eye and spinal cord (Fig. 4). While expression for all *cadm* genes was consistently stronger in the head than in the trunk and tail, their expression patterns in the spinal cord were dynamic and divergent between the *cadm* family members. Expression was evident in different domains of the spinal cord at 24 hpf (Fig.4, discussed below, see Fig. 7). Furthermore, the spinal cord expression of *cadm* genes was evident as a wave of expression during development. For example, the expression *cadm2a* was decreased in the rostral spinal cord by 48 hpf, becoming undetectable throughout the spinal cord by 72 hpf (Fig. 4C, insets). Also, the *cadm1* genes were present in a rostro-caudal gradient at 24

hpf, with no expression seen above the yolk tube and caudal to this (Fig. 4A and B, dashed lines). These patterns are confirmed for all *cadm* genes by ISH on sections at 24 and 48 hpf (not shown). Since many neurons in the spinal cord develop in a rostro-caudal gradient (Lewis and Eisen, 2003), it is probable that the *cadm* genes are important for a specific event during neuronal maturation.

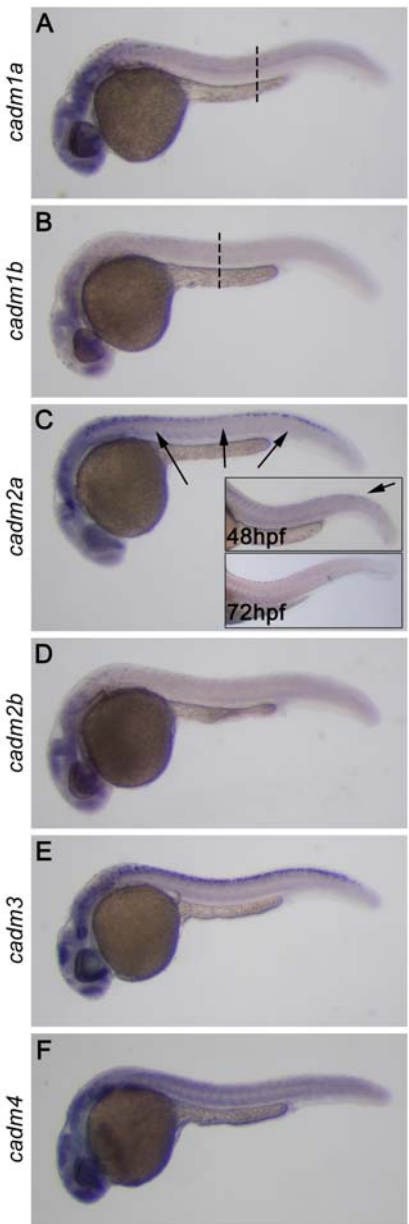


Figure 4. Expression of *cadms* at 24 hours post-fertilization (hpf). ISH performed on 24hpf whole-mount zebrafish embryos reveals that the six *cadm* genes are expressed throughout the central nervous system, in particular in the developing brain, the visual system and the spinal cord. Expression for *cadm1a* and *1b* is in a rostro-caudal gradient (A, B), being undetectable caudal to the dashed lines. *cadm2a* expression decreases rostrally at 48 hpf and is lost by 72 hpf (insets in C).

The general pattern of strong expression throughout the brain persisted to 72 hpf. However, some expression was also seen outside of the nervous system; all 6 *cadms* were expressed in the precartilage of the pectoral fin buds at 48 hpf (arrows in Fig. 5A-F), the pancreas, gut, and developing swim bladder (not shown). All *cadm* genes were expressed at low levels in the adult testis, with *cadm3* showing the strongest expression (not shown), suggesting that, as in mammals (Fujita et al., 2006), these cell adhesion molecules may play a role in the maturation of sperm. Due to the predominant expression of the *cadm* genes in the nervous system during development, we have focused our attention on the brain, visual system and spinal cord of the zebrafish.

***cadm* expression in developing and adult brain**

The *cadms* were broadly expressed throughout the brain both during development and in the adult (Fig. 4, 5). We have summarized the brain expression patterns in Tables 2 and 3, and detailed descriptions of the expression patterns are in Supplementary Data. The tables and descriptions are based on analyses of both horizontal and coronal sections of the whole brain, the majority of which are not shown here.

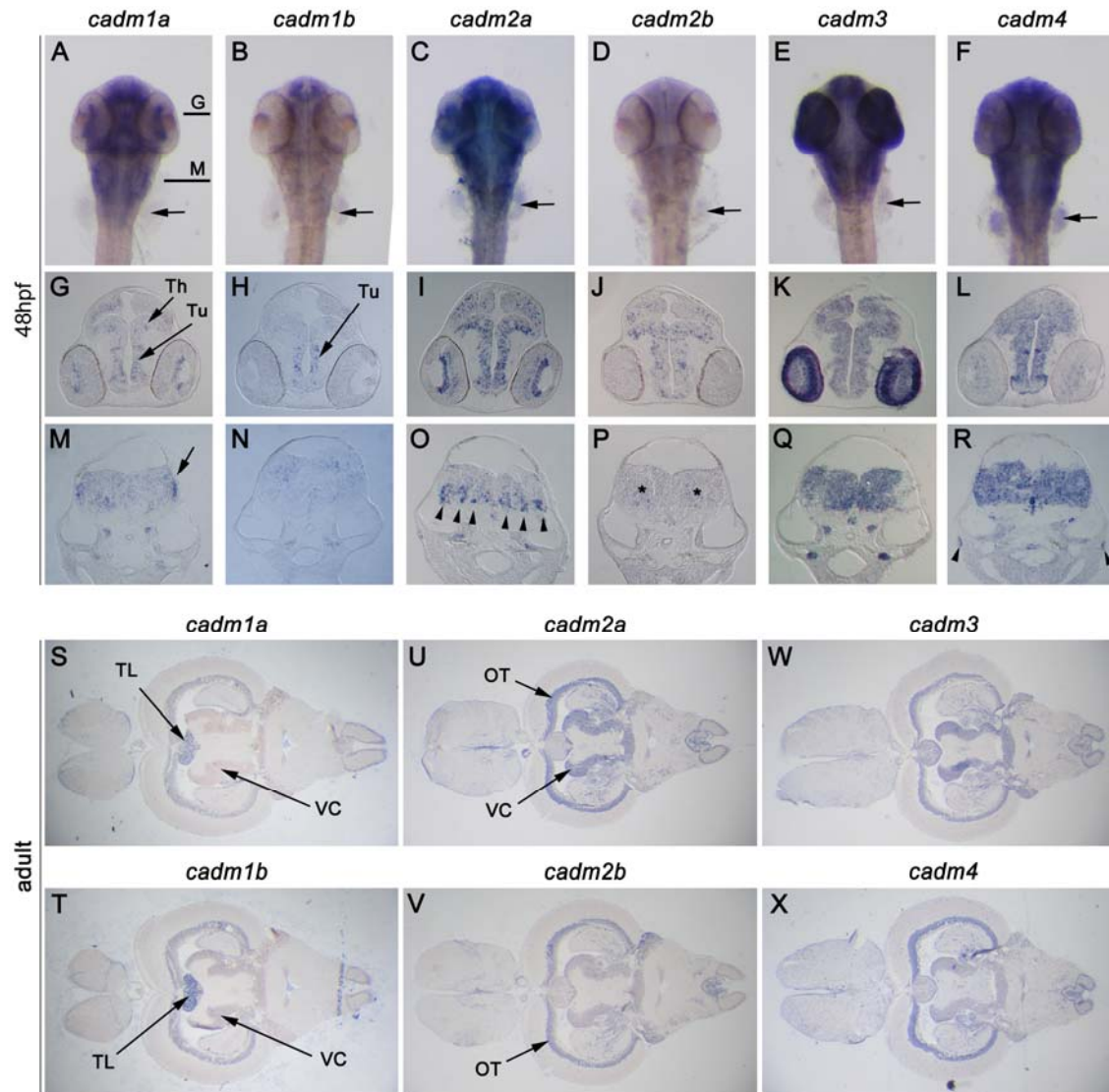


Figure 5. Expression of *cadms* in the brain. (A-R) ISH staining in 48hpf zebrafish embryos; a dorsal view of whole-mount zebrafish (A-F), and cross sections at the midbrain (G-L) and hindbrain (M-R) are presented for each *cadm* gene. Lines in A-F represent levels of the sections in G-L and M-R. (S-X) *cadm* expression visualized in horizontal sections of adult brain. *cadm* genes are expressed broadly in the developing and adult brain, and show partially overlapping domains of expression. *cadm2a* is strongly expressed in the ventral medulla oblongata (arrowheads in O), while *cadm2b* is more diffuse in this region (asterisks in P). The posterior part of the *medulla oblongata* shows strong staining for *cadm1a* (arrow in M). Ot: developing optic tectum; OT: optic tectum granular layer L3; Th: thalamus; TL: *torus longitudinalis*; Tu: tuberculum; VC: *valvula cerebellis*. Orientations are anterior at the top in A-F; dorsal at the top in G-R; anterior to the left in S-X. Scale bars: 50 μ m (G-L), 50 μ m (M-R), 0.5 mm (S-X).

In general, the *cadm1* and 2 genes showed weaker and more punctate expression than *cadm3* and 4 (Fig. 5). This may suggest that the four *cadm1* and 2 genes are expressed in subsets of cells within a structure. This expression may be in distinct cells within each structure, however, more detailed analyses will be required to determine whether this is true. Conversely, *cadm3* and 4 appeared to be expressed in more cell types and more brain regions throughout the nervous system than *cadm1a*, *1b*, *2a* and *2b* (Tables 2 and 3). Whereas as the co-orthologs were sparsely expressed in cells at 48 hpf, the same structures solidly expressed *cadm3* and 4 (for example Fig. 5K, L). This may reflect the expression of *cadm3* and 4 in both neurons and glial cells, as has been demonstrated in the mouse (Kakunaga et al., 2005; Gruber-Olipitz et al., 2006; Maurel et al., 2007; Spiegel et al., 2007).

One of the areas with the most striking expression at 48 hpf was the *medulla oblongata* (MO). Expression varied considerably for each *cadm* gene through the rostro-caudal length of the MO. While *Cadm1a* showed weak punctate expression medially in the anterior portion of the MO, it was expressed predominantly in the periphery of the posterior MO (Fig. 5M, arrow). In contrast, *cadm1b* was hardly expressed in the anterior MO, showing a scattered punctate staining towards the middle, becoming concentrated dorsally towards the posterior end of the structure (Fig 5N). *Cadm2a* showed strong staining mostly in the ventral region of the whole MO in a series of stripes (arrowheads in Fig. 5O), while *cadm2b* was only weakly expressed in the ventral region of the MO (Fig 5P, asterisks). Both *cadm3* and 4 were expressed strongly throughout the MO (Fig 5Q, R).

It was interesting to note that the co-orthologs for the *cadm* genes 1 and 2 demonstrated overlapping, yet more restricted expression patterns both at 48 hpf and in adult. For example, *cadm1a* was expressed throughout the dorsal thalamus and the posterior tuberculum at 48 hpf (arrows in Fig. 5G), while *cadm1b* was only expressed in the ventral part of the posterior tuberculum (arrow in Fig. 5M). Analogously, *cadm2a* was expressed throughout both the granular zone of the optic tectum (OT) and lateral division of the valvula cerebelli (VC) in adult zebrafish (arrows in Fig. 5U), while *cadm2b* was only present in the OT (arrows in Fig. 5V). The restriction of expression of one of the coorthologs, rather than a distinct expression pattern, may suggest a partitioning of function between the two co-orthologs.

On close examination, it was apparent that in many areas the *cadm1* and 2 genes showed inverse expression patterns in the developing and adult brain. This is especially clear in Tables 2 and 3, which reveal that inverse staining was seen for the olfactory epithelium, *griseum tectale*, VC, cerebellar plate, and the trigeminal ganglion at 48 hpf. In the adult, the olfactory bulb, the anterior thalamic nuclei, both the magnocellular and periventricular pretectal nuclei, the *torus longitudinalis* (TL), the valvula, the caudal lobe of the cerebellum and the octaval nucleus all showed inverse staining for *cadm1* and 2. Clear examples are the TL and VC. Both *cadm1* genes were expressed in the TL (arrows in Fig. 5S, T), while *cadm2a* and *2b* were absent (Fig. 5U, V). In contrast, both *cadm1a* and *1b* were not detected in the VC, whereas *cadm2a* and *2b* were present (arrows in Figs. 6 S-V). This inverse expression pattern suggests that transcription for these genes may be co-regulated in an exclusionary fashion.

Table 2. Summary of *cadm* Expression in Brain at 48 Hours Postfertilization

48hpf	<i>cadm1a</i>	<i>cadm1b</i>	<i>cadm2a</i>	<i>cadm2b</i>	<i>cadm3</i>	<i>cadm4</i>
<i>Forebrain</i>						
Pallium	■	■	■	■	■	■
Olfactory bulb	■	■	■	■	■	■
Epiphysis	■	■	■	■	■	■
Habenula	■	■	■	■	■	■
Subpallium	■	■	■	■	■	■
Olfactory epithelium	■	■	■	■	■	■
Dorsal thalamus	■	■	■	■	■	■
Ventral thalamus	■	■	■	■	■	■
Griseum tectale	■	■	■	■	■	■
Pretectum	■	■	■	■	■	■
Posterior tuberculum (dorsal part)	■	■	■	■	■	■
Posterior tuberculum (ventral part)	■	■	■	■	■	■
<i>Midbrain</i>						
Tectum opticum	■	■	■	■	■	■
Medial longitudinal fascicle nucleus	■	■	■	■	■	■
Midbrain tegmentum	■	■	■	■	■	■
Rostral hypothalamus	■	■	■	■	■	■
Intermediate hypothalamus	■	■	■	■	■	■
<i>Hindbrain</i>						
Valvula cerebelli	■	■	■	■	■	■
Cerebellar plate	■	■	■	■	■	■
Torus semicircularis	■	■	■	■	■	■
Trigeminal ganglion	■	■	■	■	■	■
Medulla oblongata	■	■	■	■	■	■
Caudal hypothalamus	■	■	■	■	■	■
Hypophysis	■	■	■	■	■	■
Rhombic lip	■	■	■	■	■	■
Anterior lateral line ganglion	■	■	■	■	■	■
Posterior lateral line ganglion	■	■	■	■	■	■
Octaval ganglion	■	■	■	■	■	■
Facial ganglion	■	■	■	■	■	■
Glossopharyngeal ganglion	■	■	■	■	■	■
Vagal ganglion	■	■	■	■	■	■

Expression for brain structures are summarized for the six *cadm* genes. A black box denotes the presence of cells expressing the *cadm* gene listed at the top of the columns.

Table 3. Summary of *cadm* Expression in Adult Brain

adult	<i>cadm1a</i>	<i>cadm1b</i>	<i>cadm2a</i>	<i>cadm2b</i>	<i>cadm3</i>	<i>cadm4</i>
<i>Telencephalon</i>						
Glomerular layer of olfactory bulb	■	■	■	■	■	■
External cellular layer of olfactory bulb			■		■	
Internal cellular layer of olfactory bulb		■	■		■	■
Lateral dorsal telencephalic cell mass		■	■	■	■	■
Medial dorsal telencephalic cell mass		■	■			
Ventral dorsal telencephalic cell mass				■	■	■
Ventral telencephalon nuclei	■	■	■	■	■	■
Entopeduncular nucleus	■	■	■		■	
<i>Diencephalon</i>						
Parvocellular preoptic nuclei (anterior)	■	■	■	■	■	
Parvocellular preoptic nuclei (posterior)	■	■	■		■	■
Magnocellular preoptic nucleus	■	■	■	■	■	■
Habenula	■	■	■	■	■	■
Suprachiasmatic nucleus	■	■	■	■	■	■
Preoptic nuclei	■	■	■	■	■	■
Thalamic nuclei (ventromedial)	■	■	■	■	■	■
Thalamic nuclei (central posterior)	■	■	■	■	■	■
Thalamic nuclei (anterior)		■	■	■	■	
Preglomerular nucleus (lateral)	■	■	■	■	■	
Preglomerular nucleus (anterior)	■	■	■	■	■	■
Corpus mamillare	■	■	■	■	■	■
Torus lateralis	■	■	■	■	■	■
Periventricular hypothalamus		■	■	■	■	■
Inferior lobe (diffuse nucleus)	■	■	■	■	■	■
Inferior lobe (central nucleus)		■	■	■	■	■
Magnocellular prethalamic nucleus		■	■	■	■	■
Periventricular prethalamic nucleus		■	■	■	■	■
<i>Mesencephalon</i>						
Tectum opticum (white matter)		■	■	■	■	■
Tectum opticum (granular zone)	■	■	■	■	■	■
Tectum opticum (periventricular zone)	■	■	■	■	■	■
Torus semicircularis (central nucleus)	■		■	■	■	■
Torus semicircularis (ventrolateral)	■	■	■	■	■	■
Torus longitudinalis	■	■		■	■	
Nucleus isthmi	■	■		■	■	■
<i>Rhombencephalon</i>						
Eminentia granularis	■	■	■	■	■	■
Corpus cerebelli		■	■	■	■	■
Valvula cerebelli (lateral division)		■	■	■	■	■
Valvulae (nucleus lateralis)		■	■	■	■	■
Lobus caudalis cerebelli		■	■	■	■	■
Facial lobe	■	■	■	■	■	■
Vagal lobe	■	■	■	■	■	■
Descending octaval nucleus		■	■	■	■	■
Anterior octaval nucleus		■	■	■	■	■
Medial octavolateralis nucleus		■	■	■	■	■
Caudal octavolateralis nucleus	■	■	■	■	■	■

Expression for brain structures are summarized for the six *cadm* genes. A black box denotes the presence of cells expressing the *cadm* gene listed at the top of the columns.

***cadm* expression in the developing and adult visual system**

We examined in detail the *cadm* gene expression patterns in retina at 48 hpf, 5 days postfertilization (dpf) and adult eyes. Lamination of the retina occurs with a central to peripheral and inner to outer gradient of maturation, and is generally complete by 48 hpf (Schmitt and Dowling, 1994). At this age of development, most *cadm* genes were expressed in a punctate, scattered manner. For instance, *cadm1b* and *2b* were expressed throughout the retina, lens and the cornea in this manner (Fig. 6B and D, respectively). A similar scattered expression was seen for *cadm1a*, *2a* and *4* in the inner nuclear layer (INL), outer nuclear layer (ONL) and the marginal zone (Fig. 6A, C and F respectively). Since the neuroepithelial cells within these regions are still actively dividing during this period of rapid growth, these expression patterns might represent mitotically active cells. Expression in mitotically active cells would then suggest a novel function for these *cadms* during early neuronal differentiation.

The ganglion cell layer (GCL) displayed the most varied expression pattern of all the layers of the retina at 48 hpf. *cadm1a* expression appeared to follow the wave of differentiation of this layer: high expression of *cadm1a* was seen in the periphery of the layer where the neuroblasts are still mitotically active at this stage, while being downregulated in the more mature GCL (Fig. 6A, arrows). Conversely, *cadm4* expression in the GCL was higher in more mature neurons (Fig. 6F, arrows), while *cadm2a* was expressed in the entire GCL independently of the level of maturation of the ganglion cells (Fig. 6B). In contrast, and as seen in the brain, *cadm3* was expressed in the vast majority of cells in the retina (Fig. 6E).

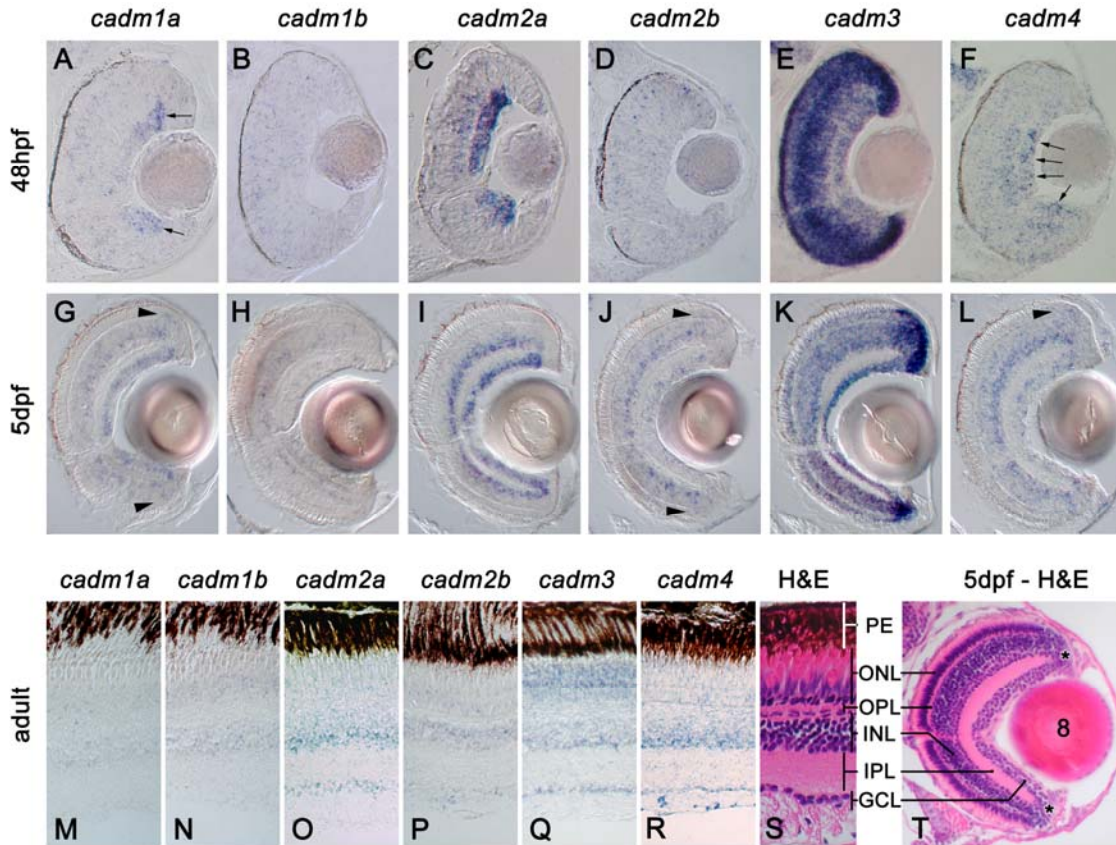


Figure 6. Expression of *cadms* in the visual system. ISH staining in sections of retina at 48hpf(A-F), 5dpf (G-L) and adult zebrafish (M-R). S and T show haematoxylin and eosin staining (H&E) of sections of adult and 5dpf, respectively; the different layers of the retina are indicated: PE: pigment epithelium; ONL: outer nuclear layer; OPL: outer plexiform layer; INL: inner nuclear layer; IPL: inner plexiform layer; GCL: ganglion cell layer. Asterisk in T denotes the location of the marginal zone. *cadm1a* is expressed in the dividing ganglion cells (arrows in A), while *cadm4* is more strongly expressed in the mature cells of the GCL (arrows in F). Arrowheads in G, J and L reveal precursors at the margin of the ONL. Scale bars: 50 μ m (A-F), 50 μ m (G-L, T).

Visual function is observed as early as 3 dpf and is fully functional by 5 dpf (Schmitt and Dowling, 1994). At this time, *cadm* genes were expressed in partially overlapping domains within most retinal layers. In the GCL, *cadm1a*, *2a* and *3* were expressed in most of the neurons (Fig. 6G, I and K), while *cadm1b*, *2b* and *4* (Fig. 6H, J and L) were seen in subsets of cells. In the INL, *cadm1a*, *1b*, *2a*, *2b* and *4* were expressed

in restricted populations of cells (Fig. 6G-J and L). These expression patterns suggest that all *cadm* genes are expressed in amacrine cells, bipolar cells and Müller glia. In addition, it appears that *cadm1a*, *2b*, *3* and *4* are expressed in horizontal cells at the outer limit of the INL (Fig. 6G, J-L) and *cadm3* and *4* in the ONL (Fig. 6K and L). Notably, the periphery of the ONL also expressed *cadm1a*, *2b* and *4*, and might represent dividing retinal precursor cells (Fig. 6G, J and L, arrowheads).

All *cadm* genes remain expressed in the adult eyes with partially overlapping domains of expression, generally mirroring the expression at 5 dpf. However, *cadm1a* and *1b* were down regulated in the GCL in adult eyes (Fig. 6M, N). *Cadm2a*, *2b*, *3* and *4* were detected in the GCL, albeit at different levels (Fig. 6O-R). *Cadm2a* and *2b* were expressed in a small subset of the GCL cells (Fig. 6O, P), while *cadm3* and *4* were present in most of the ganglion cells (Fig. 6 Q, R). All six *cadm* genes were expressed in the INL: *cadm1a*, *1b*, *2b* and *4* were restricted to the medial domain of the INL, suggesting they are expressed in bipolar, but not amacrine or horizontal cells. In contrast, *cadm2a* and *3* presented a broader expression in the INL, including the amacrine cell domain. *cadm3* was expressed at a higher level in the amacrine cells than in the other regions of the INL. The ONL presented a sparse expression of *cadm1a*, *1b*, *2a* and *4* in both inner and outer segments, suggesting they are present in a small subpopulation of rods and cones; *cadm3* was detected in virtually all cells of the ONL. In contrast, *cadm2b* was restricted to the outer segment and therefore expressed in the rod population of the ONL.

In summary, *cadm* genes are highly regulated in the course of the development of the retina. They show partially overlapping domains of expression within the retina, but

can be restricted to distinct cell populations composing each layer. These dynamic expression patterns suggest that the various *cadms* may perform distinct functions at discrete times during differentiation of retinal cells.

***cadm* expression in the developing spinal cord**

We examined the expression of the six *cadm* genes in the spinal cord at 48 hpf, since the wave of expression of these genes was in the widest variety of cell types at this time. We present both dorsal views of RNA ISH in whole mount embryos (Fig. 7A-F) and in sections (Fig. 7G-L). This allows appreciation of the spatial distribution of expression along both rostro-caudal and dorso-ventral axes. We used the following spatial subdivisions along these axes to assign expression to particular cell types. The dorsal domain is defined by the sensory Rohon-Beard neuron, while the intermediate domain is composed of various types of interneurons. Finally, the ventral domain comprises floor plate cells and motoneurons. The morphology, localization and axon projections of zebrafish spinal cord neurons have been well described (Hale et al., 2001; Lewis and Eisen, 2003).

Diffuse expression was seen for all *cadms* in the various domains of the spinal cord; however a number of the expression patterns were suggestive of strong expression in distinct populations of spinal neurons (Fig. 4, Fig. 7). *cadm1a* was mostly detected in the intermediate domain of the spinal cord, probably in a subpopulation of interneurons. It was more strongly detected in the ventral part of this domain in the caudal spinal cord, suggesting that it is expressed first in a ventral population of interneurons, before expanding to a more dorsal domain. *cadm1b* was expressed in the intermediate domain of

the spinal cord and, in particular, in its dorsal aspect, suggesting that *cadm1b* is expressed in dorsal interneurons.

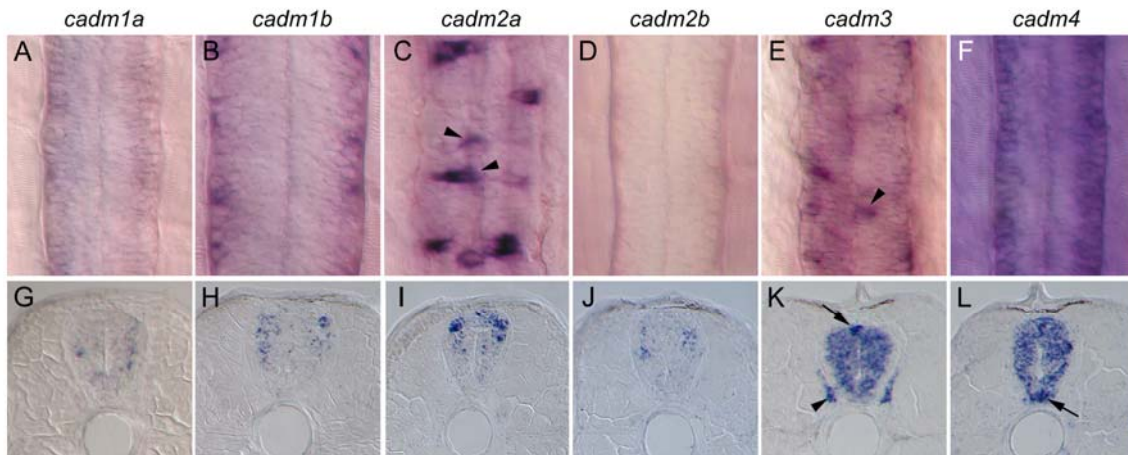


Figure 7. Expression of *cadms* in the developing spinal cord. *cadm* expression revealed by ISH in whole-mount (dorsal view, A-F) and cross sections (G-L) of 48hpf embryos. Due to the strong rostrocaudal gradient of *cadm1b* expression, panels B and H show an anterior localized region of the spinal cord (somites 3-5), immediately behind the hindbrain, whereas all other images are from a region dorsal to the anus (somites 12-15). Staining for *cadm2a* and 3 is in dorsal cells at the midline of the spinal cord, suggestive of sensory Rohon-Beard neurons (arrowheads in C and E, arrow in K). Expression for *cadm3* is also seen in the dorsal root ganglion (arrowhead in K). *cadm4* is strongly expressed in the ventral domain of the spinal cord indicative of floor plate or motoneurons. Scale bars: 20 μ m (A-F), 20 μ m (G-L).

cadm2a was expressed throughout the dorsal and intermediate region of the spinal cord and was particularly strong in cells at the midline in the dorsal spinal cord, suggesting expression in sensory Rohon-Beard neurons (Fig. 7C, arrowheads). In contrast, *cadm2b* was weakly expressed and excluded from the dorsal and ventral domain, suggesting that it may be exclusively present in interneurons.

cadm3 and 4 were widely expressed in the spinal cord, including the proliferating ventricular zone. *cadm3* showed strong staining in dorsal neurons, including Rohon-

Beard neurons (Fig. 7, arrowhead in E and arrow in K). In contrast, *cadm4* was more highly expressed in the ventral domain of the spinal cord, suggestive of floor plate cells and motoneurons (arrow Fig. 7L). Additionally, *cadm3* was present in other neuronal tissues in the trunk and tail, the localization suggesting expression in dorsal root and sympathetic ganglia (Fig. 7K, arrowhead). Interestingly, *cadm4* was also detected in the developing neuromasts of the lateral line system (Fig. 5R).

As Cadm1 is a potential mediator of synaptogenesis (Biederer et al., 2002) and the expression of all six *cadm* genes is found in discrete neuronal subtypes of the developing spinal cord at a time when neuronal circuits are becoming functional (16-48 hpf; (Drapeau et al., 2002), it is reasonable to hypothesize that these molecules could mediate synaptogenesis or determine synaptic specificity for the early circuits in spinal cord during development. With this expression data in hand, it may now be possible to perform a functional analysis of this family of cell adhesion molecules *in vivo*.

CONCLUDING REMARKS

The zebrafish *cadm* genes show strong similarities with their tetrapod orthologs in terms of genetic structure and protein organization. Their expression is highly regulated during development of the central nervous system and they show partially overlapping domains of expression within each structure. The maintenance of two duplicated *cadm* loci in zebrafish with similar expression patterns indicates the probable acquisition of novel functions or the partition of functions during the course of evolution. The dynamic expression patterns during development suggest that these cell adhesion molecules may

play multiple roles during neuronal differentiation, including steps in neuronal cell fate decisions and synaptogenesis.

SUPPLEMENTARY RESULTS

***cadm* expression in the brain: developing brain**

Forebrain

By 48hpf, the brain has begun to differentiate to such a degree that many distinct structures are identifiable. In the anterior forebrain, the *cadms* expressed throughout the pallium, olfactory bulb, epiphysis, habenula, and subpallium (Fig. 5 A, D, J, G, M, P). In the olfactory epithelium, *cadm2a* and *2b* expressed weakly, while *cadm3* expressed very strongly. *cadm1a*, *1b*, and *4* were not expressed. In thalamus, *cadm1a* expressed throughout the structure, with the strongest expression in the periphery, and *cadm1b* showed weak punctate expression throughout. *cadm2a* showed strong punctate staining throughout the thalamus, and *2b* showed a similar but weaker expression pattern, while *cadm3* and *4* showed strong expression throughout. *cadm2a*, *2b*, *3* and *4* were expressed in the *griseum tectale* at similar levels, *cadm1a* and *1b* were not expressed. In the posterior tuberculum, *cadm1a* showed weak punctate expression, with stronger expression in the ventral region (Fig. 5B). Expression of *cadm1b* and *2b* was similar, with weak punctate expression throughout, but *1b* showed stronger expression in the medial region and *2b* showed stronger expression in the peripheral region of the ventral part of the posterior tuberculum (Fig. 5E, K). All 6 *cadm* genes were expressed in the pretectum.

Midbrain

In the midbrain, all of the *cadm* genes were expressed in the optic tectum, but there was variability in where they expressed within the structure. *cadm1a* and *1b* showed weak punctate expression and *cadm3* and *4* showed strong expression (Fig. 5B, E, N, Q). *cadm2a* and *2b* showed a more complex expression pattern, with *2a* showing strong punctate expression in all but the most medial region, and *2b* showing punctate staining only in the anterior region (Fig. 6H, K). All 6 *cadm* genes expressed at similar levels in the nucleus of the medial longitudinal fascicle. The tegmentum showed expression of all 6 *cadms*, with *cadm2a*, *3*, and *4* showing stronger expression. In the hypothalamus all of the *cadms* were strongly expressed, except for *cadm2a* which only expressed in the anterior periphery, and *cadm2b*, which showed weak punctate expression in the dorsal region.

Hindbrain

The portion of the zebrafish embryonic brain that is the most variable in terms of where each *cadm* expressed was the hindbrain. In the cerebellum, both *cadm1a* and *1b* showed weak expression, while *cadm3* and *4* showed strong expression. *cadm2a* and *2b* were not expressed in the cerebellum. In the *torus semicircularis* all of the *cadms* except *1b* were expressed. In the trigeminal ganglion only *cadm2a* was expressed. In the hypophysis (pituitary gland) only *cadm1a*, *2a*, and *4* were expressed. All but *cadm1b* were expressed in the rhombic lip. Only *cadm2b*, *3* and *4* were expressed in the anterior lateral line ganglion with *3* showing the strongest expression. The octaval ganglion showed expression of all but *cadm1b*, with *1a* and *3* showing the strongest expression (Fig 5C, I,

L, O, R). In the facial ganglion only *cadm3* was expressed and in the glossopharyngeal ganglion only *cadm4* was expressed. The posterior lateral line ganglion and the vagal ganglion both expressed *cadm1a*, *2a*, *3* and *4* at similar levels. Expression in the *medulla oblongata* is described in the main text.

Adult brain

Telencephalon

cadm2a and *3* were expressed throughout the pallium. In contrast, *cadm1a*, *1b* and *2b* were not found in the central zone of the dorsal telencephalic area. *cadm4* was excluded from the lateral and medial domain only in the most dorsal part of the pallium. In the ventral pallium, *cadm4* was also expressed in the lateral domain. In the subpallium, most of the nuclei (supra and postcommissural, central and lateral nuclei) expressed all *cadm* genes, albeit at different levels.

Diencephalon

The anterior endopeduncular nuclei extend into the preoptic region at the boundary between the telencephalon and the diencephalon. These nuclei include the preoptic nucleus, parvocellular nuclei and magnocellular nuclei, as well as the suprachiasmatic nucleus. All *cadm* genes were expressed in this series of nuclei, with the exception of *cadm2b* and *cadm4* in the posterior and anterior parvocellular nuclei, respectively, and *cadm1b* in the suprachiasmatic nucleus. The epithalamus, the *saccus dorsalis* and the epiphysis did not express any of the *cadm* genes. However, *cadm* expression was detected in the habenula: *cadm2b* being only expressed in its most ventral part. *cadm*

genes were found in the thalamus. The anterior thalamic nucleus did not express *cadm4*, while the ventromedial thalamic nuclei did not express *cadm1a* and *4*. All *cadm* genes were expressed in the central posterior and dorsal posterior thalamic nuclei. *cadm* genes were detected in a few nuclei of the posterior tuberculum, however, the periventricular, posterior tuberal nuclei, as well as the paraventricular organ did not express *cadms*. In contrast, all *cadms* were found in the anterior preglomerular nucleus. *cadm1a*, *2a* and *3* were expressed in the lateral preglomerular nucleus, *corpus mamillare* and *torus lateralis*. The periventricular hypothalamus (ventral, caudal and dorsal zone including the periventricular nucleus) and the central nucleus of the inferior lobe express *cadm2a*, *2b*, *3* and *4*, but not the *cadm1* genes. In contrast, cells which presumably migrate from the periventricular zone to the diffuse nucleus of the inferior lobe expressed *cadm1a*, but not *cadm3*. The anterior tuberal nucleus, lateral to the ventral zone of the periventricular hypothalamus, did not express any of the *cadm* genes. Close to the posterior commissure, the nucleus of the medial longitudinal fascicle, as well as the subcommissural organ was devoid of *cadm* expression, while *cadm2a* and *3* were detected in the periventricular pretectal nucleus. In the pretectum, only the parvocellular pretectal and dorsal accessory optic nuclei expressed *cadm2a* and *2b*. None of the other superficial nuclei, such as the magnocellular, the posterior pretectal, or the ventral accessory optic nuclei expressed *cadm* genes.

Mesencephalon

As described for the developing brain, the optic tectum expressed all *cadm* genes. Except for *cadm1a*, cells expressing the *cadm* genes were scattered throughout the superficial

white matter and were not restricted to particular layers of the white matter of the optic tectum. However, *cadm1a* was found together with all other *cadms* in the granular zone and the periventricular zone L3. The *torus longitudinalis* is discussed in detail in the main text. The *torus semicircularis*, a sensory structure, showed expression of all *cadm* genes, except for *cadm1b* and *cadm4* in the central nucleus and a ventrolateral nucleus, respectively. The tegmentum, which includes many motor structures, was mostly devoid of *cadm* expression; while some scattered expression was detected, it was not associated with particular nuclei or cell masses in this region of the brain.

Rhombencephalon

The three parts of the cerebellum, vestibulolateralis lobe, corpus cerebelli and valvulla cerebelli expressed *cadm2a*, *2b*, and *3*. The medial subdivision of the valvulla cerebelli did not express *cadm* genes. Complementary expression was seen for *cadm1a* and *1b* in the vestibulolateral lobe, where *cadm1a* was expressed in the *eminentia granularis*, but not in the medial caudal lobe, and the inverse was seen for *cadm1b*. Posterior to the cerebellum lies the medulla oblongata, which contains a large set of sensory and motor nuclei. A scattered expression of *cadm* genes was detected, however the expression did not clearly define all the various nuclei found throughout this region. In contrast, however, all the *cadms* were clearly detected in the facial and vagal lobe, and in the caudal octavolateralis nuclei. Only *cadm2a* and *2b* were expressed in the descending octaval nuclei. *cadm2a*, *2b*, *3* and *4* were expressed in anterior octaval nuclei and the medial octavolateralis nucleus, while all *cadms* were expressed in the caudal

octavolateralis nucleus. In addition, all *cadms* were found in the rhombencephalic reticular formations.

EXPERIMENTAL PROCEDURES

Cloning the *cadm* genes

To clone the zebrafish *cadm* genes, we searched the zebrafish genome assembly Zv6 from the Sanger Institute (http://www.ensembl.org/Danio_rerio) by tBLASTn (<http://www.ncbi.nlm.nih.gov/BLAST>) comparison with the mouse *Cadm1* to *Cadm4* protein sequences (NP_997558.2, NP_848836, NP_444429 and NP_694752 respectively). This search revealed 6 *cadm* genes in zebrafish, with a duplication of the *cadm1* and *cadm2* loci. The best hits on the zebrafish genome were then compared with the Genbank database to recover published sequences. Full length cDNA for one *cadm2* (*Igsf4d*, renamed in this study *cadm2a*) and *cadm4* were found in the Genbank references NM_200664.1 (IMAGE clone 5603809) and BC085419 (IMAGE clone 7227860), respectively. Partial cloning of *cadm1a* (third Ig domain, transmembrane domain and cytoplasmic tail of the protein), based on a partial sequence of RA175 (AB183400) was performed by RT-PCR of zebrafish adult brain cDNA (forward primer: ATGCTAGCAAGGAGAGATAT reverse primer TCAGGACTCAGATATAGTAT). The database search with the mouse *Cadm1* did not allow recovery of the highly divergent 5' fragment of zebrafish *cadm1a*. Comparison of the medaka *cadm1* sequence (EnsEmbl ENSORLG00000005159) by BLASTn with the zebrafish genome revealed a 5' fragment (without the signal peptide sequence), which was cloned by RT-PCR (forward primer CAGAATCTCATATCGGACAACGTC and reverse primer

GCCTGAAAGTCCTTGACTGC). We used the FirstChoice RLM-RACE Kit (Ambion) to recover the signal peptide of *cadm1a* (outer primer: TCCTCGCGGGACTCTATGAT and inner primer: CGAGCATCTTTCAGGGGTCT). Zebrafish *cadm1b* is derived from partial zebrafish cDNA sequences (XM_001337106, XM_685581 and BU710444) and cloned by RT-PCR of 72hpf whole zebrafish embryo cDNA. These published sequences did not contain the signal peptide of *cadm1b*, which was cloned by 5'-RACE PCR (outer primer: CTCGCGGGACTCTAAGATTG and inner primer: CGGTGGATCCGTGTAGAGTT). *Cadm2b* and *cadm3* were deduced from XM_001342480 and XM_695311 (*cadm2b*) and NM_001045246 (*cadm3*) and cloned by RT-PCR from zebrafish adult brain cDNA (forward primer: TGCACGCAACAAATATCCTC and reverse primer: CTAAATGAAGTACTCTTTCTTTTCC for *cadm2b* and forward primer: CTATTGGCTGTAGCGTGCTG and reverse primer GAAGCGTGTGAAGGAAGAGG for *cadm3*).

Protein alignment and phylogenetic analysis

Deduced protein sequences for the zebrafish *cadm* genes based on the cloned cDNA sequences have been aligned with ClustalW. This alignment, using only the shortest isoforms, was used to generate a phylogenetic tree with the MEGA package, based on Poisson-corrected Neighbor-Joining amino-acid distances and considering gap pairwise deletion. Protein accession number (Genbank for human and mouse and EnsEmbl for *Xenopus*) used for the analysis were, NP_055148.3 (*Homo sapiens*; Hs_CADM1), NP_694854.2 (Hs_CADM2), NP_067012.1 (Hs_CADM3), NP_660339.1

(Hs_CADM3), NP_997559.1 (*Mus musculus*, Mm_Cadm1), NP_848836.1 (Mm_Cadm2), NP_444429.1 (Mm_Cadm3), NP_694752.1 (Mm_Cadm4), ENSXETP00000033613 (*Xenopus tropicalis*, Xt_cadm1), ENSXETG00000026489 (Xt_cadm2), ENSXETP00000041942 (Xt_cadm3) and ENSXETP00000033087 (Xt_cadm4).

Mapping and conserved synteny

The zebrafish *cadm* genes were mapped on the LN54 radiation hybrid mapping panel (Hukriede et al., 1999) as described (Postlethwait et al., 2000). The chromosomal position of each gene was determined through the use of the mapping program of Dr. I. Dawid (<http://mgchd1.nichd.nih.gov:8000/zfrh/beta.cgi>). Two sets of primers were used to confirm the localization on the LN54 panel (primer sequences available on demand). For comparative mapping with murine *Cadm* genes, zebrafish *cadm* genes were considered orthologs when the human and zebrafish genes were best hits on the reciprocal BLASTp searches on the other genome. The mouse *Cadm* sequences used for this analysis are as indicated in Protein alignment and phylogenetic analysis.

***In situ* hybridization**

Zebrafish embryos, larvae and adults (AB/Tübingen strain) were raised at 28.5°C according to standard protocols (Westerfield, 2000). Sense and antisense probes were *in vitro* transcribed and digoxigenin tagged according to the manufacturer's protocol (Roche) from linearized pCRII-TOPO (Invitrogen) *cadm1a* plasmid or from PCR fragments of *cadm1b*, *2a*, *2b*, *3* and *4* linked to a T7 or T3 promoter. *cadm1a* probes

encompass the *cadm1a* cDNA from nt 623 to 1384 of the CDS; *cadm1b*, from nt 381 to 856, *cadm2a*, from nt 331 to 1154; *cadm2b*, from nt 351 to 1048; *cadm3*, from nt 239 to 992; *cadm4*, from nt 278 to 992. ISH on frozen sections was performed according to the protocol described by Jensen et al. (2001) with the following changes. Labeled probes were diluted 1:200 in hybridization buffer and heated to 68°C for 30 min, 200 µl of diluted probe was used per slide. Hybridization was carried out at 68°C.

Posthybridization washes were increased to 3 washes in 50% formamide, 1X SSC, 0.1% Tween-20 at 68°C for 30 minutes and three washes in MABT (100 mM maleic acid, 150 mM NaCl, pH 7.5, 0.1% Tween-20) for 30 minutes at room temperature. Antidigoxigenin conjugated to AP antibody (Roche) was used at a 1:1500 dilution. Whole mount ISH was carried out according to the protocol by Moens et al. (1996). BM purple AP Substrate (Roche) was used for coloration. Images of sections and whole mount embryos were taken on a Zeiss Axioplan microscope or a Leica MZ6 stereomicroscope using a Nikon Coolpix 990 or 4500 digital camera. The images were arranged for presentation purposes using Adobe Photoshop. Annotations of the anatomy of the embryonic and adult brain are done according to Wulliman (1996) and Muller (2005).

CHAPTER IV

***CADM2A* IS NECESSARY FOR THE FORMATION OF GLUTAMATERGIC SYNAPSES IN THE DEVELOPING ZEBRAFISH SPINAL CORD**

The work described in this chapter is unpublished material co-authored by myself and P. Washbourne. The experimental work was performed by me. The analysis was performed by me with assistance from P. Washbourne. The writing is entirely mine. P. Washbourne provided editorial assistance.

INTRODUCTION

Synapses are connections between neurons that allow information to flow in a single direction. Synaptic connections between individual neurons form the basis for complex neuronal networks in the brain that drive thoughts and behaviors. For a synapse to form, a pre and post synaptic neuron must first make contact. This point of contact must be stabilized; then an array of pre and post synaptic proteins must be recruited to the site of contact, including synaptic vesicle proteins, neurotransmitter receptors, and scaffolding proteins (Ziv and Garner, 2004; Waites et al., 2005; Gerrow and El-Husseini, 2006; McAllister, 2007; Jin and Garner, 2008; Bury and Sabo, 2011).

Contacts between neurons are stabilized by cell adhesion molecules, or CAMs. These proteins act as molecular glue to physically hold together the points of contact between two neurons, and allow for the recruitment of further proteins to a developing synapse. Recently, several families of CAMs have been shown to have not just the ability to physically link neurons together, but also to induce synapse formation in the first

place, including the Neuroligins, and the Cadms (Washbourne et al., 2004; Biederer and Stagi, 2008). In a co-culture assay, non-neuronal cells expressing Cadm1 were shown to be able to induce formation of a presynaptic terminal from a hippocampal neuron onto the surface of a non-neuronal cell (Biederer et al., 2002).

The Cadms are a family of adhesion molecules that bind transynaptically in a homo and heterophilic fashion (Fogel et al., 2007; Thomas et al., 2008; Hunter et al., 2011). Cadms are transmembrane proteins that contain three extracellular Ig domains, and have short cytoplasmic tails containing a PDZ and a FERM binding domain (Biederer et al., 2002; Sara et al., 2005). These binding domains allow Cadms to bind to synaptic scaffolding proteins and adaptor proteins (Biederer et al., 2002; Biederer and Stagi, 2008), and these interactions suggest that Cadms may be required to provide a signal to drive recruitment of further proteins to a nascent synapse.

To determine the function of Cadms *in vivo*, Fujita and colleagues made a Cadm1 knockout (KO) mouse model and found it to be viable (Fujita et al., 2006). Further study showed that the Cadm1 KO mouse has a reduction in excitatory synapse number in the CA1 region of the hippocampus (Robbins et al., 2010). This work suggests that Cadms play a role in synapse formation.

To further examine the role of Cadms in synapse formation, we chose to utilize the zebrafish spinal cord as a model. Zebrafish possess a number of features useful for the study of synapse formation *in vivo*: 1) a small number of identified neurons in the spinal cord (Bernhardt et al., 1990; Hale et al., 2001; Drapeau et al., 2002), and 2) a developmentally characterized excitatory synapse (Easley-Neal et al., in review) that drives a well documented behavioral response (Saint-Amant and Drapeau, 1998).

To determine the role of *Cadm2a* in synapse formation *in vivo*, we have used the RB-CoPA synapse in the zebrafish spinal cord as a model synapse. After knocking down *Cadm2a* expression we found that behavior driven by the RB sensory neurons was dramatically impaired, and that the number of RB-CoPA synapses is reduced.

MATERIALS AND METHODS

Zebrafish husbandry

All zebrafish embryos, larvae, and adults were raised and maintained at 28.5°C according to standard protocols (Westerfield, 2000). Lines used included AB/Tübingen and *neurogenin1:GFP* (*Tg(-3.1ngn1:GFP)sb; ngn1:GFP*).

Fluorescent *in situ* hybridization

Fluorescent *in situ* hybridization (FISH) was done according to the method described by Welten (Welten et al., 2006) with modifications described by J. Talbot (Talbot et al., 2010). The full protocol is available online at (<https://wiki.zfin.org/display/prot/Triple+Fluorescent+In+Situ>). The probes used were against *Cadm2a* mRNA (Petri, 2008), and a full length probe to *islet1* mRNA (NM_130962.1).

Morpholinos

Antisense morpholino oligonucleotides (MOs) to *Cadm2a* were designed and synthesized by Genetools, LLC (Philomath, OR). The MO sequences were as follows:
Cadm2a translation blocking (*Cadm2a* TBMO)

ATGCTGCTTCACCATCATATTGCCT, Cadm2a splice blocking (Cadm2a SBMO)
GCTCCTGGAAGAGACAGACCGACTT, and Genetools standard control oligo (control
MO) CCTCTTACCTCAGTTACAATTTATA.

Morpholino injections

MOs were pressure injected into 1-2 cell stage embryos using a MPPI-2 pressure injector (ASI, Eugene, OR). MOs were injected at the following concentrations: control MO 14.99-23.32ng, Cadm2a TBMO 17.52-23.37ng, and Cadm2a SBMO 15.26-20.34ng. MOs were diluted in a 0.05% phenol red solution in water. Injection volumes were estimated to be 3-4nl.

RT-PCR

Efficacy of knock-down of wild-type transcript by the Cadm2a SBMO was assayed by RT-PCR on cDNA from MO injected embryos. Primers used were Cadm2a SB 4F ATCTGCGGGATCGTCCTTAAAG and Cadm2a SB 4R GGTGATTGGTGGCTCCACAG. cDNA was synthesized from unspliced pre-mRNA from 20 morpholino injected embryos. PCR conditions were as follows: 95°C for 5 min, followed by 40 cycles of 95°C/ 30 seconds, 55°C/ 30 seconds, 72°C/ 60 seconds, followed by 10 minutes at 72°C.

Behavioral analysis

Touch response (TR) was assayed in MO injected embryos between 27-28 hpf. Dechorionated embryos were mounted dorsal side up in a drop of 1.5% low melting

temperature agarose on a 24x60mm glass coverslip. The agarose was allowed to cure for 10 min, then a pap pen was used to make a hydrophobic barrier around the agarose drop creating a “chamber” that was flooded with embryo medium (EM). The agarose surrounding the embryo’s tail was then cut away at a 45° angle from each side of the body, starting from the yolk tube, allowing a ~270° degree range of motion of the tail. Embryos were allowed to recover at room temperature for at least 20 minutes prior to behavioral testing. The touch response (TR) test consisted of touching the embryo five times on the side of the tail between somites 14-16 with an insect pin attached to a micromanipulator, with a pause of 1-2 seconds between touches. The behavior was recorded at a rate of 100 frames/second using a stereomicroscope (Leica LZMFIII) and a monochrome digital camera (PixeLINK PL-A741).

Failure rate was calculated by counting the number of times an embryo failed to respond to the stimulus and reporting that as a percentage of the total number of stimuli. Latency was defined as the time between the frame when the probe made contact with the embryos ($t=0$) and the frame when the embryo began to move away from the probe. If the movement of an embryo occurred more than 1 second after the stimulus was applied that behavior was scored as a spontaneous contraction, not a response to touch. Analysis of the movement was performed using Image Pro Plus software. To calculate the velocity of the movement the tip of the embryo’s tail was tracked from $t=0$ to the time point at which the tail reached its apex during the coiling behavior. Two tailed unpaired Students t-tests were used to determine significance between groups. All graphs were made in Microsoft Excel.

Immunohistochemistry

Whole mount immunohistochemistry (IHC) was performed with the following primary antibodies: panMAGUK (1:100 ; NeuroMab, Davis, CA), and chicken anti-GFP (1:500; Abcam, Cambridge, MA), and secondary antibodies: anti-mouse Cy2 (1:600; Jackson Immuno, West Grove, PA), and anti-rabbit Alexa 546 (1:600; Molecular Probes, Eugene, OR). All IHC was performed as described by Easley-Neal (2011).

Imaging

IHC was imaged on an inverted Nikon TU-2000 microscope with an EZ-C1 confocal system (Nikon) with a 100x oil-immersion objective (1.45 NA). Image stacks through the depth of the dlf (~10-15 microns) were acquired to capture synaptic puncta at all points of contact between RB axons and CoPAs. Images were acquired for each channel separately.

Analysis of imaging data was performed on maximum intensity projections of the image stacks. Synaptic puncta were selected and counted using Image Pro Plus software (Media Cybernetics, Bethesda, MD) as described by Easley-Neal (2011).

RESULTS

Cadm2a is expressed in RB cells

Previous work has shown that *Cadm2a* is strongly expressed in cells in the zebrafish spinal cord that occupy a dorso-ventral position (Pietri et al., 2008). To determine whether these were Rohon Beard (RB) sensory neurons, we performed two color fluorescent in situ hybridization (FISH) for *Cadm2a* and *islet1*, a marker of RB

cells (Olesnicky et al., 2010). We found that a significant number of *islet1* expressing RB cells also expressed *Cadm2a* at 25hpf (Fig. 1). It is possible that all RB cells express *cadm2a* as development progresses. Our previous work had also shown that *cadm3* is expressed in dorso-ventrally located cells in the spinal cord that were thought to be RBs (Pietri et al., 2008). This was confirmed by *islet1/cadm3* FISH (data not shown). For the remainder of our studies we chose to examine the function of Cadm2a, as it has a much more restricted expression pattern than Cadm3 (Pietri et al., 2008).

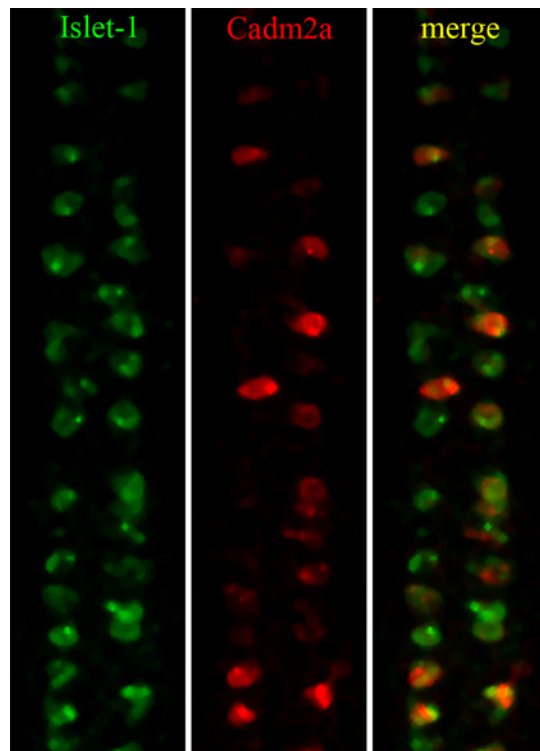


Figure 1. *cadm2a* is expressed in RB cells. Fluorescent in situ hybridization performed on 25hpf whole mount zebrafish embryos reveals that *cadm2a* is expressed in RB cells, as shown by colocalization with the RB marker *islet-1*.

Knockdown of Cadm2a leads to a decrease in touch response

To assess the role of Cadm2a in synapse function we used morpholino (MO) oligonucleotides to knock down expression of Cadm2a (Ekker, 2000; Nasevicius and Ekker, 2000; Corey and Abrams, 2001). Both translation blocking (TB) and splice blocking (SB) MOs were designed. To test the effect of Cadm knockdown, we utilized a stereotyped behavior, the touch response (TR). The TR is a sensorimotor behavior involving contralateral contractions of the tail, or c-bends, in response to a light touch on the tail (Saint-Amant and Drapeau, 1998; Fig. 2A). While it has been understood for some time that RBs are the sensory neurons responsible for transducing the signal of a touch to the skin (Roberts, 2000), work from our lab has recently established that the commissural primary ascending (CoPA) interneurons are the downstream synaptic partner of RBs (Easley-Neal et al., in review; Pietri et al., 2009).

The effect of Cadm2a knockdown by MO was assessed in 27hpf embryos. At this stage of development spontaneous contractions, which are c-bends that don't require an external stimulus, have reduced in frequency to a sufficient degree that c-bends occurring in response to touch are simple to discern (Brustein et al., 2003; Pietri et al., 2009). When the TR of Cadm2a MO injected embryos, referred to as morphants, was measured, we found that Cadm2a TB morphants showed a significant increase in failure rate and that co-injection of the MO with full length Cadm2a RNA rescued the TR failure rate to WT levels (embryos analyzed: control n=16, Cadm2a TBMO n=13, MO + RNA n=12, RNA n=12; Fig. 2B). We also measured the latency of the onset of the c-bend after the touch stimulus, and found that it was significantly increased in Cadm2a TBMO embryos versus controls (Fig. 2C). Though the MO injected embryos frequently failed to respond to

touch, in some cases they did complete a c-bend in response to the stimulus. Analysis of those movements showed that the velocity of the tail tip for the MO injected embryos was significantly slower than control or MO plus RNA injected embryos (control n = 17, MO n = 9, MO + RNA n = 14 c-bends; Fig. 2D), and that the maximum velocity achieved by MO injected embryos was significantly below that seen for either the control or rescue group (Fig. 2E). In other words, when they responded to touch, *Cadm2a* morphants performed very slow c-bends compared to the control and rescue groups.

To confirm these results, touch test analysis was performed with a second *Cadm2a* MO, one that blocked correct splicing of the fourth exon. This produces an early stop codon, yielding a truncated protein consisting of the most N-terminal amino acid sequence, stopping just prior to the first Ig domain (Pietri et al., 2008). Embryos injected with this *Cadm2a* SBMO had a 3.5 fold higher failure rate than control embryos ($p = 0.04$; data not shown). Knockdown of properly spliced *Cadm2a* transcript was confirmed by RT-PCR (data not shown).

We next wanted to ensure that the decrease in TR seen in the *Cadm2a* TB morphants was not due to a general health or musculature defect which would lead to an inability to respond in a wild type fashion to the touch stimulus. To do this we analyzed spontaneous contractions in age matched groups of fish at ~24hpf. We found that there was no significant difference in the rate of spontaneous contractions between MO, control, and rescue groups (control n = 25, MO n = 30, MO + RNA n = 25 embryos; Fig. 2E, G). Analysis of the velocity of the tip of the tail during spontaneous b-bends showed no significant difference in velocity between *Cadm2a* morphants and controls over the course of the movement (control n = 6 embryos, MO n = 6 embryos; Fig. 2H).

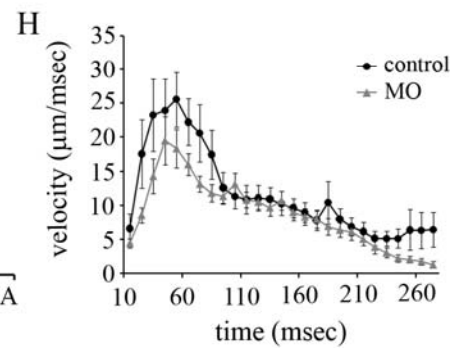
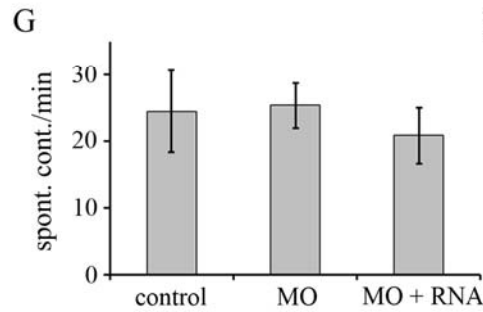
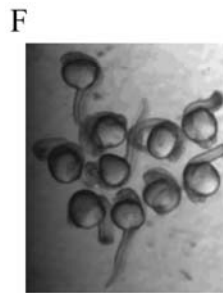
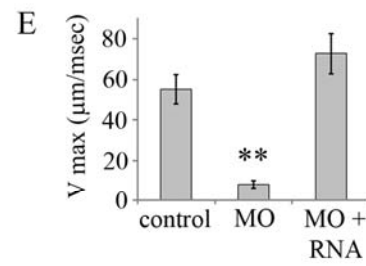
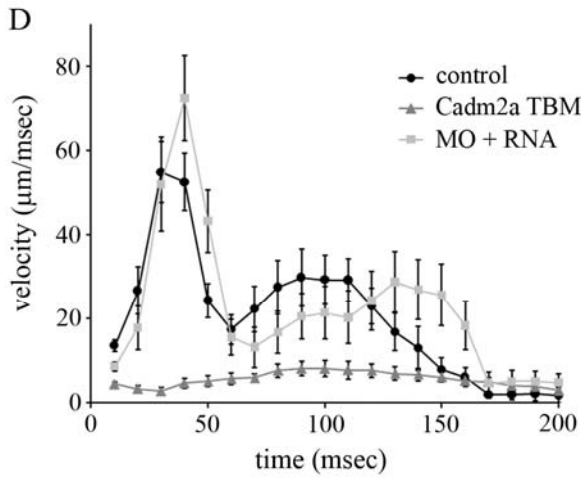
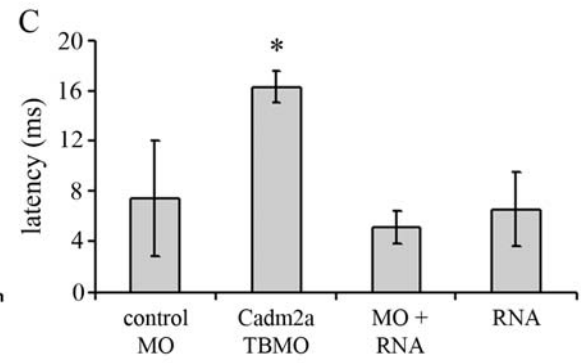
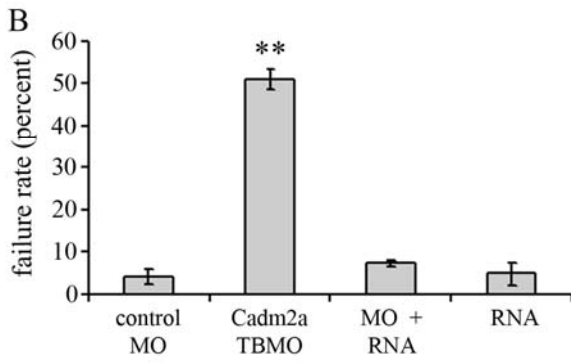
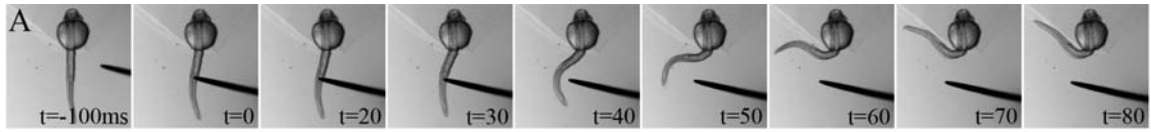


Figure 2. Cadm2a knockdown decreases touch response. **A**, Selected frames from a time lapse movie of touch response testing on a WT embryo. The probe contacts the embryo at $t=0$. **B**, Histogram quantifies the percentage TR failure rate for control, morphant, RNA rescue, and RNA injected embryos. **C**, The histogram quantifies latency, which is the time from the probe touching the embryo to the time when the embryo begins a c-bend. Groups as describes in **B**. **D**, Plot shows the average velocity of each group measured every 10ms from 0-200ms after the start of a c-bend. Groups as describes in **B**. **E**, Histogram shows the average maximum velocity (V_{max}) achieved during c-bends by each group. Groups as describes in **B**. **F**, Frame from a time lapse movie of spontaneous contractions. Note the embryos in various stages of a c-bend. **G**, The histogram quantifies average spontaneous contractions per minute for groups of control, morphant, and RNA rescue embryos. **H**, Plot depicts the average velocity of each group measured every 10ms from 10-260ms after the start of a spontaneous contraction. All error bars represent standard error of the mean (s.e.m.). * $p < 0.05$, ** $p < 0.005$.

Together, these data suggest that Cadm2a is required for the touch response circuitry to function properly. Although use of MOs leads to a global knock down of wild type Cadm2a protein levels in the developing fish, the disparity between the spontaneous contractions and c-bends in response to touch suggests that an effect on the most upstream portion of the circuit, the synapses between RBs and CoPAs, is indicated by the reduction in TR. Input from RBs has previously been shown to be indispensable for the touch response (Saint-Amant and Drapeau, 2000). Therefore we next set out to determine whether Cadm2a knockdown affects the number of RB-CoPA synapses.

Knockdown of Cadm2a leads to a decrease in synapse number

To determine the effect of Cadm2a knockdown on RB-CoPA synapse formation we performed immunohistochemistry for pan MAGUK (MAGUKs), an antibody that binds postsynaptic scaffolding proteins with MAGUK domains such as PSD-95, PSD-93, and SAP 102 (Meyer et al., 2005). This antibody has previously been shown by us to label RB-CoPA synapses (Easley-Neal et al., in review). Cadm2a TB MO embryos were

TR tested at 27hpf. Those embryos with the highest failure rates were anesthetized and fixed at 28hpf, along with age matched control MO injected embryos.

Immunohistochemistry for MAGUKs on these embryos showed that there was a significant, fifty percent decrease in the number of MAGUK puncta per micron of fascicle in the Cadm2a morphants versus the control embryos (control n = 13, MO n = 10 embryos; Fig. 3A, B). This decrease in postsynaptic MAGUK puncta in Cadm2a TB morphants suggests that knockdown of Cadm2a leads to a decrease in the number of RB-CoPA synapses.

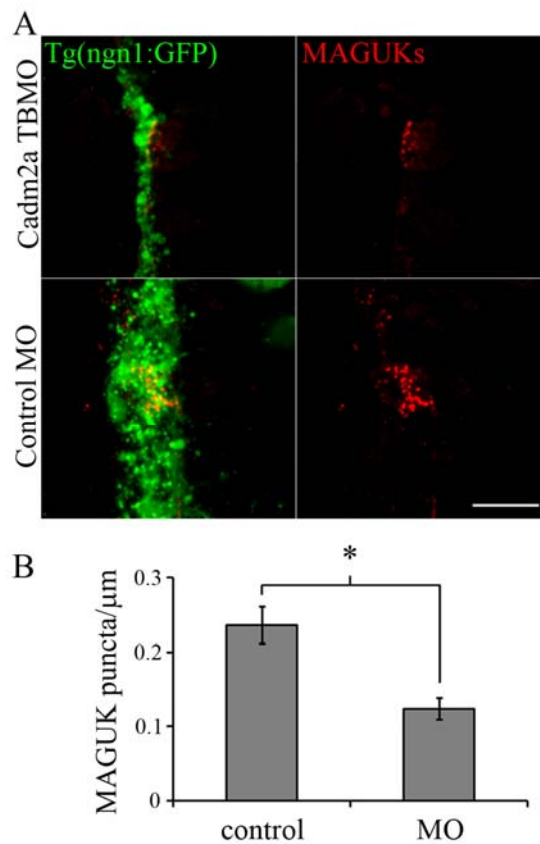


Figure 3. Cadm2a knockdown decreases RB-CoPA synapse number. **A**, Immunohistochemistry for MAGUKs on control embryos and Cadm2aTB morphants at 28hpf. **B**, The histogram quantifies the average number of MAGUK puncta per micron in the dlf of control embryos and Cadm2a morphants. Error bars represent s.e.m. $p < 0.001$.

DISCUSSION

In the current study, we have shown that Cadm2a is required for the development of glutamatergic synapses in the zebrafish spinal cord. First, we showed that knockdown of Cadm2a protein levels leads to a deficit in touch response behavior in zebrafish embryos (Fig. 2). Then, we showed that Cadm2a knockdown leads to a decrease in the number of RB-CoPA synapses (Fig. 3). This is the first work to show a role for Cadm2a in synapse formation.

Our results support work performed in mouse showing that knockout of Cadm1 leads to a decrease in excitatory synapse number (Robbins et al., 2010). We have shown that a second Cadm family member, Cadm2a, shows a decrease in excitatory synapse number when protein levels are knocked down. This suggests that all members of the Cadm family may have this ability to drive synapse formation *in vivo*. It will be interesting to explore the roles of the other Cadms in synapse formation as well.

We have also demonstrated that the RB-CoPA synapse in the touch response circuit provides an excellent model with which to study the role of Cadms in synapse formation *in vivo*. The touch response behavioral assay provides an excellent tool to assess synapse formation at a single, defined excitatory synapse. When used in conjunction with immunohistochemical techniques, this provides a unique toolset to assess synapse formation.

In this study Cadm2a knockdown lead to a decrease in synapse formation despite a lack of change in the expression levels of any of the other Cadms. This is in line with results from Cadm1 knockout in mouse (Robbins et al., 2010), where only Cadm1 expression levels were perturbed. This work provides further support for the idea that

Cadms, unlike the Neuroligins, can not functionally compensate for one another (Varoqueaux et al., 2006; Robbins et al., 2010). This work is further evidence that the Cadm family of adhesion molecules may play a unique role in synapse formation.

CHAPTER V

CONCLUSION

Trafficking proteins to the presynaptic terminal

My analysis of presynaptic protein trafficking showed that there are at least three types of transport packets that carry proteins to a nascent synapse. In addition, these transport packets arrive at the synapse in a distinct temporal order. This work opens up several avenues for future investigation. First, it will be of great interest to characterize the newly described Synapsin transport packet. Determining what, if any, other presynaptic cargo are co-transported with Synapsin, as well as what motor protein is responsible for transporting these packets will be of great interest. Another line of investigation will involve looking for the signal(s) that recruit these transport packets. Our preliminary work suggests that signaling via the FERM domain of Cadm may be required for the recruitment of additional STVs to a synapse (data not shown). Determining whether the PDZ domain of Cadm is also playing a signaling role in recruitment, and whether other signaling molecules are involved are questions ripe for exploration.

Cadm expression and function in the zebrafish spinal cord

My examination of the spatial and temporal expression patterns of the zebrafish Cadms showed that *cadm* mRNAs are expressed throughout the nervous system in both developing animals and in adults. I also assessed the effect of Cadm2a knockdown in zebrafish embryos, and found that it caused both a decrease in the response to touch and a

decrease in the number of RB-CoPA synapses. This work suggests several interesting avenues of future investigation. First, it would be of interest to examine the role of Cadms PDZ and FERM protein binding domains in synapse formation and recruitment of proteins to the presynaptic active zone and postsynaptic density. It has been proposed that synaptogenic CAMs may induce signaling to recruit proteins to the nascent synapse (Biederer and Stagi, 2008). Preliminary studies to address this question in our lab are ongoing and suggest that the FERM domain of Cadm2a is required to recruit STVs to nascent synapses (data not shown). Further investigation of the functions of the binding domains will help to further clarify the role Cadms are playing in synapse formation. Another interesting project would be to examine the roles of other Cadms in *in vivo* synapse formation. All of the Cadm family members have conserved protein architecture and highly conserved amino acid sequences (Pietri et al., 2008), and both Cadm1 and Cadm2a have now been shown to be required for synapse formation (Robbins et al., 2010; Chapter IV). This raises the question of whether the other Cadms have a similar function. Currently, the only other Cadm to be studied in the CNS is rat Cadm3. It has been shown to be important for adhesion of an axon to a myelinating oligodendrocyte (Pellissier et al., 2007), though this may not necessarily be its only function in the CNS. Addressing this question will help to further clarify the roles of the Cadms in CNS development and function.

REFERENCES CITED

- Ahmari SE, Smith SJ (2002) Knowing a nascent synapse when you see it. *Neuron* 34:333-336.
- Ahmari SE, Buchanan J, Smith SJ (2000) Assembly of presynaptic active zones from cytoplasmic transport packets. *Nat Neurosci* 3:445-451.
- Artinger KB, Chitnis AB, Mercola M, Driever W (1999) Zebrafish narrowminded suggests a genetic link between formation of neural crest and primary sensory neurons. *Development* 126:3969-3979.
- Barrow SL, Constable JR, Clark E, El-Sabeawy F, McAllister AK, Washbourne P (2009) Neuroligin1: a cell adhesion molecule that recruits PSD-95 and NMDA receptors by distinct mechanisms during synaptogenesis. *Neural Dev* 4:17.
- Bernhardt RR, Chitnis AB, Lindamer L, Kuwada JY (1990) Identification of spinal neurons in the embryonic and larval zebrafish. *J Comp Neurol* 302:603-616.
- Biederer T (2006) Bioinformatic characterization of the SynCAM family of immunoglobulin-like domain-containing adhesion molecules. *Genomics* 87:139-150.
- Biederer T, Stagi M (2008) Signaling by synaptogenic molecules. *Curr Opin Neurobiol* 18:261-269.
- Biederer T, Sara Y, Mozhayeva M, Atasoy D, Liu X, Kavalali ET, Sudhof TC (2002) SynCAM, a synaptic adhesion molecule that drives synapse assembly. *Science* 297:1525-1531.
- Bresler T, Ramati Y, Zamorano PL, Zhai R, Garner CC, Ziv NE (2001) The dynamics of SAP90/PSD-95 recruitment to new synaptic junctions. *Mol Cell Neurosci* 18:149-167.
- Brustein E, Saint-Amant L, Buss RR, Chong M, McDearmid JR, Drapeau P (2003) Steps during the development of the zebrafish locomotor network. *J Physiol Paris* 97:77-86.
- Bury LA, Sabo SL (2011) Coordinated trafficking of synaptic vesicle and active zone proteins prior to synapse formation. *Neural Dev* 6:24.
- Catchen JM, Conery JS, Postlethwait JH (2009) Automated identification of conserved synteny after whole-genome duplication. *Genome Res* 19:1497-1505.

- Chin LS, Li L, Ferreira A, Kosik KS, Greengard P (1995) Impairment of axonal development and of synaptogenesis in hippocampal neurons of synapsin I-deficient mice. *Proc Natl Acad Sci U S A* 92:9230-9234.
- Coleman WL, Bykhovskaia M (2009) Synapsin I accelerates the kinetics of neurotransmitter release in mouse motor terminals. *Synapse* 63:531-533.
- Corey DR, Abrams JM (2001) Morpholino antisense oligonucleotides: tools for investigating vertebrate development. *Genome Biol* 2:REVIEWS1015-REVIEWS1015.1013.
- Dalva MB, McClelland AC, Kayser MS (2007) Cell adhesion molecules: signalling functions at the synapse. *Nat Rev Neurosci* 8:206-220.
- Demarque M, Represa A, Becq H, Khalilov I, Ben-Ari Y, Aniksztejn L (2002) Paracrine intercellular communication by a Ca²⁺- and SNARE-independent release of GABA and glutamate prior to synapse formation. *Neuron* 36:1051-1061.
- Douglass AD, Kraves S, Deisseroth K, Schier AF, Engert F (2008) Escape behavior elicited by single, channelrhodopsin-2-evoked spikes in zebrafish somatosensory neurons. *Curr Biol* 18:1133-1137.
- Downes GB, Granato M (2006) Supraspinal input is dispensable to generate glycine-mediated locomotive behaviors in the zebrafish embryo. *J Neurobiol* 66:437-451.
- Drachman DA (2005) Do we have brain to spare? *Neurology* 64:2004-2005.
- Drapeau P, Saint-Amant L, Buss RR, Chong M, McDearmid JR, Brustein E (2002) Development of the locomotor network in zebrafish. *Prog Neurobiol* 68:85-111.
- Easley-Neal C, Buchanan J, Washbourne P Ordered assembly of the presynaptic terminal of glutamatergic synapses in vivo. *Journal of Neuroscience*, manuscript in review.
- Eisen JS, Pike SH (1991) The spt-1 mutation alters segmental arrangement and axonal development of identified neurons in the spinal cord of the embryonic zebrafish. *Neuron* 6:767-776.
- Ekker SC (2000) Morphants: a new systematic vertebrate functional genomics approach. *Yeast* 17:302-306.
- Fogel AI, Akins MR, Krupp AJ, Stagi M, Stein V, Biederer T (2007) SynCAMs organize synapses through heterophilic adhesion. *J Neurosci* 27:12516-12530.
- Fornasiero EF, Bonanomi D, Benfenati F, Valtorta F (2010) The role of synapsins in neuronal development. *Cell Mol Life Sci* 67:1383-1396.

- Fuchs A, Colonna M (2006) The role of NK cell recognition of nectin and nectin-like proteins in tumor immunosurveillance. *Semin Cancer Biol* 16:359-366.
- Fujita E, Urase K, Soyama A, Kouroku Y, Momoi T (2005) Distribution of RA175/TSLC1/SynCAM, a member of the immunoglobulin superfamily, in the developing nervous system. *Brain Res Dev Brain Res* 154:199-209.
- Fujita E, Kouroku Y, Ozeki S, Tanabe Y, Toyama Y, Maekawa M, Kojima N, Senoo H, Toshimori K, Momoi T (2006) Oligo-astheno-teratozoospermia in mice lacking RA175/TSLC1/SynCAM/IGSF4A, a cell adhesion molecule in the immunoglobulin superfamily. *Mol Cell Biol* 26:718-726.
- Fukuhara H, Masuda M, Yageta M, Fukami T, Kuramochi M, Maruyama T, Kitamura T, Murakami Y (2003) Association of a lung tumor suppressor TSLC1 with MPP3, a human homologue of *Drosophila* tumor suppressor Dlg. *Oncogene* 22:6160-6165.
- Furuno T, Ito A, Koma Y, Watabe K, Yokozaki H, Bienenstock J, Nakanishi M, Kitamura Y (2005) The spermatogenic Ig superfamily/synaptic cell adhesion molecule mast-cell adhesion molecule promotes interaction with nerves. *J Immunol* 174:6934-6942.
- Gerrow K, El-Husseini A (2006) Cell adhesion molecules at the synapse. *Front Biosci* 11:2400-2419.
- Gitler D, Takagishi Y, Feng J, Ren Y, Rodriguiz RM, Wetsel WC, Greengard P, Augustine GJ (2004) Different presynaptic roles of synapsins at excitatory and inhibitory synapses. *J Neurosci* 24:11368-11380.
- Grant SG (2006) The synapse proteome and phosphoproteome: a new paradigm for synapse biology. *Biochem Soc Trans* 34:59-63.
- Gruber-Olipitz M, Yang JW, Slave I, Lubec G (2006) Nectin-like molecule 1 is a high abundance protein in cerebellar neurons. *Amino Acids* 30:409-415.
- Grunwald DJ, Kimmel CB, Westerfield M, Walker C, Streisinger G (1988) A neural degeneration mutation that spares primary neurons in the zebrafish. *Dev Biol* 126:115-128.
- Hale ME, Ritter DA, Fetcho JR (2001) A confocal study of spinal interneurons in living larval zebrafish. *J Comp Neurol* 437:1-16.
- Han Y, Kaeser PS, Sudhof TC, Schneggenburger R (2011) RIM determines Ca²⁺ channel density and vesicle docking at the presynaptic active zone. *Neuron* 69:304-316.

- Hernandez-Lagunas L, Choi IF, Kaji T, Simpson P, Hershey C, Zhou Y, Zon L, Mercola M, Artinger KB (2005) Zebrafish narrowminded disrupts the transcription factor *prdm1* and is required for neural crest and sensory neuron specification. *Dev Biol* 278:347-357.
- Hoy JL, Constable JR, Vicini S, Fu Z, Washbourne P (2009) SynCAM1 recruits NMDA receptors via protein 4.1B. *Mol Cell Neurosci* 42:466-483.
- Hukriede NA, Joly L, Tsang M, Miles J, Tellis P, Epstein JA, Barbazuk WB, Li FN, Paw B, Postlethwait JH, Hudson TJ, Zon LI, McPherson JD, Chevrette M, Dawid IB, Johnson SL, Ekker M (1999) Radiation hybrid mapping of the zebrafish genome. *Proc Natl Acad Sci U S A* 96:9745-9750.
- Hunter PR, Nikolaou N, Odermatt B, Williams PR, Drescher U, Meyer MP (2011) Localization of *Cadm2a* and *Cadm3* proteins during development of the zebrafish nervous system. *J Comp Neurol* 519:2252-2270.
- Huttner WB, Schiebler W, Greengard P, De Camilli P (1983) Synapsin I (protein I), a nerve terminal-specific phosphoprotein. III. Its association with synaptic vesicles studied in a highly purified synaptic vesicle preparation. *J Cell Biol* 96:1374-1388.
- Ito A, Oonuma J (2006) Direct interaction between nerves and mast cells mediated by the SgIGSF/SynCAM adhesion molecule. *J Pharmacol Sci* 102:1-5.
- Ito A, Hagiwara M, Oonuma J, Murakami Y, Yokozaki H, Takaki M (2007a) Involvement of the SgIGSF/Necl-2 adhesion molecule in degranulation of mesenteric mast cells. *J Neuroimmunol* 184:209-213.
- Ito A, Jippo T, Wakayama T, Morii E, Koma Y, Onda H, Nojima H, Iseki S, Kitamura Y (2003) SgIGSF: a new mast-cell adhesion molecule used for attachment to fibroblasts and transcriptionally regulated by MITF. *Blood* 101:2601-2608.
- Ito A, Nishikawa Y, Ohnuma K, Ohnuma I, Koma Y, Sato A, Enomoto K, Tsujimura T, Yokozaki H (2007b) SgIGSF is a novel biliary-epithelial cell adhesion molecule mediating duct/ductule development. *Hepatology* 45:684-694.
- Jensen AM, Walker C, Westerfield M (2001) *mosaic eyes*: a zebrafish gene required in pigmented epithelium for apical localization of retinal cell division and lamination. *Development* 128:95-105.
- Jin Y, Garner CC (2008) Molecular mechanisms of presynaptic differentiation. *Annu Rev Cell Dev Biol* 24:237-262.
- Jontes JD, Buchanan J, Smith SJ (2000) Growth cone and dendrite dynamics in zebrafish embryos: early events in synaptogenesis imaged in vivo. *Nat Neurosci* 3:231-237.

- Jontes JD, Emond MR, Smith SJ (2004) In vivo trafficking and targeting of N-cadherin to nascent presynaptic terminals. *J Neurosci* 24:9027-9034.
- Kakunaga S, Ikeda W, Itoh S, Deguchi-Tawarada M, Ohtsuka T, Mizoguchi A, Takai Y (2005) Nectin-like molecule-1/TSSL1/SynCAM3: a neural tissue-specific immunoglobulin-like cell-cell adhesion molecule localizing at non-junctional contact sites of presynaptic nerve terminals, axons and glia cell processes. *J Cell Sci* 118:1267-1277.
- Kelly RB (1991) Neurobiology. A system for synapse control. *Nature* 349:650-651.
- Kimmel CB, Ballard WW, Kimmel SR, Ullmann B, Schilling TF (1995) Stages of embryonic development of the zebrafish. *Dev Dyn* 203:253-310.
- Kraszewski K, Mundigl O, Daniell L, Verderio C, Matteoli M, De Camilli P (1995) Synaptic vesicle dynamics in living cultured hippocampal neurons visualized with CY3-conjugated antibodies directed against the luminal domain of synaptotagmin. *J Neurosci* 15:4328-4342.
- Kwon HB, Sabatini BL (2011) Glutamate induces de novo growth of functional spines in developing cortex. *Nature* 474:100-104.
- Leal-Ortiz S, Waites CL, Terry-Lorenzo R, Zamorano P, Gundelfinger ED, Garner CC (2008) Piccolo modulation of Synapsin1a dynamics regulates synaptic vesicle exocytosis. *J Cell Biol* 181:831-846.
- Lewis KE, Eisen JS (2003) From cells to circuits: development of the zebrafish spinal cord. *Prog Neurobiol* 69:419-449.
- Lohmann C, Myhr KL, Wong RO (2002) Transmitter-evoked local calcium release stabilizes developing dendrites. *Nature* 418:177-181.
- Luscher C, Isaac JT (2009) The synapse: center stage for many brain diseases. *J Physiol* 587:727-729.
- Maletic-Savatic M, Malinow R, Svoboda K (1999) Rapid dendritic morphogenesis in CA1 hippocampal dendrites induced by synaptic activity. *Science* 283:1923-1927.
- Maurel P, Einheber S, Galinska J, Thaker P, Lam I, Rubin MB, Scherer SS, Murakami Y, Gutmann DH, Salzer JL (2007) Nectin-like proteins mediate axon Schwann cell interactions along the internode and are essential for myelination. *J Cell Biol* 178:861-874.
- McAllister AK (2007) Dynamic aspects of CNS synapse formation. *Annu Rev Neurosci* 30:425-450.

- McLean DL, Fetcho JR (2008) Using imaging and genetics in zebrafish to study developing spinal circuits in vivo. *Dev Neurobiol* 68:817-834.
- Meyer G, Varoqueaux F, Neeb A, Oschlies M, Brose N (2004) The complexity of PDZ domain-mediated interactions at glutamatergic synapses: a case study on neuroligin. *Neuropharmacology* 47:724-733.
- Meyer MP, Trimmer JS, Gilthorpe JD, Smith SJ (2005) Characterization of zebrafish PSD-95 gene family members. *J Neurobiol* 63:91-105.
- Micheva KD, Busse B, Weiler NC, O'Rourke N, Smith SJ (2010) Single-synapse analysis of a diverse synapse population: proteomic imaging methods and markers. *Neuron* 68:639-653.
- Moens CB, Yan YL, Appel B, Force AG, Kimmel CB (1996) valentino: a zebrafish gene required for normal hindbrain segmentation. *Development* 122:3981-3990.
- Muller T, Wulliman, MF. (2005) Atlas of Early Zebrafish Brain Development, A Tool for Molecular Neurogenetics: Elsevier.
- Murakami Y (2005) Involvement of a cell adhesion molecule, TSLC1/IGSF4, in human oncogenesis. *Cancer Sci* 96:543-552.
- Nasevicius A, Ekker SC (2000) Effective targeted gene 'knockdown' in zebrafish. *Nat Genet* 26:216-220.
- Nikolaou N, Meyer MP (2011) Imaging circuit formation in zebrafish. *Dev Neurobiol*.
- Ohta Y, Itoh K, Yaoi T, Tando S, Fukui K, Fushiki S (2005) Spatiotemporal patterns of expression of IGSF4 in developing mouse nervous system. *Brain Res Dev Brain Res* 156:23-31.
- Olesnicki E, Hernandez-Lagunas L, Artinger KB (2010) prdm1a Regulates sox10 and islet1 in the development of neural crest and Rohon-Beard sensory neurons. *Genesis* 48:656-666.
- Pellissier F, Gerber A, Bauer C, Ballivet M, Ossipow V (2007) The adhesion molecule Necl-3/SynCAM-2 localizes to myelinated axons, binds to oligodendrocytes and promotes cell adhesion. *BMC Neurosci* 8:90.
- Penzes P, Cahill ME, Jones KA, VanLeeuwen JE, Woolfrey KM (2011) Dendritic spine pathology in neuropsychiatric disorders. *Nat Neurosci* 14:285-293.
- Pietri T, Easley-Neal C, Wilson C, Washbourne P (2008) Six cadm/SynCAM genes are expressed in the nervous system of developing zebrafish. *Dev Dyn* 237:233-246.

- Pietri T, Manalo E, Ryan J, Saint-Amant L, Washbourne P (2009) Glutamate drives the touch response through a rostral loop in the spinal cord of zebrafish embryos. *Dev Neurobiol* 69:780-795.
- Postlethwait J, Amores A, Cresko W, Singer A, Yan YL (2004) Subfunction partitioning, the teleost radiation and the annotation of the human genome. *Trends Genet* 20:481-490.
- Postlethwait JH, Woods IG, Ngo-Hazelett P, Yan YL, Kelly PD, Chu F, Huang H, Hill-Force A, Talbot WS (2000) Zebrafish comparative genomics and the origins of vertebrate chromosomes. *Genome Res* 10:1890-1902.
- Rasband WS (1997-2011) ImageJ. In. Bethesda: U. S. National Institutes of Health.
- Robbins EM, Krupp AJ, Perez de Arce K, Ghosh AK, Fogel AI, Boucard A, Sudhof TC, Stein V, Biederer T (2010) SynCAM 1 adhesion dynamically regulates synapse number and impacts plasticity and learning. *Neuron* 68:894-906.
- Roberts A (2000) Early functional organization of spinal neurons in developing lower vertebrates. *Brain Res Bull* 53:585-593.
- Sabo SL, Gomes RA, McAllister AK (2006) Formation of presynaptic terminals at predefined sites along axons. *J Neurosci* 26:10813-10825.
- Saint-Amant L (2006) Development of motor networks in zebrafish embryos. *Zebrafish* 3:173-190.
- Saint-Amant L, Drapeau P (1998) Time course of the development of motor behaviors in the zebrafish embryo. *J Neurobiol* 37:622-632.
- Saint-Amant L, Drapeau P (2000) Motoneuron activity patterns related to the earliest behavior of the zebrafish embryo. *J Neurosci* 20:3964-3972.
- Sara Y, Biederer T, Atasoy D, Chubykin A, Mozhayeva MG, Sudhof TC, Kavalali ET (2005) Selective capability of SynCAM and neuroligin for functional synapse assembly. *J Neurosci* 25:260-270.
- Schmitt EA, Dowling JE (1994) Early eye morphogenesis in the zebrafish, *Brachydanio rerio*. *J Comp Neurol* 344:532-542.
- Scott DA, Das U, Tang Y, Roy S (2011) Mechanistic logic underlying the axonal transport of cytosolic proteins. *Neuron* 70:441-454.
- Scott EK, Mason L, Arrenberg AB, Ziv L, Gosse NJ, Xiao T, Chi NC, Asakawa K, Kawakami K, Baier H (2007) Targeting neural circuitry in zebrafish using GAL4 enhancer trapping. *Nat Methods* 4:323-326.

- Shapira M, Zhai RG, Dresbach T, Bresler T, Torres VI, Gundelfinger ED, Ziv NE, Garner CC (2003) Unitary assembly of presynaptic active zones from Piccolo-Bassoon transport vesicles. *Neuron* 38:237-252.
- Shcherbo D, Souslova EA, Goedhart J, Chepurnykh TV, Gaintzeva A, Shemiakina, II, Gadella TW, Lukyanov S, Chudakov DM (2009) Practical and reliable FRET/FLIM pair of fluorescent proteins. *BMC Biotechnol* 9:24.
- Spiegel I, Adamsky K, Eshed Y, Milo R, Sabanay H, Sarig-Nadir O, Horresh I, Scherer SS, Rasband MN, Peles E (2007) A central role for Necl4 (SynCAM4) in Schwann cell-axon interaction and myelination. *Nat Neurosci* 10:861-869.
- Takai Y, Irie K, Shimizu K, Sakisaka T, Ikeda W (2003) Nectins and nectin-like molecules: roles in cell adhesion, migration, and polarization. *Cancer Sci* 94:655-667.
- Talbot JC, Johnson SL, Kimmel CB (2010) *hand2* and *Dlx* genes specify dorsal, intermediate and ventral domains within zebrafish pharyngeal arches. *Development* 137:2507-2517.
- Tallafuss A, Constable JR, Washbourne P (2010) Organization of central synapses by adhesion molecules. *Eur J Neurosci* 32:198-206.
- Tao-Cheng JH (2007) Ultrastructural localization of active zone and synaptic vesicle proteins in a preassembled multi-vesicle transport aggregate. *Neuroscience* 150:575-584.
- Thevenaz P, Ruttimann UE, Unser M (1998) A pyramid approach to subpixel registration based on intensity. *IEEE Trans Image Process* 7:27-41.
- Thomas LA, Akins MR, Biederer T (2008) Expression and adhesion profiles of SynCAM molecules indicate distinct neuronal functions. *J Comp Neurol* 510:47-67.
- Valor LM, Grant SG (2007) Integrating synapse proteomics with transcriptional regulation. *Behav Genet* 37:18-30.
- van der Weyden L, Arends MJ, Chausiaux OE, Ellis PJ, Lange UC, Surani MA, Affara N, Murakami Y, Adams DJ, Bradley A (2006) Loss of TSLC1 causes male infertility due to a defect at the spermatid stage of spermatogenesis. *Mol Cell Biol* 26:3595-3609.
- Varoqueaux F, Aramuni G, Rawson RL, Mohrmann R, Missler M, Gottmann K, Zhang W, Sudhof TC, Brose N (2006) Neuroligins determine synapse maturation and function. *Neuron* 51:741-754.

- Waites CL, Craig AM, Garner CC (2005) Mechanisms of vertebrate synaptogenesis. *Annu Rev Neurosci* 28:251-274.
- Wakayama T, Ohashi K, Mizuno K, Iseki S (2001) Cloning and characterization of a novel mouse immunoglobulin superfamily gene expressed in early spermatogenic cells. *Mol Reprod Dev* 60:158-164.
- Wakayama T, Koami H, Ariga H, Kobayashi D, Sai Y, Tsuji A, Yamamoto M, Iseki S (2003) Expression and functional characterization of the adhesion molecule spermatogenic immunoglobulin superfamily in the mouse testis. *Biol Reprod* 68:1755-1763.
- Washbourne P, Bennett JE, McAllister AK (2002) Rapid recruitment of NMDA receptor transport packets to nascent synapses. *Nat Neurosci* 5:751-759.
- Washbourne P, Dityatev A, Scheiffele P, Biederer T, Weiner JA, Christopherson KS, El-Husseini A (2004) Cell adhesion molecules in synapse formation. *J Neurosci* 24:9244-9249.
- Waterhouse AM, Procter JB, Martin DM, Clamp M, Barton GJ (2009) Jalview Version 2--a multiple sequence alignment editor and analysis workbench. *Bioinformatics* 25:1189-1191.
- Welten MC, de Haan SB, van den Boogert N, Noordermeer JN, Lamers GE, Spaink HP, Meijer AH, Verbeek FJ (2006) ZebraFISH: fluorescent in situ hybridization protocol and three-dimensional imaging of gene expression patterns. *Zebrafish* 3:465-476.
- Westerfield M (2000) *The Zebrafish Book*, 4th Edition. Eugene OR: Institute for Neuroscience, University of Oregon.
- Wulliman M, Rupp, B., Reichert, H. (1996) *Neuroanatomy of the Zebrafish Brain, A Topological Atlas*: Birkhauser Verlag.
- Yageta M, Kuramochi M, Masuda M, Fukami T, Fukuhara H, Maruyama T, Shibuya M, Murakami Y (2002) Direct association of TSLC1 and DAL-1, two distinct tumor suppressor proteins in lung cancer. *Cancer Res* 62:5129-5133.
- Yamada D, Yoshida M, Williams YN, Fukami T, Kikuchi S, Masuda M, Maruyama T, Ohta T, Nakae D, Maekawa A, Kitamura T, Murakami Y (2006) Disruption of spermatogenic cell adhesion and male infertility in mice lacking TSLC1/IGSF4, an immunoglobulin superfamily cell adhesion molecule. *Mol Cell Biol* 26:3610-3624.

Zhai RG, Vardinon-Friedman H, Cases-Langhoff C, Becker B, Gundelfinger ED, Ziv NE, Garner CC (2001) Assembling the presynaptic active zone: a characterization of an active one precursor vesicle. *Neuron* 29:131-143.

Ziv NE, Garner CC (2004) Cellular and molecular mechanisms of presynaptic assembly. *Nat Rev Neurosci* 5:385-399.